Mechanisms controlling natural aging and its effect on artificial aging in Al-Mg-Si alloys with and without trace element additions

A PhD thesis presented by

Dipl.-Ing. Marion Werinos

Leoben, February 16

AFFIDAVIT

I declare in lieu of oath, that I wrote this thesis and performed the associated research myself, using only literature cited in this volume.

_____
Marion Werinos

_____
Leoben, January 2016

Place and date of issue

ACKNOWLEDGEMENTS

Mechanisms controlling natural aging and its effect on artificial aging in Al-Mg-Si alloys with and without trace element additions

Al-Mg-Si alloys (6xxx series) represent the commercially most important group of age hardenable aluminum alloys. The wish to control natural aging kinetics and to find a solution to the negative effect of room temperature storage on artificial aging, discovered in 1939, is of major importance for the aluminum manufacturing industry. Based on preliminary results of a preceding study, the main objectives of this thesis were the minimization of natural aging and maximization of the artificial aging potential of Al-Mg-Si alloys with and without trace element additions to commercial Al-Mg-Si alloys.

A general understanding could be acquired how trace Sn additions to the alloy AA6061 are able to temporarily suppress natural aging and simultaneously enhance artificial aging kinetics: The strong Sn-vacancy binding energy results in trapping of most quenched-in excess vacancies in predominantly Sn-vacancy pairs. This generates a reduced number of untrapped vacancies which can control diffusional processes of other alloying atoms (Mg, Si or Cu) and thus significantly retards all natural aging clustering processes, whereas the maximum suppression of natural aging is obtained for Sn contents above the solubility limit of ~100 at.ppm. While suppression of natural aging prevails, the release of vacancies allows diffusion on demand for the precipitation of the peak hardening phase.

It could be shown that the effect of Sn is phenomenological similar to the positive effect of natural pre-aging at high temperatures > 210 °C in the commercial alloy. Additionally trace Sn addition generates both ultrafast artificial aging kinetics and superior peak hardness. This is supposed to result from the vacancy release besides a contribution of Sn-vacancy pairs to diffusion during artificial aging and/or a retardation of the annihilation of quenched-in vacancies by Sn.

Usually processing parameters and compositional limits of different Al-Mg-Si alloys and products vary. Lower solution treatment temperatures than 570 °C yield a decreasing delay of natural aging hardening, which is explained by a lower maximum quenchable Sn solubility. Thermodynamic calculations were also able to explain the effect and role of Mg, Si and Cu on natural aging kinetics and in clustering processes. The significant decrease in the suppressive effect of Sn with Si addition is attributed to Si-related clustering that controls the beginning of natural aging and its kinetics, while Si additionally lowers the quenchable Sn solubility. Cu does not influence the Sn solubility and is therefore believed to show a similar, but weaker effect as Sn, whereas Mg lowers the quenchable Sn solubility only.

For an industrial implementation of the trace element effect, the knowledge that material produced in laboratory behaves comparably as industrially produced wrought sheets or plates is important. Industrially produced material only shows a higher as-quenched hardness.

Finally, a design strategy for a maximum suppression of natural aging in Al-Mg-Si alloys was developed and led to a new Sn-added Al-Mg-Si alloy that shows natural aging stability of > 6 months for high solution treatment temperatures and a significant artificial aging potential. Further, combined Sn and indium (In) addition show comparable natural aging kinetics after quenching from different solution treatment temperatures.

A strong dependence of natural aging kinetics on the storage temperature was measured for various AA6061 alloys. For the Sn- and Sn+In-added alloys an additional contribution of a thermally activated vacancy release from Sn- and In-vacancy pairs is assumed. Applying this knowledge the developed alloy should show up to one month of stability for natural aging at 45 °C or ~7 years at 5 °C.

Based on an in-depth analysis of recent literature on natural aging in Al-Mg-Si alloys and its effect on artificial aging and the connections we have drawn, the picture about underlying mechanisms could be refined. With this background, the trapping of quenched-in excess vacancies by Sn and/or In could be interpreted to decrease the cluster number density during natural aging while increasing the cluster size. Also the effect of natural aging temperature and of prolonged natural aging (up to years) on artificial aging could be interpreted.

Furthermore, preliminary results about the influence of stretching and the quenching rate were discussed.

In this view, the project succeeded in the development of an alloy that shows maximum suppression of natural aging and simultaneous high artificial aging potential which may pave the way for a new class of Al-Mg-Si alloys with their own property profile.

Kontrollmechanismen der Kaltaushärtung in Al-Mg-Si-Legierungen und ihr Einfluss auf die Warmaushärtung mit und ohne Zugabe von Spurenelementen

Al-Mg-Si-Legierungen (6xxx Serie) sind die kommerziell wichtigste Gruppe aushärtbarer Aluminiumwerkstoffe. Der Wunsch die Kaltaushärtungskinetik kontrollieren zu können und eine Lösung für den negativen Effekt der Raumtemperaturlagerung auf die Warmauslagerung zu finden, welcher bereits 1939 entdeckt wurde, ist der Triebfaktor für Forschungsanstrengungen der aluminiumverarbeitenden Industrie. Basierend auf vorläufigen Ergebnissen einer vorangegangenen Studie waren die Hauptziele dieser Dissertation die „Minimierung der Kaltaushärtung" bei gleichzeitiger „Maximierung der Warmaushärtung" von Al-Mg-Si-Werkstoffen mit und ohne Zugaben von Spurenelementen in kommerziellen Legierungen.

Es wurde ein grundlegendes Verständnis erarbeitet, wie Sn-Zugaben zur Legierung AA6061 die Kaltauslagerung temporär unterdrücken und gleichzeitig die Warmaushärtungskinetik erhöhen. Die starke Sn-Leerstellen-Bindungsenergie resultiert in einer „Gefangennahme" der meisten eingeschreckten Überschussleerstellen in Sn-Leerstellenpaaren. Dies reduziert die Anzahl an freien Leerstellen, welche die Diffusionsprozesse anderer Legierungselemente wie Mg, Si oder Cu kontrollieren, was die Kaltaushärtung signifikant verzögert. Die maximale Verzögerung der Kaltauslagerung resultiert bei Sn-Gehalten an oder über der Löslichkeitsgrenze von ~100 at.ppm. Während die Unterdrückung der Kaltaushärtung vorherrscht, bewirkt die „Freilassung" von Leerstellen eine verstärkte Diffusion für die Ausscheidungsbildung der aushärtenden Phase bei höheren Temperaturen.

Es konnte gezeigt werden, dass der Effekt von Sn phänomenologisch mit dem positiven Effekt einer Kaltvorauslagerung bei Warmauslagerungstemperaturen von > 210 °C vergleichbar ist. Zusätzlich bewirkt eine Sn-Zugabe sowohl eine ungewöhnlich schnelle Warmauslagerungskinetik als auch hohe Maximalhärte. Dies rührt neben der Freilassung von Leerstellen von einem Beitrag diffundierender Sn-Leerstellenpaare während der Warmauslagerung und/oder einer Verzögerung der Annihilation von Überschussleerstellen durch Sn her.

Üblicherweise variieren Prozessparameter und Zusammensetzungslimits von Al-Mg-Si-Legierungen. Geringere Lösungsglühtemperaturen als 570 °C resultieren in einer abnehmenden Verzögerung der Kaltaushärtung, was mit einer Abnahme der maximal einschreckbaren gelösten Sn-Menge erklärbar ist. Thermodynamische Berechnungen konnten ebenfalls den Effekt und die Rolle von Mg, Si und Cu auf die Kaltauslagerungskinetik und in Clusterprozessen erklären. Ein erhöhter Si-Gehalt verkürzt die Verzögerungsdauer der Kaltaushärtung mit Sn. Dies wird damit erklärt, dass Si die Clusterbildung zu Beginn der Kaltaushärtung und deren Kinetik kontrolliert, während Si zusätzlich die gelöst einschreckbare Sn-Menge reduziert. Cu beeinflusst die Sn-Löslichkeit nicht, weswegen angenommen wird,

dass es einen ähnlichen, aber schwächeren Effekt als Sn zeigt. Mg hingegen verringert nur die gelöst einschreckbare Sn-Menge.

Für eine industrielle Umsetzung ist es wichtig zu wissen, ob im Labor hergestelltes Material mit industriell produzierten Feinblechen oder Platten vergleichbar ist. Dies konnte bestätigt werden wobei industriell produziertes Material nur eine etwas höhere Anfangshärte zeigte.

Schließlich wurde eine Designstrategie für eine lange Unterdrückung der Kaltaushärtung in Al-Mg-Si-Legierungen entwickelt, welche zu einem neuen Sn-legierten Al-Mg-Si-Werkstoff führte. Diese zeigt eine Kaltauslagerungsstabilität von > 6 Monaten für hohe Lösungsglüh-temperaturen und ein signifikantes Warmaushärtepotenzial. Kombinierte Sn- und In-Zugaben ergeben weiters vergleichbare Kaltauslagerungskinetik nach dem Abschrecken von verschiedenen Lösungsglühtemperaturen.

Eine starke Abhängigkeit der Kaltaushärtungskinetik von der Lagertemperatur wurde für verschiedene 6061-Werkstoffe festgestellt. Für die Sn- und Sn+In-legierten Materialien wird ein zusätzlicher Beitrag von einer thermisch aktivierten „Freilassung" von Leerstellen von Sn- und In-Leerstellenpaaren angenommen. Bei Anwendung dieses Wissens sollte die entwickelte Legierung bis zu einem Monat Stabilität bei 45 °C oder sogar ~7 Jahre bei 5 °C zeigen.

Basierend auf einer gründlichen Analyse von jüngster Literatur zur Kaltaushärtung in Al-Mg-Si-Legierungen und deren Effekt auf die Warmaushärtung, konnte durch das Erkennen neuer Zusammenhänge das Bild der zugrunde liegenden Mechanismen verfeinert werden. Mit diesem Wissen wurde für die „Blockierung" von eingeschreckten Überschussleerstellen durch Sn und/oder In interpretiert, dass sich die Clusterzahldichte während der Kaltauslagerung reduziert und gleichzeitig die Clustergröße erhöht. Weiters konnte der Effekt der Kaltauslagerungstemperatur und jener von langer Kaltaushärtung (bis zu Jahren) auf die Warmaushärtung interpretiert werden.

Abschließend kam es zur Diskussion der vorläufigen Ergebnisse über den Einfluss eines Reckprozesses und der Abschreckrate.

Zusammenfassend liegt der Erfolg dieser Arbeit in der Entwicklung einer Legierung, welche die Kaltaushärtung maximal verzögert und gleichzeitig ein hohes Warmaushärtungspotenzial zeigt. Dies könnte den Weg für eine neue Klasse von Al-Mg-Si-Werkstoffen mit einem eigenen Eigenschaftsprofil bereiten.

CONTENTS

1 INTRODUCTION

1.1   History and challenges of Al-Mg-Si alloys

Not long after Alfred Wilm accidentally discovered aging in an Al-Cu-Mg alloy in the 1900s [1], age-hardenable Al-Mg-Si alloys were developed in the 1920s by Robert S. Archer and Zay Jeffries as a new type of "High strength Aluminum Alloys" [2]. Today Al-Mg-Si alloys (6xxx series) in wrought, cast or extruded form represent the commercially most important group of age hardenable aluminum alloys [3,4]. They are widely used in the transport, shipbuilding, construction as well as aviation industry as rolled, extruded, forged and die-cast products [4–6]. In the automotive industry, for example, they are used as outer skin alloys, for inner parts, and structural or crash components with individual property criteria. 6xxx-series are especially attractive as they combine good formability with medium to high strength after age hardening, good corrosion resistance, and weldability [4–8]. In the last decade the interest in aluminum products in the transportation industry significantly increased as they allow lightweight construction for improved fuel efficiency and reduced CO_2-emissons. Especially automobile manufacturers have to increase the percentage of lightweight components until the year 2030 from 30% to 70% to compensate for the vehicle weight increase caused by an electric drive and fuel-efficient engine technology [9].

1.1.1 Industrial impact of natural aging

As schematically shown in Figure 1.1, natural aging is hardening at low temperatures (in this work defined as < 80 °C) attributed to solute clustering of Mg and Si atoms [11–15] and is characterized by a continuous increase in hardness which persists for years; at room temperature even hundreds of years are possible [10]. In this context directly after quenching from solution treatment treatments of 500-580 °C [6,11,12], an industrial alloy never stops hardening until the artificial aging treatment at typically 150-190 °C [6]. Artificial aging is typically performed after ~30 min for extruded products [13], after days for plates or even months for sheet products [7].

In this thesis special focus has been laid on the impact of natural aging on the processing of semi-finished sheets and plates, which are products delivered by the industrial partner of this thesis – AMAG rolling. After extensive scientific investigations in the 1960s and 1970s, only in the last decade aluminum producing companies started to systematically investigate the mechanisms underlying natural aging intensively [12]. The reason for this is that natural aging hardening not only reduces the formability of semi-finished products, it also shows a major negative effect on subsequent artificial aging (Figure 1.1). This phenomenon which has been revealed by Brenner and Kostron [13] in 1939, retards artificial aging kinetics and lowers the achievable strength compared to material directly aged after the solution heat treatment

[11,12,14–17]. Yet, for numerous products an intermediate storage at room temperature is unavoidable and thus the negative effect additionally results in reduced energy efficiency, production capacity and profitability. But the ever-growing demand to increase formability and strength for more complex parts of lower weight drives the alloy development e.g. in the transportation industry considerably [7,8,18,19].
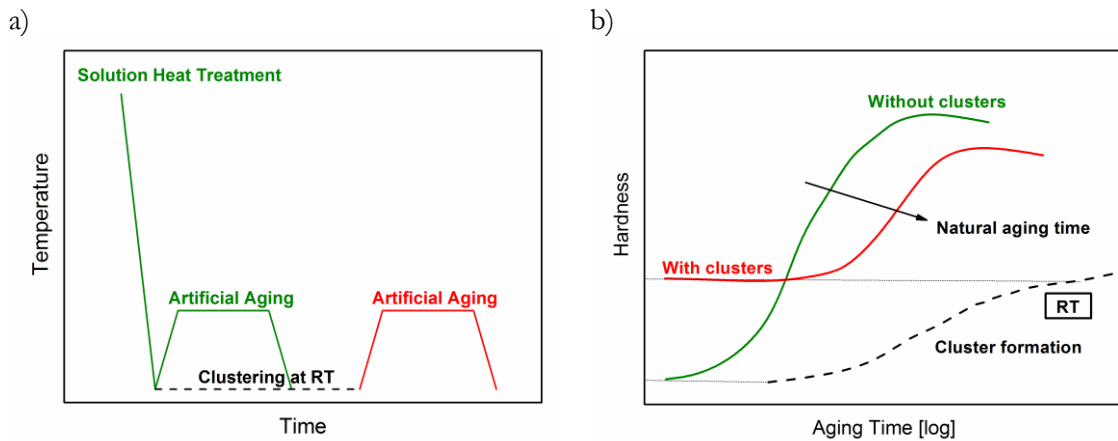
Figure 1.1. Schematic representation of natural aging and the negative effect of room temperature (RT) storage after a solution heat treatment on subsequent artificial aging kinetics and the reachable strength

1.2 Preceding studies on the effect of trace elements

To achieve the main objectives of this thesis, i.e. the minimization of natural aging and maximization of the artificial aging potential of Al-Mg-Si alloys, a fundamental knowledge of the compositional and processing parameters that influence natural aging kinetics with and without trace elements had to be acquired. In a preceding study conducted in the course of the present author's diploma thesis [20], the major impact of trace element additions on natural aging and subsequent artificial aging kinetics has been found. Sn addition in laboratory scale achieved to suppress natural aging for up to 2 weeks while accelerating the subsequent artificial aging kinetics significantly compared to a Sn-free reference alloy. In this view, the project aimed at a sustainable alloy development for industrial application with the simultaneous aim to significantly improve the current understanding of underlying mechanisms.

The approach of the preceding study [20] was based on the model of the "vacancy prison mechanism" formulated by Pogatscher et al. in 2011 [16]. According to this model, interactions of the main alloying elements Si and Mg with quenched-in excess vacancies are responsible for the negative effect of natural aging on artificial aging. The idea was to (i) find another proof that natural aging clusters trap vacancies and act as vacancy prisons during artificial aging and

(ii) if possible, suppress or modify cluster formation during room temperature storage with trace element additions.

Selected trace elements (Li, Ca, Sr, Ba, Ag, In, Ge, Sn, Sb, Pb and Bi) were added to the industrial important alloy AA6061, see Figure 1.2. The diffusion of all these trace elements in aluminum is believed to be dominated by solute-vacancy interchanges [21], but only Sn, In and Cd were able to temporarily suppress natural aging. The low effect of e.g. Sb, Pb, Bi, Ca and Sr could be interpreted with the insolubility in the alloy AA6061 (< 0 at.ppm, Sr ~ 2 at.ppm) as calculated with thermodynamic calculations based on the CALPHAD approach. The positive effect of trace elements such as Sn and In on temporary suppression of natural aging, however, is known for Al-Cu alloys [22,23], but before not many investigations existed for Al-Mg-Si alloys. Further tests showed that trace Sn or In additions not only significantly retard natural aging kinetics, but also improve artificial aging kinetics and increase the achievable peak hardness values as long as artificial aging starts before the onset of hardening during natural aging.
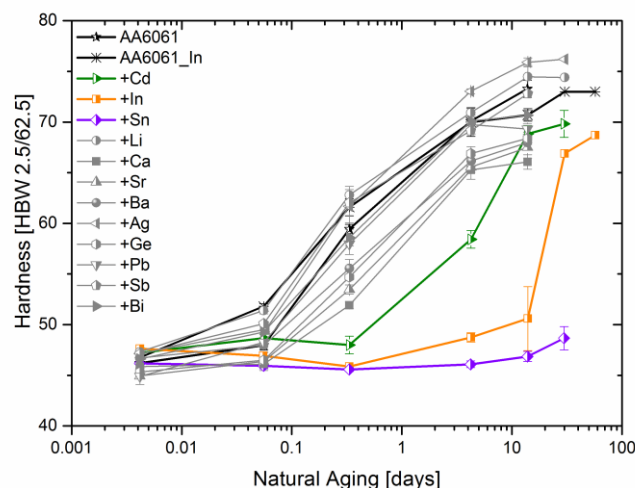
Figure 1.2. Natural aging of the alloy AA6061 with and without trace element addition tested in ref. [20]

For more detailed investigations four Sn-added and a nearly Sn-free reference alloy were produced in laboratory scale. Sn was chosen as it showed best preliminary results (Figure 1.2) and the potential of a cost-efficient industrial implementation due to moderate production costs for alloying ~0.04 wt.% Sn, whereas also Sn-containing scrap alloys may be usable. The ~200 and ~430 at.ppm Sn-added alloys both suppressed natural aging for > 14 days and showed comparable natural aging and artificial aging kinetics during subsequent artificial aging at 170 °C and 250 °C, see Figure 1.3. With this approach and in combination with APT investigations, performed at the ETH Zurich, the maximum Sn solubility at the solution treatment temperature of 570 °C could be estimated with ~100 at. ppm.

a)

b)
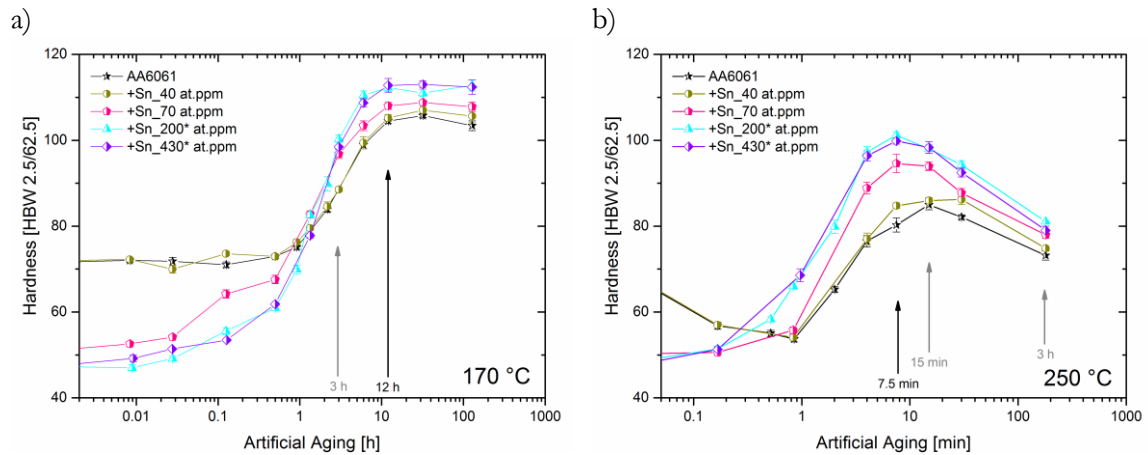
Figure 1.3. Artificial aging kinetics at a) 170 °C and b) 250 °C of Sn-added AA6061 alloys and a nearly Sn-free reference alloy after 14 days natural pre-aging at 25 °C tested in ref [20]

The temporary suppression of natural aging with trace Sn addition could be explained with the formation of Sn-vacancy complexes instead of clusters due to (i) high Sn-vacancy correlation and Sn-vacancy binding energy (~0.26 eV) [21] and (ii) a sufficient solubility of Sn in the fcc aluminum matrix.

1.3 Influences on natural aging

Based on background information about scientific achievements in investigating natural aging, partly also from this thesis, the industrial processing parameters of wrought sheets and plates which influence natural aging are discussed in more detail.

1.3.1 Scientific achievements in investigating natural aging

As wrought Al-Mg-Si alloys normally contain less than 1.5 wt.% of Mg plus Si, direct microstructural observations of natural aging clustering are challenging and higher resolution characterization methods are required. Atom probe tomography (APT) is the only method that is able to visualize natural aging clusters [12,24] whereas the earliest known experiments only start ~100 min after quenching from solution heat treatment [25]. During these 100 min most pure and commercial alloys are already significantly naturally aged as the start of natural aging ranges from several minutes to about one hour depending on the Mg, Si and Cu content [26,27] and, in commercial alloys, on additional alloying elements and impurities [3]. Moreover, for the visualization of natural aging clusters which consist of just a few atoms the APT technique operates at its limit due to limited detection efficiencies and restrictions of cluster search algorithms available today [12]. Also high resolution scanning transmission electron

microscopy (HRSTEM) studies as the most promising TEM method were not able to resolve natural aging clusters up to now. Other typical measurements techniques such as X-ray small angle scattering or small-angle neutron scattering (SANS) also only provide weak contrast as Mg and Si neighbor Al in the periodic table, thus X-rays are diffracted comparably due to the similar electron density and the scattering lengths of SANS are similar [12].

Hence, for the investigation of the earliest natural aging processes, which are most decisive for the latter property development of an individual alloy, only indirect techniques are available such as hardness, electrical resistivity, positron annihilation, differential scanning calorimetry (DSC) [3,12] and, more exotic, the muon spin relaxation technique [28] or, more recently, time dependent magnetization [29]. Yet, a combined approach of various techniques can contribute significantly to the understanding of mechanistic processes underlying natural aging.

Such investigations by Banhart et al. [3,12] revealed five distinct temporal stages of clustering that are associated with a characteristic behavior of positron lifetime, hardness, electrical resistivity, differential scanning calorimetry (DSC) with times that coincide for many of these measurements. Although numerous further important publications by their group in the last few years [30–38] were able to further specify their interpretations about processes in individual clustering stages and the dependency on e.g. the natural aging temperature or the Mg/Si ratio of the alloy, no complete picture could be derived up to today. In short as schematically shown in Figure 1.4, it is believed that quenched-in excess structural vacancies and solute-vacancy complexes dominate in the first minutes after quenching (stages 0 and I). The following stage II is dominated by Si-related clustering followed, around the transition to stage III, by Mg addition to pre-existing clusters. For the last stage, stage IV, a coarsening or ordering and zone formation of clusters were proposed as possible mechanisms. By investigating the effect of natural aging on subsequent artificial aging at unconventionally high temperatures of ≥ 200 °C with hardness, electrical resistivity and APT, Pogatscher et al. [16] concluded that Mg,Si co-clusters contain quenched-in excess vacancies and thus act as "vacancy prisons" during artificial aging. Figure 1.4 also includes a preview of interpretations derived in this thesis.
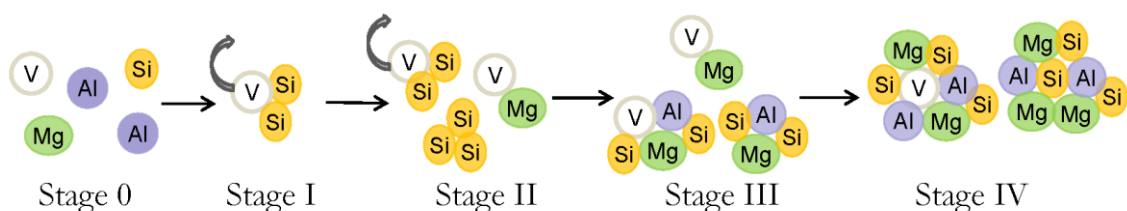
Figure 1.4. Schematic representation of processes that take place during the five stages of natural aging clustering introduced by Banhart et al. [3,12] including a preview of interpretations derived in this thesis

An in-depth analysis of recent literature and therefrom generated new cross-links in combination with our interpretation of the effect of trace elements and solute-vacancy

interactions on natural aging hardening and kinetics enabled us to understand our results and to derive a more complete picture of the mechanisms controlling natural aging and its influence on artificial aging.

1.3.2 Industrial processing parameters influencing natural aging

The duration of each clustering stage (Figure 1.4) is not fixed and thus natural aging kinetics of commercial Al-Mg-Si alloys depends on the chemical composition, the heat treatment history, and on trace elements [27]. In the following the industrial processing parameters which influence natural aging of Al-Mg-Si products are discussed. Note that some experimental results obtained in this thesis are already anticipated to better understand the importance of individual processing parameters for this thesis.

Process chain of sheets

Figure 1.5 illustrates the processing of Al-Mg-Si alloys for automotive outer skin applications. After the production of Al-Mg-Si ingots, the in-house processing of sheets covers, in this order: hot rolling and cold rolling followed by a solution heat treatment between 500 °C and 580 °C on a continuous annealing line and immediate pre-aging. After the pre-aging treatment, the coil is packaged and delivered to the customer where the sheet is formed and finally artificially aged during the paint bake process at ~150-220 °C for ~20-30 min. Yet, for a sheet material that has undergone room temperature storage for up to months ~20-30 min are much too short to reach "T6 strength" (peak aged condition), which would require ~5-7 h at e.g. 180 °C [6].

DC Cast　Preheat　　　Hot Roll　　　Cold Roll　　Solutionize

Pre-age　　Cut & Package　　　Form　　Age / Paint Bake
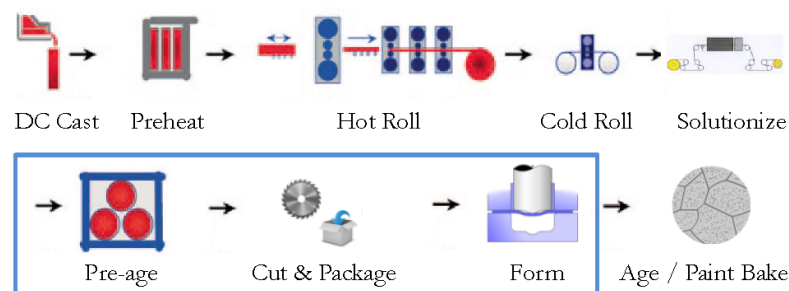
Figure 1.5. Processing of Al-Mg-Si alloys for auto body sheet purposes. Partly reproduced from ref. [6]

Pre-aging treatments that are performed immediately after quenching for several hours around 100 °C have been developed to improve the artificial aging performance and to achieve a relatively "stable" material state [39–44]. Pre-aging treatments, however, result in undesired hardness increase [43] and are often only with difficulty able to preserve the desired formability needed by the customer due to additional natural aging at room temperature. Still, OEMs in the

automotive industry require at least 6 months of stable formability and even an increase in the overall formability and strength for more complex parts of lower weight. Hence, currently frequently used sheet alloys for automotive outer skin applications like AA6016, which has also been investigated in this thesis, might soon not be able to fulfill the requirements any more.

Therefore it would be a milestone in the history of 6xxx sheet alloys if an alloy could be developed that (i) saves the pre-aging step, (ii) preserves the as-quenched soft hardness after the solution heat treatments for > 6 months and (iii) shows a significant artificial aging potential with (iv) a cost-efficient modification of the alloy composition.

Process chain of plates

Al-Mg-Si plates are mainly used as semi-finished products for milling operations in the engineering and transportation industry and have many applications in electronics and the semiconductor industry. A frequently used alloy is AA6061. After the production of Al-Mg-Si ingots, the processing of plates covers, in this order: the homogenization treatment of the milled ingots between 500 °C and 580 °C, hot rolling and cooling to room temperature, a solution heat treatment between 500 °C and 580 °C for 10 to 60 min to obtain a homogeneous solid solution, water-quenching to room temperature, stretching between 1.5 and 3% plastic deformation to reduce internal stresses caused by the quenching procedure and artificial aging for more than 24 h at 150 °C to 190 °C to reach T6 strength.

Due to logistic reasons the storage period between the solution heat treatment and artificial aging lasts between several days to sometimes weeks. Thus for the processing of plates, natural aging mainly affects the in-house artificial aging treatment by increasing the time to reach T6 strength by a factor of 10 compared to direct artificial aging and by the decrease in the reachable T6 strength. By a closer investigation these are rather qualitative statements as the individual final product profile after artificial aging depends on several parameters, which have also been investigated in this thesis.

Influence of Mg, Si, Cu and trace element content

The alloy composition with regard to the Mg, Si and Cu content distinctly determines natural aging kinetics and the amount of natural aging hardening. Recent literature [26,37] and investigations performed in the course of this thesis show that an increasing Si content significantly increases natural aging kinetics straight after quenching from solution heat treatment and also the amount of hardness increase, compare Figure 1.6. Our results support the theory that Mg does not take part in early stage clustering [3,12,25,35,36,45], which explains why increasing Mg content, in contrast to Si, only increases natural aging kinetics of the later stages III and IV (see Figure 1.6). Rich alloys (Mg+Si ≥ 0.8 at.%, Mg and Si ≥ 0.4 at.%) with a Mg/Si ratio of ~1-1.5 show fastest natural aging kinetics [26].
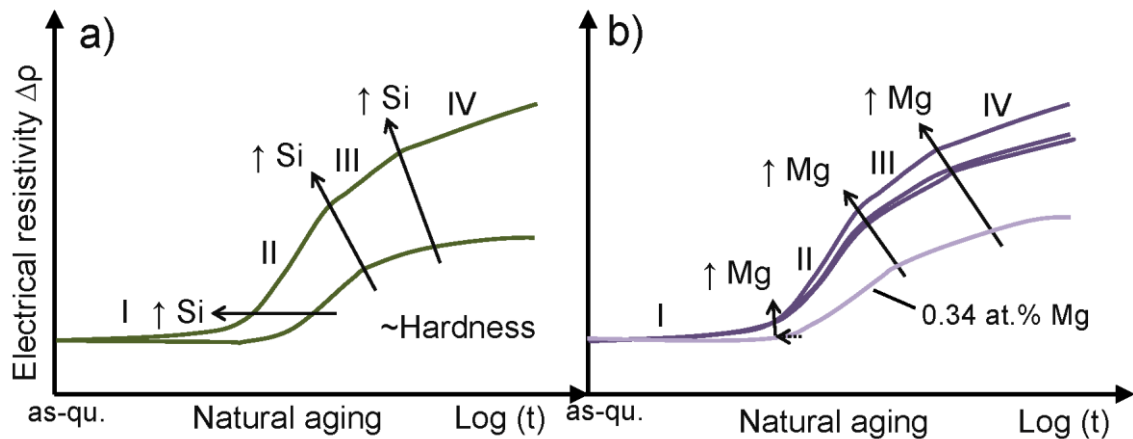
Figure 1.6. Schematic dependence of natural aging kinetics on a) Si content and b) Mg content. With increasing Si content all transition times between clustering stages occur earlier, with increasing Mg content stage I-II transition times are similar (except for very lean alloys) [46]. Reproduced from ref. [26]

As shown in Figure 1.7 Cu addition slightly reduces early stage hardening kinetics whereas in the later stages III and IV hardness increases more than in Cu-free alloys [27,47]. First, this information is valuable as for an alloy development which aims at the maximum suppression of natural aging the influence of the Si, Mg and Cu content can be exploited to maximize the trace element effect. Secondly, an industrial alloy production process always needs the definition of compositional limits to achieve the desired alloy properties. These compositional limits are mostly smaller than the compositional limits of standard alloys. Thirdly, the precondition to achieve the maximum trace element effect is to quench in the maximum concentration of dissolved Sn atoms. We found that Mg and Si addition reduce the maximum quenchable Sn solubility at solution treatment temperature which is just ~100-150 at.ppm or ~0.04-0.06 wt.%. This is especially critical in the case of Si addition as Si dominates early stage clustering (Figure 1.4).
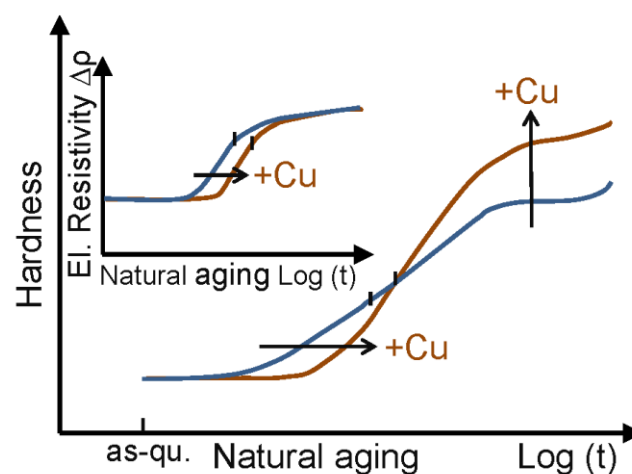
Figure 1.7. Comparison of hardness and electrical resistivity change $\Delta\varrho$ for the influence of Cu addition on natural aging kinetics [46]. Reproduced from ref. [26]

Influence of solution treatment temperature

For the commercial alloys AA6016 and AA6061 investigated in this thesis, solution treatment temperatures above ~530 °C followed by water-quenching only negligibly influence natural aging kinetics. This can be explained by equilibrium thermodynamic calculations which show that the Mg and Si solubility above ~530 °C varies negligible.

For the Sn-added Mg-rich alloy AA6061 it was found early in this thesis that a decrease of the solution treatment temperature below 570 °C strongly reduces the suppressive effect of Sn on natural aging. The reason is a decrease of the maximum quenchable Sn solubility due to the formation or pre-existence of the equilibrium phase Mg_2X, X stands for Sn and Si, at temperatures up to ~560 °C.

Influence of natural aging temperature

Between individual processing steps after the solution heat treatment, sheet and plate products are often opposed to or stored at room temperature. Storage rooms or transport vehicles are often not air-conditioned so that ambient or material temperatures in the winter season can temporarily reach ~5 °C and in the summer season ~45 °C are possible. It is known from literature that with decreasing temperature (< 80 °C) natural aging kinetics of Al-Mg-Si alloys is reduced, i.e. hardening starts retarded [10,48]. For prolonged natural aging in stage IV (Figure 1.4), the long-term hardness of rich alloys with a high Mg+Si content increases with rising temperature whereas for lean alloys hardness decreases [48]. Thus in industrial practice an increasing natural aging temperature and prolonged natural aging reduce the formability of the commercially more important rich alloys and can significantly influence the artificial aging behavior. Both phenomena have been observed and analyzed for the commercial alloy AA6061 investigated in this thesis with and without trace Sn or Sn+In addition. For the alloy development with trace Sn addition this means that the reachable suppression of natural aging and the achievable artificial aging behavior strongly depend on the storage temperature.

Influence of stretching and pre-straining

The time and amount of a plastic deformation applied during industrial processing also influences natural aging kinetics, the long-term hardness and formability of 6xxx series alloys as well as the artificial aging behavior [44,49,50]. For example pre-straining before a pre-aging treatment accelerates artificial aging kinetics according to DSC measurements, whereas pre-straining after pre-aging destabilizes the structure created by pre-aging and therefore has a negative effect on subsequent artificial aging [44].

Influence of quenching rate

High strength 6xxx alloys such as AA6061 or AA6082 show a higher quench sensitivity than medium and low strength alloys such as AA6016 or AA6060 because they contain Mn and/or Cr which form Al(MnFeCr)Si dispersoids [6,13]. Dispersoids contribute to a more homogenous slip behavior of artificially aged products and hamper recrystallization and grain growth during processing or thermal treatment of plates or extruded products. With regard to natural and artificial aging kinetics, Mn and Cr containing alloys require a high quenching rate from solution treatment temperature to avoid the heterogeneous precipitation of super-saturated Si or Mg atoms, i.e. Mg-Si phases, on dispersoids during cooling [6]. For insufficient quenching rates dispersoids additionally bind super-saturated Si which is no longer available during an artificial aging treatment [6] or for natural aging. Thus the reachable strength and hardness of 6xxx alloys containing dispersoids strongly depends on the quenching rate [13].

1.3.3 Negative Effect: dependency on processing parameters

It should be noted that the negative effect of natural aging on artificial aging which reduces the achievable artificial kinetics and strength is only observed in alloys with a total content of Mg+Si > 1 wt.% [21,33,51], whereas commercially less relevant alloys with less than 1 wt.% Mg+Si content show a higher reachable strength than without natural aging [41,52,53]. The severity of the negative effect depends on the composition of pre-formed clusters or phases [21,33].

Influence of Mg and Si content and Mg/Si ratio

Whereas Mg/Si ratios of natural aging clusters resemble the alloy composition [17,25], positive pre-aging clusters which form at $\geq$ 80 °C favor Mg/Si-ratios of ~1 similar to artificial aging precipitates with a composition close to $(Al+Mg)_5Si_6$ [51,52] for the peak hardening phase β´´ [25]. The reason is that due to the limited atomic mobility at low-temperature aging only agglomerated clusters can form [17]. Therefore it is accepted in literature that from metastable natural aging clusters with compositions that differ significantly from a Mg/Si ratio of 1, more stable artificial aging precipitates form with difficulty [17,25].

It has been found that the severity of the negative effect depends not only on the composition of pre-formed clusters or phases [17,53], i.e. for natural aging the Mg/Si ratio of the alloy, but also on the duration of natural aging before artificial aging, i.e. the clustering stage (Figures 1.4 and 1.6). Si-rich clusters which form in Si-rich alloys or are present during early stage aging in every alloy type (see stage II in Figure 1.4), first need to dissolve or change chemistry to a Mg/Si ratio of $\geq$ 1 with Mg enrichment before a structural change and synchronous growth into elongated precipitates during artificial aging [25,52]. As for Si-rich alloys this behavior

persists up to long-term natural pre-aging in stage IV, no coarsening of the artificial aging microstructure in TEM is observed accompanied by a relative low decrease in the reachable artificial aging peak hardness, see Figure 1.8 [53]. This is in contrast to the Mg/Si ratio 1 and Mg-rich alloys investigated in ref. [53]. Until the end of clustering stage III after ~1 week natural aging, the Mg/Si ratio ~1 alloy reaches the highest and the Mg-rich alloy medium artificial aging peak hardness followed by a significant hardness decrease for longer natural aging times in stage IV. The hardness decrease is attributed to a coarsening of the artificial aging microstructure due to preferential growth of few stable natural aging clusters, while slowly re-precipitated solutes produce small precipitates [53].
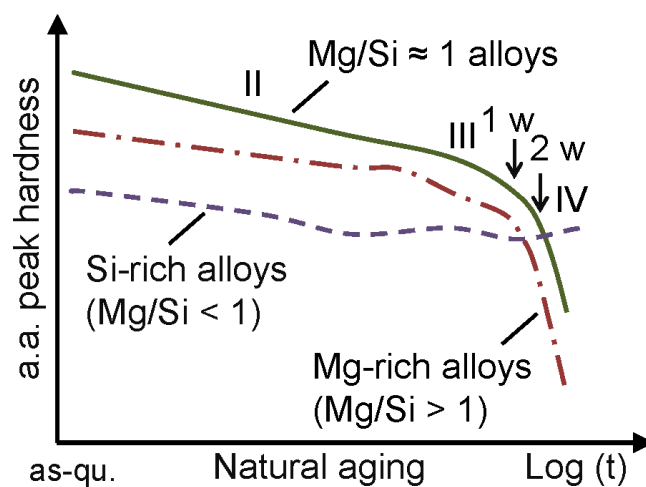
Figure 1.8. Schematic evolution of the reachable artificial aging (a.a.) peak hardness after increasing natural aging time for Mg-rich, Si-rich and Mg/Si ratio 1 alloys [46]. Reproduced from ref. [53]

For the industrial processing of Mg-rich and Mg/Si ≈ 1 alloys this means that the achievable artificial aging peak hardness strongly depends on the duration of the room temperature storage before the heat treatment.

Influence of artificial aging temperature

Recently, the origin of the negative effect on artificial aging has been linked to the clustering processes at room temperature. Pogatscher et al. [16] found that during artificial aging at conventional, low artificial aging temperatures (i.e. 170 °C-200 °C), clusters of Mg and Si atoms act as relative stable vacancy prisons for quenched-in vacancies which results in a reduced contribution of quenched-in excess vacancies to diffusion during the nucleation of the major hardening phase β´´. The "vacancy prison mechanism" is the only model that can explain why faster cluster dissolution with a simultaneous vacancy release at high aging temperatures (> 200 °C-250 °C) results in faster artificial aging kinetics than direct artificial aging.

1.4 Approach

Summing up, the wish to control natural aging kinetics and to find a solution to the negative effect of room temperature storage on artificial aging is of major importance for the aluminum manufacturing industry. The main objectives of this thesis thus were (i) the minimization of natural aging and (ii) maximization of the artificial aging potential of Al-Mg-Si alloys and (iii) to simultaneously acquire a fundamental knowledge of the compositional and processing parameters that influence natural aging kinetics with and without trace element additions to commercial Al-Mg-Si alloys. Because after the preceding study [20], which reached first promising results in laboratory scale, a significant gap of knowledge remained for the planned transfer of the trace element effect to industrial scale production and how the ultimate goal of a suppression of natural aging for > 6 months could be achieved for automotive application.

Yet, many experimental investigations are not restricted to industrially common processing parameters. Therefore also experiments which are not straight forward can result in unexpected results and from a scientific point of view deepen the understanding of underlying mechanisms. From a commercial point of view, this understanding can be used to develop new products with a maybe totally new property profile.

In general, the following fundamental issues have been dealt with in this thesis:

- Influence of processing parameters and history on natural aging kinetics with and without trace element addition

- Compositional limits for a maximum suppression of natural aging

- Investigation of the effect of combined trace element addition (Sn+In)

- Development of a theoretical model that explains the trace element effect of Sn and/or In during natural aging based on existent and refined clustering theories

- Closer interpretation of the trace element effect at conventional artificial aging temperatures (≤ 200 °C)

- Analysis and interpretation of microstructural processes at unconventionally high artificial aging temperatures (210 °C-250 °C) with and without trace Sn addition for direct aging compared to the naturally pre-aged case

- Influence of prolonged natural aging (up to years) on the negative effect of Al-Mg-Si alloys with and without trace elements

In the end, for the investigation and manipulation of natural aging clustering processes and artificial aging, only an experimental approach combined with theoretical models and a critical literature review were able to push the understanding of underlying mechanisms. In the course of this PhD thesis 33 alloys with either different composition or production history were produced and investigated. With this background the main results were obtained by hardness measurements which monitored natural aging kinetics for sometimes up to 2 years and/or which followed complex heat treatments. The interpretation of results was assisted by thermodynamic calculations based on the CALPHAD approach (software FactSage™ [54,55]), which provided equilibrium data of phases and their stabilities, compositions and element solubility. Further, the thermokinetic software package MatCalc [56,57] provided data about e.g. the evolution of the excess-vacancy concentration during artificial aging. With the help of a thermodynamic model and first-principles computations of Sn-vacancy binding the mechanism controlling aging could be supposed. For specific questions differential scanning calorimetry (DSC), atom probe tomography (APT) and scanning transmission electron microscopy (STEM) measurements were performed.

Finally, the generated data and knowledge are expected also to be helpful for computer-aided predictions and thermokinetic simulations of natural aging and artificial aging processes and microstructure, and ultimately for a sustainable alloy development in future.

References

[1]   Wilm A. Metallurgie: Zeitschrift für die gesamte Hüttenkunde 1911; 8:225–7.

[2]   Archer RS, Jeffries Z. Transactions; 1925:828–45.

[3]   Banhart J, Lay M, Chang C, Hill A. Physical Review B 2011; 83:14101.

[4]   Kammer C. Aluminium-Taschenbuch. 16th ed. Düsseldorf: Aluminium-Verl; 2002.

[5]   Polmear IJ. Light alloys: From traditional alloys to nanocrystals. 4th ed. Oxford, Burlington, MA: Elsevier/Butterworth-Heinemann; 2006.

[6]   Ostermann F. Anwendungstechnologie Aluminium. 3rd ed. Berlin, Heidelberg: Springer Berlin Heidelberg; 2014.

[7]   Prillhofer R, Rank G, Berneder J, Antrekowitsch H, Uggowitzer PJ, Pogatscher S. Materials 2014; 7:5047–68.

[8]   Hirsch J. Transactions of Nonferrous Metals Society of China (English Edition) 2014; 24:1995–2002.

[9]   Prillhofer R. Information AMAG Rolling. accessed on January 15 2016.

[10]   Panseri C, Federighi T. Journal of the Institute of Metals 1966; 94:99–105.

[11]   Kovaćs I, Lendvai J, Nagy E. Acta Metallurgica 1972; 20:975–83.

[12]   Banhart J, Chang C, Liang Z, Wanderka N, Lay M, Hill A. Advanced Engineering Materials 2010; 12:559–71.

[13]   Strobel K, Lay M, Easton MA, Sweet L, Zhu S, Parson NC, Hill AJ. Materials Characterization 2016; 111:43–52.

[14]   Ried A, Schwellinger P, Bichsel H. Aluminium 1977; 53:595–9.

[15]   Brenner, P., Kostron, H. Zeitschrift für Metallkunde 1939; 4:89–97.

[16]   Pogatscher S, Antrekowitsch H, Leitner H, Ebner T, Uggowitzer P. Acta Materialia 2011; 59:3352–63.

[17]   Torsaeter M, Hasting H, Lefebvre W, Marioara C, Walmsley J, Andersen S, Holmestad R. Journal of Applied Physics 2010; 108:073527-1 - 073527-9.

[18]   Hirsch J. Materials Transactions 2011; 52:818–24.

[19]   Hirsch J. Materials Forum 2004; 28:15–23.

[20]   Werinos M. Influence of microalloying elements on the precipitation behavior of Al-Mg-Si alloys. Diploma thesis; 2012.

[21]   Simonovic D, Sluiter M. Physical Review B - Condensed Matter and Materials Physics 2009; 79.

[22]   Hardy HK. Journal of the Institute of Metals 1950; 78:169.

[23]   Wolverton C. Acta Materialia 2007; 55:5867–72.

[24]   Lay M, Zurob HS, Hutchinson CR, Bastow TJ, Hill AJ. Metallurgical and Materials Transactions A: Physical Metallurgy and Materials Science 2012; 43:4507–13.

[25]   Zandbergen MW, Xu Q, Cerezo A, Smith G. Acta Materialia 2015; 101:136–48.

[26]   Kim S, Kim J, Tezuka H, Kobayashi E, Sato T. Materials Transactions 2013; 54:297–303.

[27]   Kim J, Kobayashi E, Sato T. Materials Transactions 2015; 56:1771–80.

[28]   Nishimura K, Matsuda K, Komaki R, Nunomra N, Wenner S, Holmestad R, Matsuzaki T et al. Archives of Metallurgy and Materials 2015; 60:925–9.

[29]   Nishimura K, Matsuda K, Namiki T, Nunomra N, Matsuzaki T, Hutchison W. Materials Transactions 2015; 56:1307–9.

[30]   Liu M, Čížek J, Chang C, Banhart J. Acta Materialia 2015; 91:355–64.

[31]   Liang Zd, Chang C, Abromeit C, Banhart Jb, Hirschc J. International Journal of Materials Research 2012; 103:980–6.

[32]   Liu M, Čížek J, Chang C, Banhart J. Materials Science Forum 2014; 794-796:33–8.

[33]   Liu M. Clustering Kinetics in Al-Mg-Si Alloys Investigated by Positron Annihilation Techniques. PhD thesis. Berlin; 2014.

[34]   Liang Z. Clustering and Precipitation in Al-Mg-Si Alloys. PhD thesis. Berlin; 2012.

[35] Chang C, Liang Z, Schmidt E, Banhart J. International Journal of Materials Research 2012; 103:955–61.

[36] Chang C, Banhart J. Metallurgical and Materials Transactions A: Physical Metallurgy and Materials Science 2011; 42:1960–4.

[37] Liang Z, Chang C., Wanderka N., Banhart J., Hirsch J. The Effect of Fe, Mn and Trace Elements on Precipitation in Al-Mg-Si Alloy, in: Proceedings of the 12th International Conference on Aluminium Alloys. p. 492–497.

[38] Liang Z, Chang C, Banhart J, Hirsch J. The effect of Cu and Cr on clustering and precipitation in Al–Mg–Si alloys., in: ICAA13: 13th International Conference on Aluminum Alloys: John Wiley & Sons, Inc; 2012. p. 1125–1130.

[39] Miao W, Laughlin D. Journal of Materials Science Letters 2000; 19:201–3.

[40] Shen C. Journal of Materials Science and Technology 2011; 27:205–12.

[41] Cao L, Rometsch PA, Zhong H, Muddle BC. Materials Science Forum 2010; 654-656:918–21.

[42] Abouarkoub A, Thompson GE, Zhou X, Hashimoto T, Scamans G. Metallurgical and Materials Transactions A 2015:1–14.

[43] Birol Y. Materials Science and Engineering A 2005; 391:175–80.

[44] Yan Y, Liang ZQ, Banhart J. Materials Science Forum 2014; 794-796:903–8.

[45] Fallah V, Langelier B, Ofori-Opoku N, Raeisinia B, Provatas N, Esmaeili S. Acta Materialia 2016; 103:290–300.

[46] Werinos M, Antrekowitsch H, Uggowitzer P, Pogatscher S. Hardening of Al-Mg-Si alloys: Effect of trace elements and prolonged natural aging; submitted to Current Opinion in Solid State & Materials Science.

[47] Zandbergen MW, Cerezo A, Smith G. Acta Materialia 2015; 101:149–58.

[48] Røyset J, Stene T, Saeter JA, Reiso O. Materials Science Forum 2006; 519-521:239–44.

[49] Yan Y. Investigation of the negative and positive effects of natural aging on artificial aging response in Al-Mg-Si alloys; 2014.

[50] Birol Y, Karlik M. Scripta Materialia 2006; 55:625–8.

[51] Zandbergen H, Andersen S, Jansen J. Science 1997; 277:1221–5.

[52] Chen JH, Costan E, van Huis MA, Xu Q, Zandbergen HW. Science 2006; 312:416–9.

[53] Tao GH, Liu CH, Chen J, Lai YX, Ma PP, Liu LM. Materials Science and Engineering A 2015; 642:241–8.

[54] Bale C, Chartrand P, Degterov S, Eriksson G, Hack K, Ben Mahfoud R, Melançon J et al. Calphad: Computer Coupling of Phase Diagrams and Thermochemistry 2002; 26:189–228.

[55] Bale C, Bélisle E, Chartrand P, Decterov S, Eriksson G, Hack K, Jung I et al. Calphad: Computer Coupling of Phase Diagrams and Thermochemistry 2009; 33:295–311.

[56] Svoboda J, Fischer FD, Fratzl P, Kozeschnik E. Materials Science and Engineering A 2004; 385:166–74.

[57] Kozeschnik E, Svoboda J, Fratzl P, Fischer FD. Materials Science and Engineering A 2004; 385:157–65.

2   DIFFUSION ON DEMAND

The investigations presented in this chapter explore the question how trace Sn additions to the alloy AA6061 are able to suppress natural aging for up to weeks with a simultaneous enhancement of artificial aging kinetics. It shows that for Sn addition above the solubility limit of ~100 at.ppm the retardation of hardening saturates. Supported by a thermodynamic model and first-principles computations of Sn-vacancy binding a mechanism controlling the aging is supposed. The trapping of vacancies in predominantly Sn-vacancy pairs suppresses room temperature aging and the vacancy release at elevated temperatures results in diffusion on demand for precipitation processes and thus solves the problem of the negative effect in Al-Mg-Si alloys.

Diffusion on Demand to Control Precipitation Aging:
Application to Al-Mg-Si Alloys[*]

We demonstrate experimentally that part-per-million addition of Sn solutes in Al-Mg-Si alloys can inhibit natural aging and enhance artificial aging. The mechanism controlling the aging is argued to be vacancy diffusion, with solutes trapping vacancies at low temperature and releasing them at elevated temperature, which is supported by a thermodynamic model and first-principals computations of Sn-vacancy binding. This "diffusion on demand" solves the long-standing problem of detrimental natural aging in Al-Mg-Si alloys, which is of great scientific and industrial importance. Moreover, the mechanism of controlled buffering and release of excess vacancies is generally applicable to modulate diffusion in other metallic systems.

2.1   Main Part

Al-Mg-Si alloys are the most widely used age-hardenable aluminium alloys, with industrial applications in lightweight construction, automotive, aircraft, and architecture [1]. The preferential heat treatment for hardening is artificial aging via baking at ~430 - 460 K after quenching from ~800 K. However, detrimental natural aging appears within minutes of RT storage after quenching [2, 3] making it unavoidable since there are logistical, technological and physical time-constraints in commercial production. The effect retards artificial aging kinetics by an order of magnitude and reduces the achievable strength. Consequently, the material properties, scope of applications, and energy efficiency in the production of Al-Mg-Si alloys are impaired.

Discovered 75 years ago [4] just one year after the origin of age-hardening was explained [5, 6] many researchers have addressed this problem since [3, 7-12]. Nevertheless the mechanisms of natural aging in Al-Mg-Si alloys and their competition with artificial aging processes remain unsolved. Excess vacancies formed upon quenching are essential for fast artificial aging [10, 12] by governing the precipitation of the hardening phase β" [13]. However, such vacancies also allow sufficient diffusion at low temperatures to cause natural aging. Thus, eliminating the negative effect of natural aging is achievable in principle by preventing excess vacancy-mediated diffusion at RT and facilitating such diffusion during elevated temperature artificial aging. Here, we demonstrate that such diffusion on demand concept can be executed by adding

trace amounts of solutes with sufficient solubility in the aluminum matrix and optimal binding energy to vacancies.

A strong binding of vacancies to solutes [14] has previously been used to explain sluggish natural aging kinetics reported for Al-Cu alloys with additions of Sn [15]. But natural aging in Al-Cu is not deleterious and, more importantly, there has thus been no consideration of vacancy release during artificial aging – the key feature for solving the negative effect of natural aging in Al-Mg-Si alloys. For Al alloys containing Mg, it was also believed that the Sn solubility is insufficient for trapping vacancies, because of Mg_2Sn phase formation [16]. However, we are able to dissolve ~100 at. ppm (atomic parts per million) of Sn in the well-known alloy Al-Mg-Si alloy AA6061 [17] at a solution treatment temperature of 843 K (see Supplemental Material (SM)). Thus, as described below, control of diffusion by the buffering and releasing of vacancies during natural and artificial aging, respectively, is realizable for Al-Mg-Si alloys and solves the 75-years-old problem of natural aging in these alloys [4] with great economic consequences for their application as lightweight alloys.

Alloys were prepared by melting an industrial AA6061 alloy (Mg 0.90, Si 0.59, Cu 0.09, Fe 0.28, Cr 0.07, Mn 0.05, Zn 0.02 and Ti 0.05, all in at.%) and adding pure Sn (99.9 at.%). Argon gas purging was applied to reduce the hydrogen content before the alloys were cast to slabs (150×90×35 mm³). To check the chemical composition, optical emission spectrometry (SPECTROMAXx from SPECTRO) was applied during the alloying procedure and to the final plates using an appropriate calibration sample as standard. After cutting and homogenization (43.2×10³ s at 773 K and 43.2×10³ s at 843 K), hot rolling (823 K) from 20 to 4.2 mm thickness was conducted. Solution heat treatment was performed at 843 K for 1.2×10³ s. Subsequent quenching was carried out in water at RT and for natural aging samples were kept in a peltier-cooled incubator at RT. Artificial aging was carried out in an oil bath at 443 K. Brinell hardness measurements (HBW 2.5/62.5/15) were performed on polished samples (17×10×3.4 mm³) using an EMCO-Test M4 unit. Needle-shaped specimens for atom probe tomography [18, 19] (APT) were prepared via a standard two-step electropolishing method [20]. APT was performed on a LEAP™ 4000 X HR atom probe at a specimen temperature of 23.7 K with a pulse fraction of 20%, a pulse rate of 200 kHz and a detection rate of 1% under ultra-high vacuum (< 10^{-10} mbar). The software package IVAS 3.6.4™ from Cameca was used for the reconstruction procedure and analysis. For the calculations the Perdew-Wang-91 generalized gradient density functional theory (DFT) as implemented in VASP was used [21]. A Monkhorst-Pack k-mesh equivalent to 9×9×9 in the fcc-Al cell was used with a kinetic energy cut-off of 250 eV [22]. Energy barriers were calculated using the Nudged Elastic Band method [23]. Calculations were performed in 4×4×4 cubic unit cells at fixed volume, and energy

contributions due to any induced pressures were verified to be negligible. Relaxation calculations were converged to 10^{-4} eV and nudged elastic band to 0.1 eV/Å.

Figure 1 shows the effect of Sn on the evolution of hardness during RT storage after quenching from 843 K. Sn additions delay the observed hardening by orders of magnitude, from the time scale of 1 hour up to several weeks, depending on the Sn content. For attempted Sn additions above the solubility limit (~100 at. ppm, also indicated by Sn additions marked with an asterisk) the retardation of hardening saturates, consistent with the solubility limit for Sn in the alloy at 843 K.
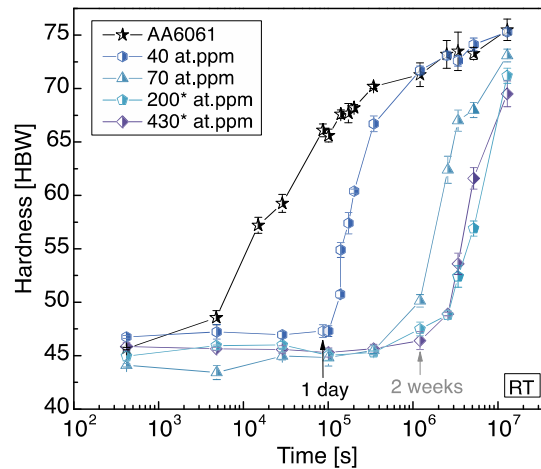
FIG 1. Evolution of hardness during RT storage after quenching for the Al-Mg-Si alloy AA6061 with and without Sn addition. The increase in hardness is retarded with increasing amount of Sn added. Sn additions above the solubility limit (~100 at. ppm) are marked with an asterisk.

Since natural aging in Al-Mg-Si alloys during RT storage has been explained by the clustering of Mg and Si [11], we attribute the retardation of hardening to the impeding of such cluster formation. Figure 2 shows a three-dimensional (3d) map of the positions of Mg, Si and Sn atoms in the alloy with an addition of 200* at. ppm Sn after two weeks of RT storage measured by APT (see SM for APT reconstruction details). A nearest-neighbor (NN) distribution analysis [24] shows no statistically significant difference between the measured distribution and a calculated random distribution of the solute elements. This indicates that no clusters of Mg and Si exist within the detection limit of a few atoms, which agrees well with the hardness data in Fig. 1. In addition, although data are noisy due to the very low Sn concentration, there is no hint of Sn clustering.
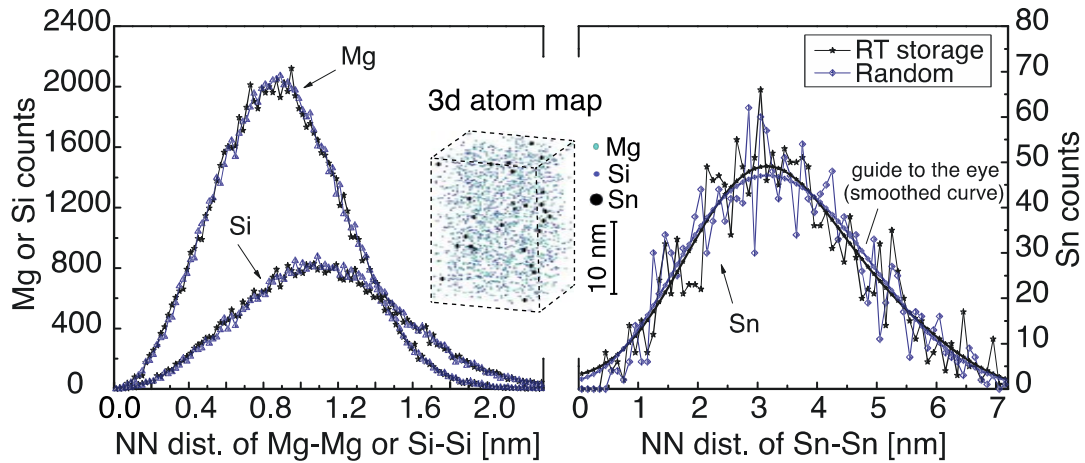
FIG 2. Analysis of solute clustering during RT storage. Results are obtained by APT for Sn addition of 200* at. ppm and two weeks of RT storage after quenching. A 3d atom map of Mg, Si and Sn (magnified) is shown. No solute clusters are recognizable by eye. (For better visibility the reader is referred to the video included in the SM.) An analysis of NN distances of Mg, Si and Sn revealed no significant difference between the measured and a calculated randomized distribution of these elements.

Figure 3 shows the evolution of the hardness in AA6061 during artificial aging at the standard temperature of 443 K after both 1 day and 2 weeks of RT storage, with and without Sn addition. Also shown are data generated from laboratory samples without Sn addition and with RT storage shorter than 60 s; even though not commercially feasible, this would be the "best-case" reference of maximum kinetics and hardening potential that can be achieved due to the absence of natural aging. The results in Fig. 3 show that Sn not only retards hardening during RT storage over orders of magnitude (Fig. 1), but it then also accelerates the kinetics during artificial aging, relative to the Sn-free "commercial case", as shown exemplarily for AA6061 stored at RT. In fact, the hardening kinetics can even approach that of the "best case" reference AA6061. The effectiveness of Sn can be controlled by the amount added and the period of RT storage. Lower Sn additions (~40 at. ppm) delay natural aging for a period sufficient to overcome most logistical, technological, and physical constraints in the production of semi-finished Al-Mg-Si products (1 day; see Fig. 1) but then allow for artificial aging that approaches the "best case" and is 6 times faster than the current "commercial case". Higher Sn additions at the ~100 at. ppm solubility limit prevent natural aging at RT even for much longer times, (e.g. 2 weeks; see Fig. 1) and still accelerates artificial aging, but somewhat less pronounced. However, at all these Sn additions, a 10% higher hardness relative to the "commercial case" of AA6061 is ultimately achieved.
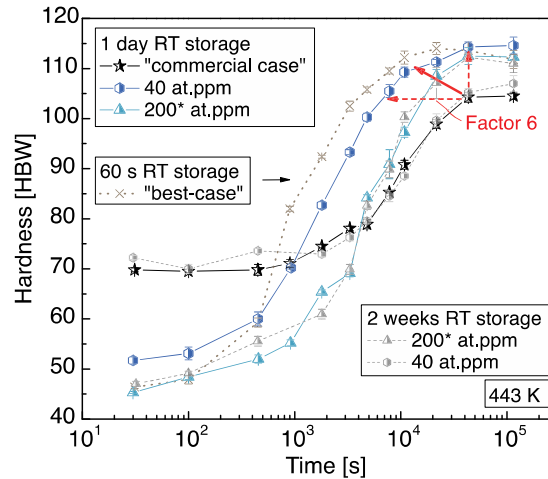
FIG 3. Evolution of hardness during artificial aging at 443 K with and without Sn addition for various periods of RT storage. Data generated from laboratory scaled samples without Sn addition and RT storage < 60 s is shown as a "best-case" reference, where the maximum kinetics and hardening potential is achieved. This "best-case" scenario cannot be realized in a commercial process, where the material undergoes a significantly longer RT storage (see "commercial case" in the figure; a similar curve is obtained for RT storages of 2 weeks). The negative effect of RT storage can be eliminated by minute additions of Sn, which enhance kinetics and hardness (red arrows).

It has been proposed that Sn could form small precipitates that act as heterogeneous nucleation sites for precipitation [25]. However, APT results for AA6061 with Sn addition of 200* at. ppm and artificial aging at 443 K after two weeks of RT storage reveal no small Sn precipitates (Fig. 4). Sn does appear in the MgSi precipitates, which indicates a finite solubility of Sn in the precipitates, possibly due to its tendency to bind with Mg [16]. This also suggests that Sn can diffuse during artificial aging.
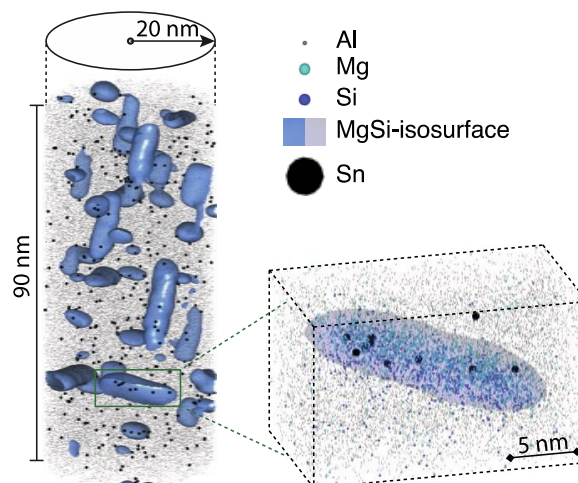
FIG 4. Artificially aged microstructure. Data obtained by APT for Sn addition of 200* at. ppm and artificial aging of 12 h at 443 K after two weeks of RT storage. A 3d map of Al and Sn atoms is shown. MgSi precipitates are indicated by semi-transparent iso-concentration surfaces of Mg and Si (4 at. %). Sn is found within the matrix and the MgSi precipitates and forms no individual precipitates (see magnified insert).

Empirically, the results in Figures 1-4 are consistent with the mechanistic concept proposed in the introduction: solutes S trap vacancies V at low temperatures and thus prevent natural aging, but release the vacancies at elevated aging temperatures, thereby allowing the desired aging processes to occur without the detrimental influence of processes that would normally happen during RT storage. This mechanistic concept is supported by thermodynamic and kinetic models using first-principles calculations of Sn-vacancy binding and vacancy migration around Sn solutes. The general thermodynamic model considers a low concentration c_S of solutes dissolved in the metal lattice, with binding energies ΔE_{SV}^i (positive values indicating binding) for various possible vacancy-solute binding complexes. Considering the solutes at fixed position in the metal lattice, we compute the concentrations c_V of untrapped vacancies and the concentrations c_{SV}^i of the vacancy-solute complexes at the effective quench temperature T_Q where annihilation of vacancies essentially ceases [26]. As the temperature of the alloy is quenched below T_Q, further vacancy annihilation is not possible but re-partitioning of the vacancies among the untrapped and trapped solute-vacancy complexes is allowed because such trapping requires very limited vacancy transport. Any vacancy-mediated diffusional processes at temperature T are then controlled by the residual untrapped vacancy concentration $c_V(T)$, and so vacancy-mediated diffusion is retarded by a factor $R = c_V(T_Q)/c_V(T)$.

The thermodynamic model uses simple solution theory, which includes only the entropy due to mixing, and assumes low concentrations $c_V, c_S \ll 1$. Rather than present the detailed model (see SM for a full presentation), we show here a simplified model that is numerically accurate for Sn. The simplified model assumes that one S can bind only one V at a time with a binding energy ΔE_{SV}, at one of the 12 nearest-neighbor (NN) sites of the S atom in the fcc lattice, and that the total quenched vacancy concentration is much smaller than the solute concentration, $c_V^{tot}(T_Q) \ll c_S$. At any temperature $T < T_Q$, the total concentration of V in the material is fixed at $c_V^{tot}(T_Q)$, i.e. $c_V^{tot}(T_Q) = c_V(T) + 12 c_S c_{SV}(T)$. Furthermore, the ratio of the trapped and untrapped V concentrations is governed by the Boltzmann factor, $\frac{c_{SV}(T)}{c_V(T)} = e^{\Delta E_{SV}/kT}$, where k is Boltzmann's constant. Combining the above two equations yields

$$R = \frac{c_V(T_Q)}{c_V(T)} = \frac{1 + 12 c_S (e^{\Delta E_{SV}/kT})}{1 + 12 c_S (e^{\Delta E_S/kT_Q}} \tag{1}$$

This ratio is unity in the limits of zero V-S binding, $T = T_Q$, or $c_S = 0$, as necessary physically. For Sn in Al, we have computed the binding energies ΔE_{S-V}^i using quantum DFT for an S-V pair, an S-V-V triplet where the vacancies are NN of each other, and of various V-S-V triplets where the vacancies are not NN. The value of ΔE_{SV} shown in Fig. 5a agrees well with previous

DFT calculations [14, 27]. For Sn, the calculated binding energies indicate that the V-S-V complexes are negligible but the S-V-V complexes are not (see SM for the values). Nonetheless, a full analysis shows that the net effect of the S-V-V complexes on trapping and on R is small, and that the second term in the denominator of Eq. (1) is negligible for all reasonable quenching temperatures (600 K < T_Q < 800 K). Thus, over a range of temperatures, and for sufficient Sn concentrations, the retardation factor is approximately

$$R = 1 + 12c_S(e^{\Delta E_{SV}/kT}) \tag{2}$$

which is conveniently independent of the effective quenching temperature and the quenched vacancy concentration $c_V^{tot}(T_Q)$.

Figure 5b shows the approximate factor R computed using Eq. (2) for Sn at concentrations of 40, 70, and/or 100 at. ppm at both RT and 443K (artificial aging), using the V-Sn binding energy determined by DFT. R is significant at RT and at the Sn solubility limit, but is fairly small at the artificial aging temperature. Thus, trapping of V by Sn suppresses RT aging processes significantly but has a much smaller effect on artificial aging. Fig. 5b also shows the R-value from experiments, computed as the ratio of the times required to achieve 50% of the hardening with and without Sn, respectively. Such an experimental R-value assumes that all aging processes are kinetically limited by vacancy-mediated diffusion, which is the mechanism proposed here. Quantitatively, the R-values obtained using the DFT-computed V-Sn binding energy are somewhat smaller than measured. Better quantitative agreement can be obtained using a larger V-Sn binding energy, as shown in Fig. 5b for ΔE_{SV} = 0.3 eV which is within the range of experimentally-derived values [28]. While the differences between the computed and deduced binding energies remains to be resolved, the model nonetheless captures the major trends shown experimentally.

The above model is applicable if the V-S complex cannot diffuse rapidly. For the Sn-V pair, we have computed, using DFT and the Nudged Elastic Band method [23], all of the migration barriers relevant for assessing Sn diffusion within the context of the 5-frequency model [29], as shown in Fig. 5a. Application of the 5-frequency model to Sn, neglecting differences in the vibrational attempt frequencies among the different migration steps, shows that the migration of Sn is also controlled by the reduced untrapped vacancy concentration, and thus by the same factor of R as for the alloying elements (Mg, Si) in AA6061. Hence, the addition of ~100 at. ppm Sn only affects diffusional processes through the reduction of available vacancies in the matrix.

In summary, we have shown that a modification of excess vacancy motion by minute additions of Sn offers the long-sought solution to the negative effect of RT storage in Al-Mg-Si alloys, with great importance for the application of this group of lightweight alloys. The advantage in kinetics and/or achievable strength (indicated by arrows in Fig. 3) in the industrial production of Al-Mg-Si alloys will increase the freedom either to decrease the necessary heat treatment time by a factor of 6 or to increase the hardness by 10%. The methodology of buffering excess vacancies at low temperature such that they are available for diffusion on demand at a later time during processing at a higher temperature is in fact not limited to Sn additions to Al-Mg-Si alloys. The mechanism is expected to be possible using other solute elements as well, e.g. In for Al-Mg-Si alloys, and in other metallic systems (e.g. Mg and Cu-alloys) where key microstructural evolution processes are controlled by vacancy-mediated diffusion. Furthermore, the selection of suitable trace element additions can be guided by a combination of the used first-principles modeling and an understanding of achievable trace element solubility in the alloy, thereby providing new directions for advanced and accelerated development of new or improved metal alloys.

Acknowledgements

2.2   Supplemental Material

Solution treatment

Figure SM1 demonstrates the importance of the temperature dependence of the solubility of Sn in the aluminum lattice. A thermodynamic calculation based on the CALPHAD approach illustrates that the solubility of Sn in Al-Mg-Si alloys is much lower than in pure aluminum (Fig. SM1(a)). However, it increases with temperature, and sufficient Sn can be dissolved in Al-Mg-Si alloys because of the high solidus temperature (~870 K for alloy AA6061). Such calculations may not be precise for the current application, but they can still serve as an estimate. They in fact confirm literature evidence of the Mg influence [16] on the solubility of Sn in Al, and acceptably match the experimentally derived concentration in solid solution at 843 K.

Figure SM1(b) shows the effect of Sn on the evolution of hardness during RT storage as a function of the solution treatment temperature. The time (Δt_{80}) when 80 % of the maximal difference between the hardness of AA6061 and AA6061 plus 430* at. ppm Sn is reached during natural aging (indicated in the insert for 843 K solution treatment temperature) is used as a measure of the retardation effect of Sn. Obviously the hardening/slowing-down depends strongly on the solution treatment temperature. We attribute this to an increasing amount of Sn dissolved in the aluminum matrix.
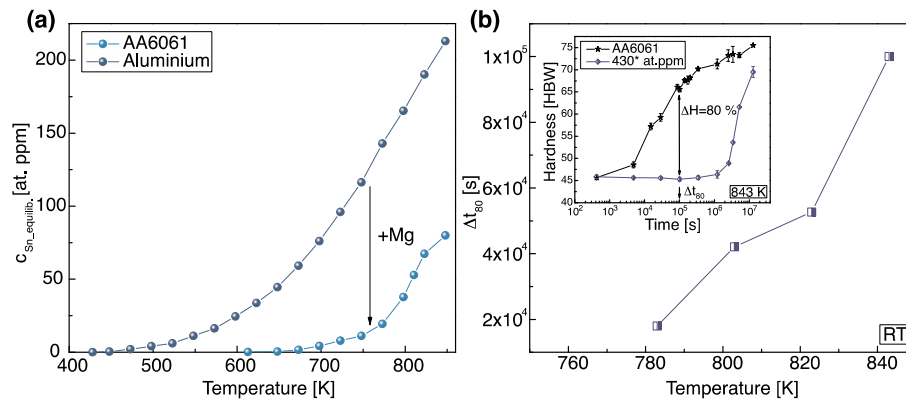
FIG SM1. (a) The solubility of Sn in pure aluminum and the alloy AA6061 is estimated for an increasing temperature from thermodynamic data (FactSage™ 6.1 software [30] together with the FACT FTlite light alloy database (2009)). (b) The influence of Sn on the evolution of hardness during RT storage is shown as a function of the solution treatment temperature. The time (Δt_{80}) when 80 % of the maximal difference between the hardness of the alloy AA6061 and AA6061 plus 430* at. ppm Sn is reached during natural aging (indicated in the insert for 843 K solution treatment temperature) is used as a measure of the retardation effect of Sn. A strong dependence on the solution treatment temperature is obvious.

Atom Probe Tomography

The reconstruction of the measured data was performed using the IVAS 3.6.4™ software package (Cameca). Figure SM2(a) shows an example desorption map on the detector, obtained during an APT experiment on the investigated alloys, revealing indexable crystallographic poles and zone lines. Such patterns are typically observed for pure metals and diluted alloys in wide-field-of-view atom probe instruments and can be used to optimize the reconstruction parameters [31]. Spatial distribution maps (SDMs) [32], a statistical tool which makes possible the measurement of lattice spacing in real space, were deployed and included in the reconstruction explorer of the IVAS software package [33]. The initial tip radius used for reconstruction was adjusted iteratively so that the SDM-measured and the expected crystallographic interplanar spacing agreed well. To confirm the validity of the reconstruction, the lattice spacing around different poles was measured again within the reconstructed data (Fig. SM2) and compared to the known crystallographic values. In the example shown in Fig.

SM2, four different poles ([002], [1-13], [0-24], [204]) were evaluated; the mean variance to the known lattice spacings agreed with the values obtained for pure aluminum [34].
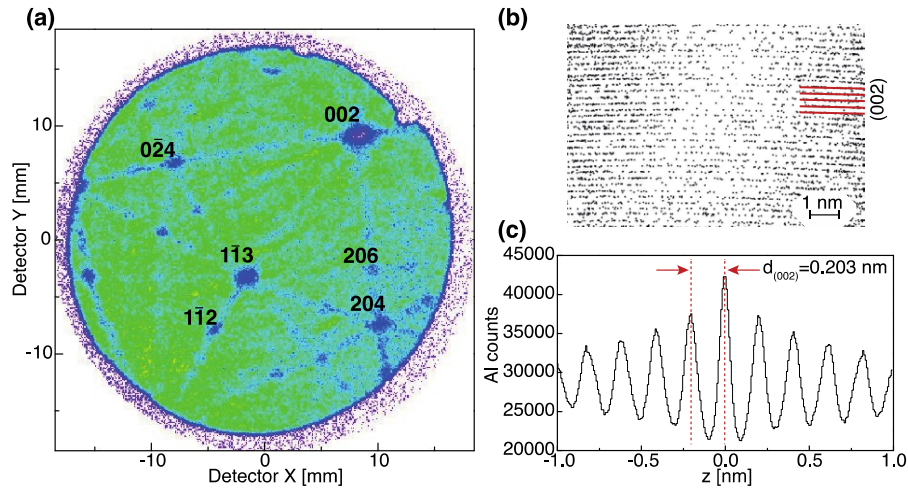
FIG SM2. (a) Desorption map showing ion hits on the detector obtained during an ATP experiment. The main crystallographic poles have been indexed. (a) Cut of a small part of the reconstructed data around the [002] pole revealing lattice planes; only Al atoms are displayed. (c) Spatial distribution map (SDM) of the reconstructed data around the [002] pole; the distance between the peaks represents the interplanar spacing.

The concentration of Sn in solid solution after solution treatment at 843 K was determined as an average from four naturally aged samples with an addition of 200* at. ppm Sn. The value of 96 ± 9 at. ppm Sn was deduced by taking background subtraction of the IVAS software package[5] into account.

Thermodynamic Model

In the general model, each solute atom is considered fixed in the metal lattice and can have zero V neighbors, one vacancy neighbor (S-V with binding energy ΔE_{SV}, having $n_{SV} = 12$ possible configurations) or two vacancy neighbors (with the vacancies being (i) near neighbors, S-V-V with binding energy ΔE_{SVV}, having $n_{SVV} = 24$ possible configurations, or (ii) further neighbors, V-S-V with various binding energies ΔE_{VSV} that are all quite similar, with a total of $n_{VSV} = 42$ possible configurations; see Fig. SM3.

$\Delta E_{SVV} = 0.54$ eV $\qquad$ $\Delta E_{VSV} = 0.29$ eV $\qquad$ $\Delta E_{VSV} = 0.26$ eV $\qquad$ $\Delta E_{VSV} = 0.29$ eV
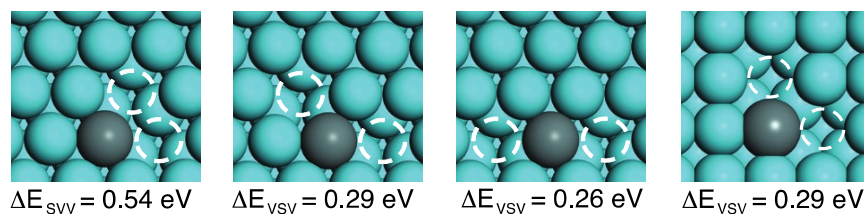
FIG SM3. Configurations and binding energies for different types of Sn-V-V triplets. The binding energies indicate that the V-Sn-V complexes are negligible.

These various complexes are considered as different "molecules" and are assumed to be independent, i.e. S-S neighbors and S-S second neighbors, for which some vacancy sites would belong to both solutes, are not considered; this is accurate for $c_S << 1$. At the effective quench temperature T_Q, standard thermodynamic equilibrium for the distribution of vacancies among the different molecules then applies. Within simple solution theory for the entropy contributions, the vacancy concentration in the metal lattice is governed by the vacancy formation energy E_V^f and is $c_V(T_Q) = e^{-E_V^f/kT_Q}$. The various solute-vacancy complex concentrations can then be written as

$$c_V(T_Q) = \frac{c_S c_V n_{SV} e^{\Delta E_{SV}/kT_Q}}{1 + c_V n_{SV} e^{\Delta E_{SV}/kT_Q} + c_V^2 n_{SVV} e^{\Delta E_{SVV}/kT_Q} + c_V^2 n_{VSV} e^{\Delta E_{VSV}/kT_Q}}$$

$$c_{SVV}(T_Q) = \frac{c_S c_V^2 n_{SVV} e^{\Delta E_{SVV}/kT_Q}}{1 + c_V n_{SV} e^{\Delta E_{SV}/kT_Q} + c_V^2 n_{SVV} e^{\Delta E_{SVV}/kT_Q} + c_V^2 n_{VSV} e^{\Delta E_{VSV}/kT_Q}}$$

$$c_{SVV}(T_Q) = \frac{c_S c_V^2 n_{VSV} e^{\Delta E_{VSV}/kT_Q}}{1 + c_V n_{SV} e^{\Delta E_{SV}/kT_Q} + c_V^2 n_{SVV} e^{\Delta E_{SVV}/kT_Q} + c_V^2 n_{VSV} e^{\Delta E_{VSV}/kT_Q}}$$

The total number of vacancies at the quench temperature is then

$$c_V^{tot}(T_Q) = c_V(T_Q) + c_{SV}(T_Q) + 2c_{SVV}(T_Q) + 2c_{VSV}(T_Q).$$

After quenching, these vacancies repartition among the different solute-vacancy complexes and the metal lattice such that the chemical potentials of all vacancies in the system remain equal. The concentrations of the solute-vacancy complexes and the isolated vacancies then satisfy the following set of coupled equations at temperature T:

$$c_V^{tot}(T_Q) = c_V(T) + c_{SV}(T) + 2c_{SVV}(T) + 2c_{VSV}(T).$$

$$c_V(T) = \left(\frac{c_{SV}}{c_S - c_{SV} - c_{SVV} - c_{VSV}}\right)\left(\frac{e^{-\Delta E_{SV}/kT}}{n_{SV}}\right)$$

$$c_V(T) = \left(\frac{c_{SV}^2}{c_S - c_{SV} - c_{SVV} - c_{VSV}}\right)\left(\frac{n_{SVV} e^{-(2\Delta E_{SV} - \Delta E_{SVV}/kT)}}{n_{SV}^2}\right)$$

$$c_{VSV}(T) = \left(\frac{c_{SV}^2}{c_S - c_{SV} - c_{SVV} - c_{VSV}}\right)\left(\frac{n_{VSV}e^{-(2\Delta E_{SV} - \Delta E_{VSV}/kT)}}{n_{SV}^2}\right)$$

The appearance of the term $(c_S - c_{SV} - c_{SVV} - c_{VSV})$ in the denominator reflects the "Fermi-Dirac-like" exclusion among the various solute-vacancy complexes: the maximum concentration of all solute-vacancy complexes cannot exceed the concentration of solutes. These equations can be combined to yield one cubic equation for $c_{SV}(T)$, from which the other quantities can then be computed, but the solution is unwieldy and does not provide any direct insight. From these equations and the binding energies shown in Fig. 3(a), it is clear that the additional binding energy of V-S-V complexes cannot compensate for the additional concentration factor c_{SV}, and thus the V-S-V complexes are negligible for Sn solutes. The simple result presented in the main text can be obtained from the full analysis above by neglecting the S-V-V and V-S-V complexes in the analysis.

Supporting Files

MOVIE S1. 3d atom map of Mg, Si and Sn (magnified). No solute clusters are recognizable by eye. Weblink:

https://journals.aps.org/prl/supplemental/10.1103/PhysRevLett.112.225701/MovieS1.m4v

References

[1] C. Kammer, *Aluminium handbook* (Beuth, Berlin, 2011), Vol. 1 Fundamentals and materials.

[2] I. Kovaćs, E. Nagy, and J. Lendvai, Acta Metall. Mater. 20, 975 (1972).

[3] J. Banhart, C. S. T. Chang, Z. Q. Liang, N. Wanderka, M. D. H. Lay, and A. J. Hill, Adv. Eng. Mater. 12, 559 (2010).

[4] P. Brenner and H. Kostron, Z. Metallkd. 4, 89 (1939).

[5] A. Guinier, Nature 142, 569 (1938).

[6] G. D. Preston, Nature 142, 570 (1938).

[7] J. Banhart, M. D. H. Lay, C. S. T. Chang, and A. J. Hill, Phys. Rev. B 83, 014101 (2011).

[8] M. J. Starink, L. F. Cao, and P. A. Rometsch, Acta Mater. 60, 4194 (2012).

[9] S. Esmaeili, D. J. Lloyd, and W. J. Poole, Acta Mater. 51, 3467 (2003).

[10] C. D. Marioara, S. J. Andersen, J. E. Jansen, and H. W. Zandbergen, Acta Mater. 51, 789 (2003).

[11] M. Murayama and K. Hono, Acta Mater. 47, 1537 (1999).

[12]   S. Pogatscher, H. Antrekowitsch, H. Leitner, T. Ebner, and P. J. Uggowitzer, Acta Mater. 59, 3352 (2011).

[13]   H. W. Zandbergen, S. J. Andersen, and J. Jansen, Science 277, 1221 (1997).

[14]   C. Wolverton, Acta Mater. 55, 5867 (2007).

[15]   H. K. Hardy, J. Inst. Met. 78, 169 (1950).

[16]   I. J. Polmear, Mater. Sci. Forum 13-14, 195 (1987).

[17]   G. A. Edwards, K. Stiller, G. L. Dunlop, and M. J. Couper, Acta Mater. 46, 3893 (1998).

[18]   D. Blavette, A. Bostel, J. M. Sarrau, B. Deconihout, and A. Menand, Nature 363, 432 (1993).

[19]   T. F. Kelly, D. J. Larson, Annu. Rev. Mater. Res. 42, 31 (2012)

[20]   M. K. Miller, A. Cerezo, M. G. Hetherington, and G. D. W. Smith, *Monograhs on the Physics and Chemistry of Materials* (Oxford University Press, Oxford, 1996), Atom Probe Field Ion Microscopy.

[21]   G. Kresse and J. Furthmuller, Phys. Rev. B 54, 11169 (1996).

[22]   H. J. Monkhorst and J. D. Pack, Phys. Rev. B 13, 5188 (1976).

[23]   G. Mills, H. Jonsson, and G. K. Schenter, Surf Sci 324, 305 (1995).

[24]   E. A. Marquis and J. M. Hyde, Mater. Sci. Eng. R. 69, 37 (2010).

[25]   T. Homma, M. P. Moody, D. W. Saxey, and S. P. Ringer, Metall. Trans. A 43, 2192 (2012).

[26]   F. D. Fischer, J. Svoboda, F. Appel, and E. Kozeschnik, Acta Mater. 59, 3463 (2011).

[27]   D. Simonovic and M. H. F. Sluiter, Phys. Rev. B 79 (2009).

[28]   G. Fioeito, S. Ceresara, and T. Federighi, Acta Metall. Mater. 14, 452 (1966).

[29]   M. Mantina, Y. Wang, L. Q. Chen, Z. K. Liu, and C. Wolverton, Acta Mater. 57, 4102 (2009).

[30]   C. W. Bale, P. Chartrand, S. A. Degterov, G. Eriksson, K. Hack, R. Ben Mahfoud, J. Melancon, A. D. Pelton and S. Petersen, Calphad **26**, 189 (2002)

[31]   B. Gault, F. De Geuser, L. T. Stephenson, M. P. Moody, B. C. Muddle and S. P. Ringer, Microsc. Microanal. **14**, 296 (2008)

[32]   B. P. Geiser, T. F. Kelly, D. J. Larson, J. Schneir and J. P. Roberts, Microsc. Microanal. **13**, 437 (2007)

[33]   Cameca. IVAS™ User Guide 3.6.4. (2012)

[34]   B. Gault, D. Haley, F. de Geuser, M. P. Moody, E. A. Marquis, D. J. Larson and B. P. Geiser, Ultramicroscopy **111**, 448 (2011)

3 ULTRAFAST ARTIFICIAL AGING

This chapter continues the work which led to the formulation of the "vacancy prison mechanism" model. The comparative analysis of direct artificial aging kinetics and the naturally pre-aged case with and without trace Sn addition sheds more light on the mechanisms controlling aging at unconventionally high temperatures of 210-250 °C. The effect of Sn is shown to be phenomenologically similar to the known positive effect of natural pre-aging on artificial aging at high temperatures in commercial Al-Mg-Si alloys. Additionally trace Sn addition generates both ultrafast aging kinetics and superior peak hardness. The observed trends are explained by a detailed analysis of the contribution of quenched-in excess structural vacancies to the nucleation and growth of age-hardening precipitates.

Ultrafast artificial aging of Al–Mg–Si alloys[*]

This study investigates the effect of trace Sn additions on the artificial aging of an Al–Mg–Si alloy at unconventionally high temperatures (>210 °C), where such additions generate both ultrafast aging kinetics and superior peak hardness. The study shows that the effect of Sn is comparable to the influence of natural pre-aging on high-temperature artificial aging, and explains this by solute-vacancy interactions, proposing that during artificial aging Sn-vacancy pairs contribute to diffusion and/or Sn retards the annihilation of quenched-in vacancies.
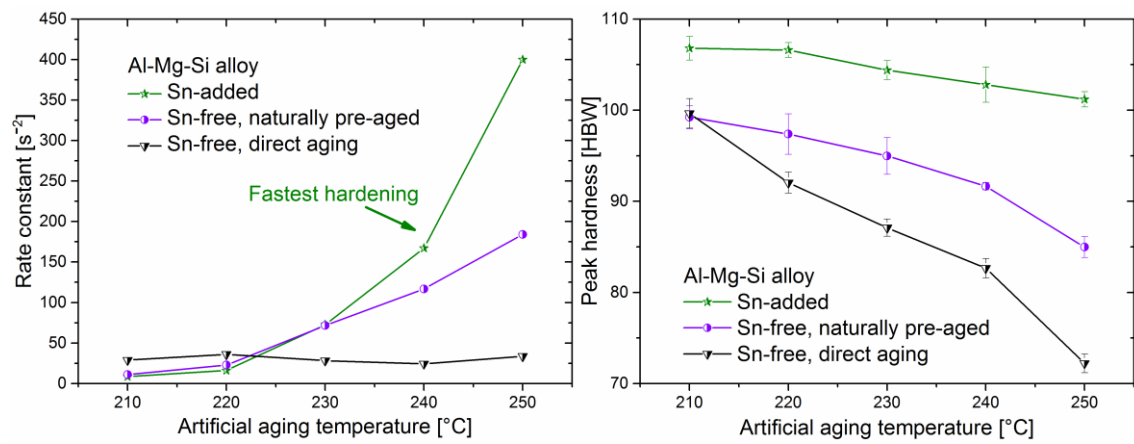
Main Part

Most commercial Al-rich Al–Mg–Si alloys such as AA6061 reveal a strong negative influence of natural pre-aging (n.p.a.) on subsequent artificial aging (a.a.). This negative effect retards kinetics and lowers T6 strength [1–4]. This phenomenon has been attributed to clustering processes at room temperature (r.t.) [5,6]. During a.a. at conventional, low a.a. temperatures (i.e. 170 °C-200 °C), clusters of Mg and Si atoms act as efficient traps for quenched-in vacancies [5]. Higher aging temperatures positively enhance the dissolution kinetics of these clusters, which thereby release vacancies, resulting in a faster nucleation rate of the major hardening phase β´´ [5,7]. Recently a concept was presented which avoids the formation of clusters by adding trace amounts of Sn to the alloy AA6061, leading to the suppression of clustering during natural aging (n.a.) for >2 weeks [8,9]. This behavior was explained by strong Sn-vacancy binding [8,10–12], which results in trapping of vacancies (mainly Sn-vacancy pairs). This generates a reduced number of quenched-in vacancies in the matrix which can control diffusional processes. While suppression of n.a. prevails, a.a. kinetics at 170 °C in Sn-

*Werinos M, Antrekowitsch H, Kozeschnik E, Ebner T, Moszner F, Löffler JF, Uggowitzer PJ et al. Scripta Materialia 2016;112:148–51.

microalloyed AA6061 is significantly enhanced compared to the n.p.a. commercial case and is even close to ideal direct aging (d.a.), which avoids the negative effect of r.t. storage [8]. To quantify the retarding effect of Sn on n.a., we proposed a retardation factor R which mainly accounts for the effect that any diffusional processes at a given temperature are controlled by a residual untrapped excess vacancy concentration. Maximum retardation of n.a. kinetics is achievable by adding Sn at the solubility limit, i.e. ~100 at. ppm Sn in AA6061 [8,9]. So far, the effect of Sn in Al–Mg–Si alloys has only been studied at conventional a.a. temperatures (of ~170 °C). In the following we present the additional phenomenon of ultrafast aging with simultaneous great hardness, which was discovered in Sn-modified AA6061 at unconventionally high a.a. temperatures (>210 °C).

Sheets with the composition Mg 0.90, Si 0.59, Cu 0.09, Fe 0.28, Cr 0.07, Mn 0.05, Zn 0.02 and Ti 0.05, all in at.% (plus ~200 at. ppm Sn for the Sn-added variant) were produced by a procedure described elsewhere [8]. Solution heat treatment occurred in a circulating air furnace at 570 °C for 1.2×10^3 s. Subsequent quenching was carried out in water at r.t., and for n.a. the samples were kept at 25 °C. Artificial aging was undertaken in an oil bath. Brinell hardness measurements (HBW 2.5/62.5/15) were performed on polished samples. Needle-shaped specimens for atom probe tomography (APT) were prepared via a standard two-step electropolishing method [13]. APT was performed on a LEAP™ 4000X HR from Cameca in laser mode using a specimen temperature of 30 K, at a pulse frequency of 250 kHz and a detection rate of 1%. The software package IVAS 3.6.4™ was used for the reconstruction procedure and analysis.

Simulation of the excess-vacancy evolution during a.a. was carried out on the basis of the FSAK model [14], which predicts the evolution of the structural vacancy concentration as a function of thermo-mechanical treatment history. In this approach, the excess vacancies are assumed to be annihilated or generated at perfect sinks or sources at dislocation jogs and grain boundaries. The corresponding model is implemented in the thermokinetic simulation software package MatCalc, which was introduced originally in refs. [15,16]. The microstructural parameters for the present simulations were set in accordance to the AA6061 alloy investigated, which had a grain size of 100 $\square$ m and a dislocation density of 10^{11} m^{-2}. The trapping enthalpy between Sn atoms and vacancies was taken with a value of $\square E$=0.3 eV and the coordination number (number of trapping sites per Sn atom) was set to 12. The distribution / partitioning of vacancies between trapped and free lattice sites was assumed to be in local equilibrium at all times.

The inset to Fig. 1 shows the n.a. behavior of the alloys studied up to 1.2×10^6 s. Whereas the Sn-free commercial alloy shows hardening shortly after quenching, the Sn-added variant preserves the as-quenched hardness. Subsequent hardening kinetics of the Sn-free alloy (Fig. 1)

during a.a. at 250 °C (n.p.a. for 1.2×10^6 s) is significantly faster than that of the d.a. case (n.p.a shorter than 60 s) and generates higher maximum values. At 250 °C, the Sn-added alloy achieves even higher maximum hardness within a short period of 450 s. Note that in the commercial case without Sn-addition (e.g. a.a. at 170 °C after 1.2×10^6 s of n.p.a.), maximum hardness is only reached after several hours (see [5,8]).
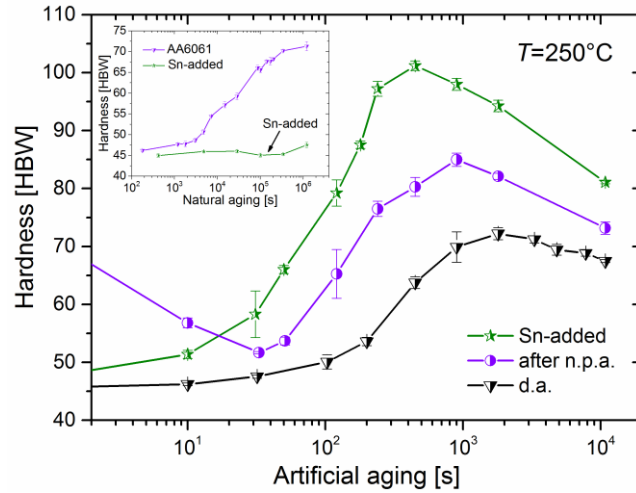
Fig. 1. Hardness evolution of alloy AA6061 at 250 °C after natural pre-aging (n.p.a.) of less than 60 s ("d.a." case, black) and after n.p.a. for 1.2×10^6 s ("after n.p.a." case, violet). Also shown is the "Sn-added" case (green) after n.p.a. for 1.2×10^6 s. The natural aging curves are shown in the inset.

With increasing a.a. temperature (>170 °C), the achievable maximum hardness is known to decrease [5], which is why a benefit in kinetics at high temperatures cannot be used to shorten the necessary time for heat treatments. This is also observed in the present study. As can be seen in Fig. 2a, the trend is most significant for the Sn-free alloy subjected to d.a., where hardness declines from ~100 HBW at 210 °C to ~72 HBW at 250 °C. Starting from the same hardness at 210 °C, but with n.p.a. for 1.2×10^6 s, the alloy still achieves ~85 HBW at 250 °C. The Sn-added alloy, however, reaches a superior value of 101 HBW at 250 °C.

To illustrate the temperature dependence of the precipitation kinetics during a.a., all hardness curves were fitted and analyzed according to Eq. 1 (for details see ref. [5]):

$$\left(\frac{H - H_{\text{a.q.}}}{H_{\text{peak}} - H_{\text{a.q.}}}\right)^2 = 1 - \exp(-kt^n) \tag{1}$$

Here, $H_{\text{a.q.}}$ equals the as-quenched hardness and was set to 46.2 HBW for the Sn-free and 45 HBW for the Sn-added alloy, respectively. The as-quenched hardness is usable for all heat treatments investigated because in the Sn-added case (n.p.a. for 1.2×10^6 s) the same artificial aging response is achievable as long as a.a. starts from the soft as-quenched hardness (ref. [8]). Fits for a.a. after n.p.a. in the Sn-free case start after the dissolution of 95% of n.a. clusters

which produces a state of the material similar to the as-quenched state (see ref. [5]). The T6 hardness values H_{peak} are shown in Fig. 2a, and k is a temperature-dependent rate constant plotted in Fig. 2b. An optimum value of n to reach a high $R^2 > 0.98$ for fitting all hardness curves analyzed was found to be 2.

Figure 2b shows for d.a. of the Sn-free alloy comparable rate constants k at all a.a. temperatures >210 °C (all curves show the onset of hardening after ~100 s and maximum hardness after ~1800 s). In contrast, after n.p.a. the alloy reveals increasing rate constants k with increasing temperature (time to the maximum decreases from ~4800 s at 210 °C to ~900 s at 250 °C). The Sn-added variant exhibits similar rate constants k at 210 °C, but increasing kinetics with increasing temperature and the highest rate constant k at 250 °C (compare also Fig. 2b with Fig. 1).
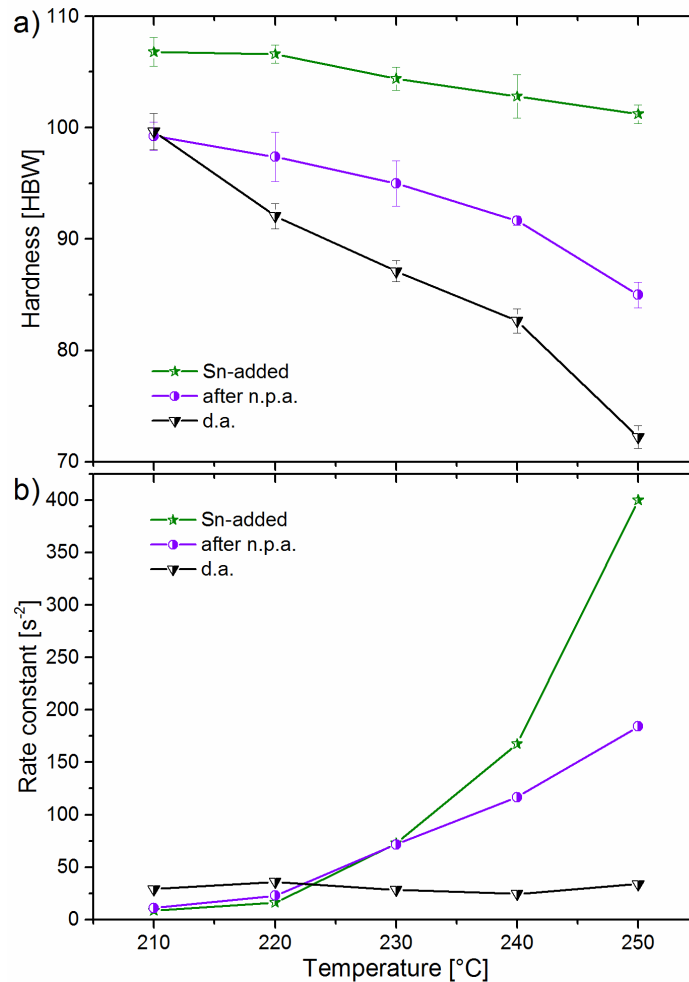
Fig. 2. (a) Peak hardness and (b) rate constant k, deduced from Eq. 1, for temperatures between 210 °C and 250 °C; for direct aging and after natural pre-aging (in the latter case with and without Sn addition).

To explain these findings, let us first consider the d.a. situation shown in Fig. 1 and 2. One of the possible reasons for the stagnation of the rate constants k above 210 °C (Fig. 2b) has been

claimed in ref. [5] to be a more pronounced annihilation of mobile quenched-in vacancies, which are necessary for precipitate nucleation (see also ref. [17]). Generally, apart from solute super-saturation the nucleation rate depends on the mobility of atoms and hence on the availability of excess structural vacancies [18,19]. Ref. [5] discussed the decreasing solute super-saturation with increasing temperature as another possible reason for comparable rate constants k above 210 °C and concluded that it does not control kinetics in this case [5]. Nucleation processes occur at the beginning of a.a., and thus the concentration of vacancies available at this stage is critical.

Figure 3 shows MatCalc simulations of the characteristic time scale for excess-vacancy annihilation during d.a., calculated for pure Al with and without the addition of Sn. In pure Al, the time to decrease the quenched-in vacancy concentration to 1% above equilibrium vacancy concentration $c_{vac,equilib}$ decreases from ~21 s at 210 °C to ~6.6 s at 250 °C; see star mark in the annihilation curve for 250 °C (inset). Thus, the concentration of excess vacancies is supposed to decrease to the temperature-dependent equilibrium level prior to the onset of hardening at ≈ 100 s of a.a., i.e. early within the nucleation stage (Fig. 1, [20]). The more brief availability of excess vacancies with increasing d.a. temperature will thus generate a decreasing number of forming nuclei. During the subsequent growth stage, the equilibrium concentration of excess vacancies is supposed to control the diffusion of atoms. Due to rising equilibrium concentration and rising diffusional mobility with increasing temperature, atoms diffuse faster. Thus two opposing trends may produce the decreasing hardness maxima and comparable rate constants k over temperature for d.a.: first, the briefer availability of excess quenched-in vacancies for nucleation produces a reduced number of nuclei; second, with increasing vacancy mobility atoms overcome larger distances in comparable time scales. Consequently, fewer nuclei of greater distance can grow to larger precipitates, which contribute less to hardness (Fig. 2a).
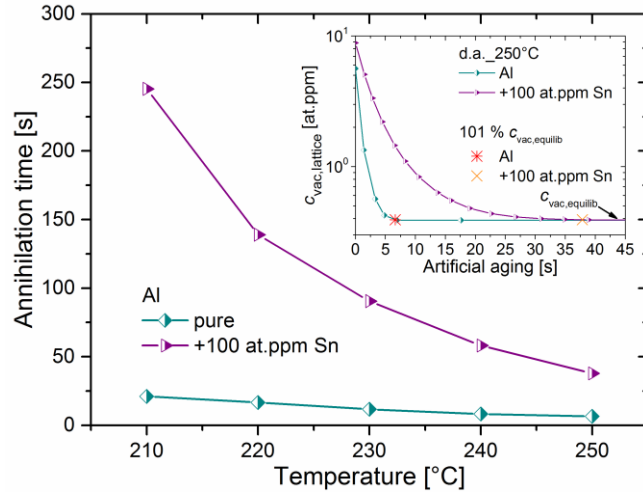
Fig. 3. Calculated characteristic time scale for annihilation of quenched-in free vacancies to nearly reach equilibrium vacancy concentration ($c_{vac,equilib}$) during d.a. for temperatures between 210 °C and 250 °C; for Al with or without addition of 100 at. ppm Sn. The inset shows the time dependence of the vacancy concentration for $T = 250$ °C, where the characteristic times for reaching 1.01 $c_{vac,equilib}$ are marked with a star (Sn-free case) and a cross (Sn-added case).

In contrast to d.a., after n.p.a and thus already at the beginning of a.a., a dense distribution of clusters is present, which is supposed to trap quenched-in excess vacancies [5,21]. Due to the faster dissolution of clusters at higher a.a. temperature, vacancies are released faster, but continuously and over a longer period compared to d.a. (see also ref. [5]). The local accumulation of alloying elements around dissolving clusters might also trigger the subsequent nucleation. Therefore the increasing rate constant k (Fig. 2b) with increasing temperature can be explained via faster dissolution of clusters. During a.a., the decreasing cluster density results in continuous vacancy release, which supports nucleation over a longer time period than for d.a. and, consequently, produces more nuclei, and thus smaller precipitates and higher peak hardness than in the case of d.a. (Fig. 2a). However, due to shorter excess vacancy availability for nucleation, the peak hardness for n.p.a. decreases from 210 °C to 250 °C, but less pronounced compared to d.a..

Based on the knowledge elaborated from the d.a. and n.p.a. treatments of commercial Sn-free AA6061, suggestions for understanding the Sn-added case are now discussed below. We propose that (i) small Sn precipitates act as heterogeneous nucleation sites; (ii) due to Sn-addition more vacancies can be quenched-in, (iii) Sn-vacancy pairs contribute to faster diffusion; and (iv) Sn retards annihilation of quenched-in vacancies.

Suggestion (i) is based on investigations of 2xxx alloys, which show that small Sn precipitates can accelerate hardening kinetics during a.a. at elevated temperatures by acting as heterogeneous nucleation sites for the maximum hardening phase Θ´ [22–26]. Figure 4a shows APT results for the Sn-added AA6061 sample aged at 250 °C for 450 s. Typical precipitates are indicated via isoconcentration surfaces of Mg+Si (2.5 at. %). Comparable to findings for a.a.

after n.p.a. at 170 °C [8], Sn is found within the matrix and within the precipitates. Although the precipitates are enriched in Sn, no individual Sn particles are found and we see no similarity with the effect in 2xxx alloys here (Fig. 4a,b).

(ii) In Al–Mg–Si and Al–Sn alloys, quenching after solution heat treatment generates solute/vacancy complexes at r.t. [27,28]. Hence, compared to commercial Al–Mg–Si alloys and due to the high solute-vacancy binding energy of Sn, a higher concentration of vacancies is assumed to be quenched-in in the case of Sn-added alloys and thus are available at the beginning of a.a. This is supported by our thermokinetic simulations (see start value in the inset to Fig. 3).
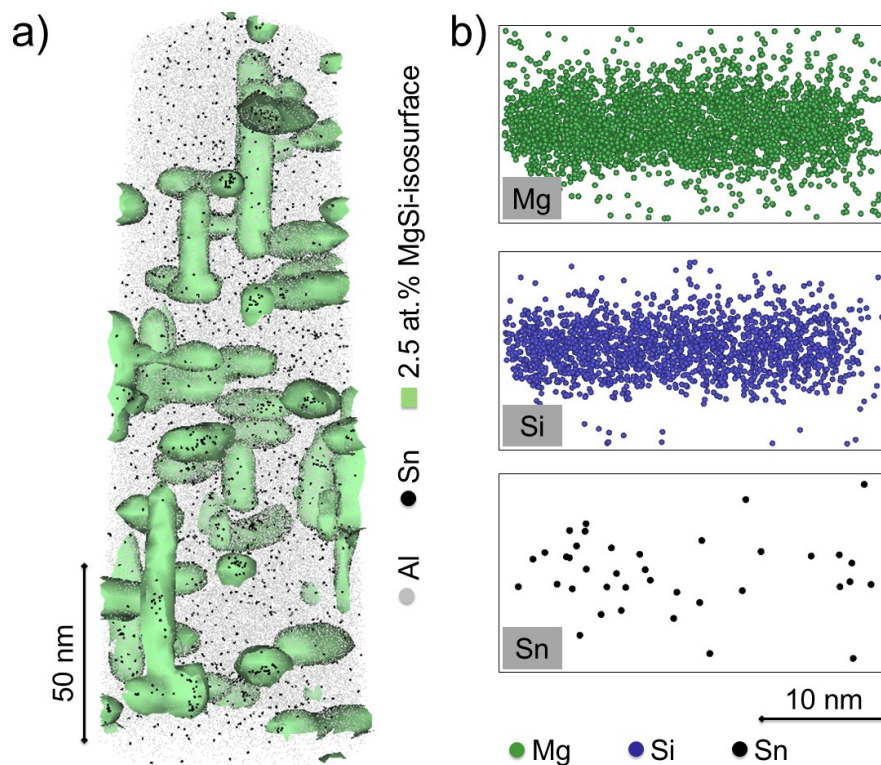
Fig. 4. a) Three-dimensional atom map of the Sn-added AA6061 sample aged at 250 °C for 450 s. Precipitates are indicated via 2.5 at.% MgSi-isoconcentration surfaces. b) Magnified atom map (Mg, Si and Sn) of a precipitate, where no Sn clustering is observed.

(iii) The trapping of vacancies by Sn, as proposed in ref. [8], shows an Arrhenius-like temperature dependency, which indicates that the trapping efficiency of Sn decreases with rising a.a. temperature. However, Sn-vacancy pairs still exist at a.a. temperatures as high as 250 °C [28] and their mobility is expected to be higher than at r.t. [8,23,24,28]. Consequently, mobile Sn-vacancy pairs may contribute to the diffusion of other solutes at these high temperatures.

Suggestion (iv) is based on the assumption that annihilation kinetics of vacancies depends on the chemical composition of the alloy, as proposed in refs. [19,29]. According to our

simulations, 100 at. ppm of Sn-addition to Al (in accordance with the solubility limit in AA6061) retards the annihilation of quenched-in vacancies, as seen in Fig. 3. The annihilation time for Sn-added Al is significantly higher than for the Sn-free case, i.e, decreases from ~245 s at 210 °C to ~37.8 s at 250 °C; see cross mark in the inset. This can be understood by Sn-atoms causing a non-random walk motion of these vacancies due to their high solute-vacancy binding energy. This effect is therefore somehow comparable to the positive effect of n.p.a. on high-temperature a.a. (>210 °C) in Sn-free AA6061 [5], because in both cases there is more time for quenched-in vacancy-assisted nucleation, until the equilibrium vacancy concentration is reached (inset to Fig. 3). The observed ultrafast a.a. kinetics can in particular be understood via the reasonable assumptions that Sn generates a higher quenched-in vacancy concentration for a longer time. Compared to n.p.a. and d.a. of Sn-free AA6061, the Sn-added situation implies a finer distribution of nuclei, generating significantly improved hardness values (Fig. 1 and 2a), which do not even decrease strongly in the range from 210 °C to 250 °C. Apparently, the effect of Sn solutes on vacancy annihilation reveals a smaller temperature dependency than that of dissolving clusters.

In summary, adding Sn to alloy AA6061 has been shown to result in superior aging performance at high temperatures (210-250 °C).

- With 100 ppm of Sn-addition, ultrafast aging kinetics and high peak hardness can be achieved simultaneously.
- The effect of Sn is shown to be phenomenologically similar to the known positive effect of natural pre-aging on artificial aging at high temperatures (>210 °C).
- The observed trends can be explained well by a detailed analysis of the contribution of quenched-in excess structural vacancies to the nucleation and growth of age-hardening precipitates.

References

[1] J. Banhart, C. Chang, Z. Liang, N. Wanderka, M. Lay, A. Hill, Advanced Engineering Materials 12 (2010) 559–571.

[2] I. Kovaćs, J. Lendvai, E. Nagy, Acta Metallurgica 20 (1972) 975–983.

[3]   A. Ried, P. Schwellinger, H. Bichsel, Aluminium 53 (1977) 595–599.

[4]   Brenner, P., Kostron, H., Zeitschrift für Metallkunde 4 (1939) 89–97.

[5]   S. Pogatscher, H. Antrekowitsch, H. Leitner, T. Ebner, P. Uggowitzer, Acta Materialia 59 (2011) 3352–3363.

[6]   S. Esmaeili, D. Lloyd, W.J. Poole, Acta Materialia 51 (2003) 3467–3481.

[7]   S. Pogatscher, H. Antrekowitsch, H. Leitner, D. Pöschmann, Z. Zhang, P. Uggowitzer, Acta Materialia 60 (2012) 4496–4505.

[8]   S. Pogatscher, H. Antrekowitsch, M. Werinos, F. Moszner, S. Gerstl, M.F. Francis, W.A. Curtin, J.F. Löffler, P.J. Uggowitzer, Physical Review Letters 112 (2014) 225701–225705.

[9]   M. Werinos, H. Antrekowitsch, W. Fragner, T. Ebner, P. Uggowitzer, S. Pogatscher, TMS Light Metals (2015) 367–371.

[10]   C. Wolverton, Acta Materialia 55 (2007) 5867–5872.

[11]   D. Simonovic, M. Sluiter, Physical Review B - Condensed Matter and Materials Physics 79 (2009).

[12]   G. Fioeito, S. Ceresara, T. Federighi, Acta Metallurgica 14 (1966) 452–454.

[13]   D.J. Larson, T.J. Prosa, R.M. Ulfig, B.P. Geiser, T.F. Kelly, Local electrode atom probe tomography: A user's guide, 2013rd ed., Springer, New York, 2013.

[14]   F. Fischer, J. Svoboda, F. Appel, E. Kozeschnik, Acta Materialia 59 (2011) 3463–3472.

[15]   J. Svoboda, F.D. Fischer, P. Fratzl, E. Kozeschnik, Materials Science and Engineering A 385 (2004) 166–174.

[16]   E. Kozeschnik, J. Svoboda, P. Fratzl, F.D. Fischer, Materials Science and Engineering A 385 (2004) 157–165.

[17]   J. Takamura, M. Koike, K. Furukawa, Journal of Nuclear Materials 69-70 (1978) 738–740.

[18]   F. Liu, F. Sommer, C. Bos, E.J. Mittemeijer, International Materials Reviews 52 (2007) 193–212.

[19]   S. Pogatscher, H. Antrekowitsch, P. Uggowitzer, Acta Materialia 60 (2012) 5545–5554.

[20]   S. Pogatscher, E. Kozeschnik, H. Antrekowitsch, M. Werinos, S. Gerstl, J.F. Löffler, P.J. Uggowitzer, Scripta Materialia 89 (2014) 53–56.

[21]   S. Esmaeili, D.J. Lloyd, Scripta Materialia 50 (2004) 155–158.

[22]   I.J. Polmear, Materials Science Forum 13-14 (1987) 195–214.

[23]   J. Silcock, H. Flower, Scripta Materialia 46 (2002) 389–394.

[24]   L. Bourgeois, T. Wong, X. Xiong, J. Nie, B. Muddle, Materials Science Forum 519-521 (2006) 495–500.

[25] L. Bourgeois, C. Dwyer, M. Weyland, J.-F. Nie, B. Muddle, Acta Materialia 60 (2012) 633–644.

[26] T. Homma, M.P. Moody, D.W. Saxey, S.P. Ringer, Metallurgical and Materials Transactions A: Physical Metallurgy and Materials Science 43 (2012) 2192–2202.

[27] C. Chang, J. Banhart, Metallurgical and Materials Transactions A: Physical Metallurgy and Materials Science 42 (2011) 1960–1964.

[28] J. Čížek, O. Melikhova, I. Procházka, J. Kuriplach, I. Stulíková, P. Vostrý, J. Faltus, Physical Review B - Condensed Matter and Materials Physics 71 (2005).

[29] S. Pogatscher, H. Antrekowitsch, T. Ebner, P. Uggowitzer, TMS Light Metals (2012).

4 INFLUENCE OF TRACE ELEMENT SOLUBILITY

Up to now only the solution treatment temperature of 570 °C and Sn addition to the alloy AA6061 with a fixed Mg, Si and Cu content had been investigated. For a reproducibility of the achievable product properties and a flexible industrial production also the effect of the solution treatment temperature and the Mg, Si and Cu content are of valuable knowledge. This chapter reveals that the influence of Sn on natural aging is controlled by its maximum quenched-in solubility, which decreases below the solution treatment temperature of 570 °C. A variation of the Mg, Si and Cu content additionally affects the quenchable Sn-solubility, but discloses a significant influence of Si and a lower effect of Mg and Cu on kinetics.

Influence of Sn-Solubility on Suppression of Natural Aging in an AA6061 Al Alloy[*]

It has been shown that minute additions of Sn to Al-Mg-Si alloys suppress and/or reduce the negative effect of natural pre-aging on artificial aging. This is of great importance for their application in precipitation hardened lightweight structures, particularly in automotive components. Sn not only retards the hardness increase during natural aging, it also enhances artificial aging kinetics and maximum hardness. Hardness measurements after varying solution heat treatment reveal slower natural aging kinetics at higher solution treatment temperature. Variation of Mg-, Si- and Cu-content disclose the significant influence of Si and a lower effect of Mg and Cu on kinetics. These results are interpreted by thermodynamic calculations based on the CALPHAD approach. It is shown that the influence of Sn on natural aging is controlled by its maximum quenched-in solubility, which increases with solution heat treatment temperature and also depends on the chemical composition.

4.1   Introduction

Today the Al-Mg-Si alloy system is the basis of numerous age hardenable wrought and casting alloys. Al-Mg-Si alloys are used as structural materials in many different ways such as rolled, extruded, forged and die-cast products. Numerous applications are found in automotive, shipbuilding, architecture and aviation industries [1–3]. They can be hardened by artificial aging (AA), i.e. by heat treating a solid solution at temperatures of about 150 to 180 °C after quenching from solution treatment temperature (SHT) [3]. A characteristic property of many Al-Mg-Si alloys is the so-called adverse effect of room temperature (RT) natural aging (NA) on subsequent AA [2–5]. In industrial processing of Al-Mg-Si alloys RT storage is practically unavoidable. Hence, the material undergoes NA and will exhibit the negative effect. Forming of profiles or sheets, however, commonly occurs in the quenched and subsequently NA state, where low strength is required and consequently hardening by NA should be prevented [1].

To understand the negative effect of NA on AA, a simple concept is proposed [2], which assumes that Mg/Si-clusters formed during NA act as traps for quenched-in thermal vacancies during AA. The mobility of these vacancies is then largely dependent on the thermal stability of the Mg/Si-clusters. On account of the slow dissolution kinetics of Mg/Si-clusters at typical AA temperatures, Mg/Si-clusters act as stable vacancy prisons during AA. Hence, a reduced

contribution of quenched-in vacancies to diffusion during the nucleation of the major hardening phase β" [6] can explain the negative effect of NA on AA [7].

Recently we presented a concept to solve this problem. Eliminating the negative effect of NA is achievable by suppressing vacancy diffusion at RT while allowing such diffusion during elevated temperature (e.g. AA) [8]. This concept has been realized by adding trace amounts of the element Sn to the alloy AA6061. Although the Mg$_2$Sn phase forms in Al-Mg-Si alloys [9], about 100 at. ppm of Sn could be dissolved in in the fcc Al matrix of AA6061 [8]. Hardness measurements and atom probe tomography revealed no NA during > 2 weeks of NA for a solution heat treatment (SHT) at 570 °C and water-quenching to RT. Without trace amounts of Sn, however, NA starts already after several minutes. Sn exhibits a high binding energy to vacancies of 0.24 eV (calculated for Sn-vacancy pairs using quantum DFT [8]). This results in trapping of vacancies by Sn and suppresses NA at RT significantly. Thus, trapping of quenched-in vacancies in Mg/Si clusters can be avoided.

Our previous studies focused on a SHT temperature of 570 °C and only the Sn-content added to AA6061 was systematically varied [8,10]. Here we will show results of NA kinetics after varying SHT and the amount of Mg, Si and Cu present in Sn-modified AA6061 alloys. The results will be interpreted in terms of theoretical Sn-solubility in fcc Al and its impact on the suppression of NA.

4.2   Experimental

Alloys 1 and 2 (**Table 1**) were prepared by melting an industrial AA6061 alloy and adding pure Sn (99.9 wt.%). For alloys 3 to 9 an AA6061 base alloy, already containing ~95 at. ppm Sn (as well as Mg 0.80, Si 0.59, Cu 0.21, Fe 0.47, Cr 0.15, Mn 0.12, Zn 0.05 and Ti 0.04, all in wt.%), was produced by the Austrian Institute of Technology (AIT) in Ranshofen (Austria) using a continuous caster in laboratory scale. To obtain the compositions listed in Table 1, the base alloy was re-melted and Mg, Si and Cu were added. After alloying, Ar gas purging was applied to reduce the hydrogen content before the alloys were cast to slabs (150 × 90 × 35 mm³). To check the chemical composition, optical emission spectrometry (SPECTROMAXx) was performed on the final plates using an appropriate calibration sample for Al-Mg-Si alloys as standard (Mg 0.85, Si 1.00, Cu 0.08, in wt.%). After cutting and homogenization, hot rolling from 20 to 4.2 mm thickness was conducted. Solution heat treatment of hardness test samples (17 × 10 × 4 mm³) was performed in a circulating air furnace (Nabertherm N60/85 SHA) at different temperatures (510 °C, 530 °C, 550 °C or 570 °C) for 20 min. Subsequent quenching

was carried out in water at RT and samples were kept in a Peltier-cooled incubator IPP (Memmert) at RT for NA.

Whereas alloys 1 and 2 differ in their Sn-content (70 at. ppm for alloy 1, 430 at. ppm in alloy 2), the specimens numbered 3 to 9 vary in the Mg-, Si- and Cu-amount added. Compared to the reference alloy 3 with average concentrations of these elements, alloys 4 and 5 are intended to reveal the influence of Mg (h: high Mg, l: low Mg). Alloys 6 to 7 demonstrate the effect of Si and alloys 8 to 9 investigate in the effect of Cu.

Table 1 Composition of alloys (Al in balance)

Alloy	Symbol MgSiCu	Sn [at.ppm]	Sn [wt.%]	Mg [wt.%]	Si [wt.%]	Cu [wt.%]	Fe [wt.%]	Mn [wt.%]	Cr [wt.%]	Zn [wt.%]	Ti [wt.%]
1	lll	70	0.030	0.82	0.63	0.232	0.59	0.111	0.147	0.059	0.079
2	lll	430	0.188	0.79	0.58	0.213	0.482	0.110	0.147	0.057	0.088
3	~~~	~95	0.041	0.87	0.72	0.300	0.510	0.118	0.148	0.045	0.041
4	h~~	~95	0.041	0.96	0.71	0.288	0.456	0.116	0.147	0.044	0.043
5	l~~	~95	0.042	0.77	0.73	0.298	0.462	0.117	0.148	0.045	0.042
6	~h~	~95	0.040	0.85	0.83	0.287	0.449	0.116	0.147	0.045	0.043
7	~l~	~95	0.041	0.86	0.61	0.245	0.456	0.116	0.148	0.045	0.042
8	~~h	~95	0.040	0.84	0.70	0.379	0.443	0.115	0.150	0.043	0.043
9	~~l	~95	0.039	0.86	0.74	0.203	0.476	0.116	0.151	0.045	0.044

Brinell hardness measurements (HBW 2.5/62.5) were carried out using an EMCO-Test M4 unit. A maximum standard deviation of 2.0 HBW was achieved. Thermodynamic calculations were performed using FactSage™ 6.3.1 software [11] together with the FACT FTlite light alloy database (2013).

4.3 Results

The following text illustrates the effect of SHT as well as variations of Mg, Si and Cu on AA6061 NA kinetics when Sn is present in Al-Mg-Si alloy.

4.3.1 Solution Treatment Temperature

As shown in **Figure 1**a the alloy containing 430 at. ppm Sn solution heat treated at 570 °C preserves the as-quenched hardness for about 14 days of NA. A decreased SHT temperature leads to earlier hardening after ~4 days (550 °C), 2 days (530 °C) and 8 h for 510 °C.

The alloy with a Sn-content of 70 at. ppm (**Figure 1**b) SHT treated at 570°C exhibits an initial hardness increase after about 4 days of RT storage. Also for this alloy the same dependence

from decreasing SHT is perceived; hardening starts at ~2 days (550 °C), ~28 h (530 °C) and ~8 h (510 °C).
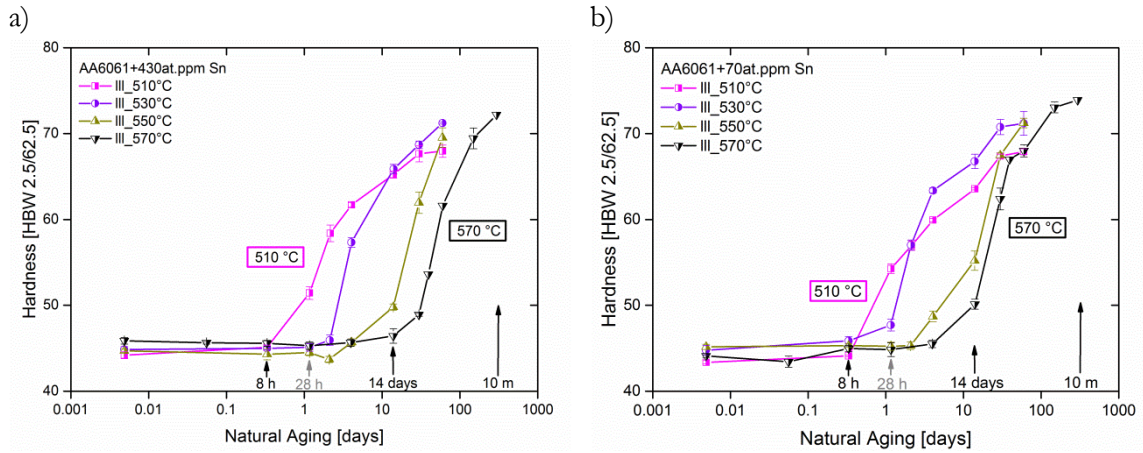
Figure 1. Effect of the SHT temperature on NA kinetics for AA6061 with the addition of a) 430 at. ppm Sn and b) 70 at. ppm Sn. With decreasing SHT an earlier initial hardness increase is perceived.

4.3.2 Composition

To monitor the influence of the main alloying elements Mg, Si and Cu a reference alloy with average amounts is compared with alloys containing one element either at high (h) or low concentration (l), **Table 1**. As depicted in **Figure 2**, for a SHT of 570 °C the average alloy starts hardening after about 1 day, followed by a steep hardness increase. It reaches its maximum hardness after ~90 days. **Figure 2**a indicates a significant influence of Si on hardening kinetics. With low amounts of 0.61 wt.% the alloy stays ~7 days in its soft state, with a high content (0.83 wt.%) it already hardens after ~8 h. The Mg-influence on NA kinetics for Sn added AA6061 is shown in **Figure 2**b. The hardening kinetics are not strongly dependent on the Mg-content, although the trend is similar to Si; a lower Mg-content slightly decreases the rate of hardening kinetics and vice versa. Cu variation leads to only small differences in the NA kinetics.
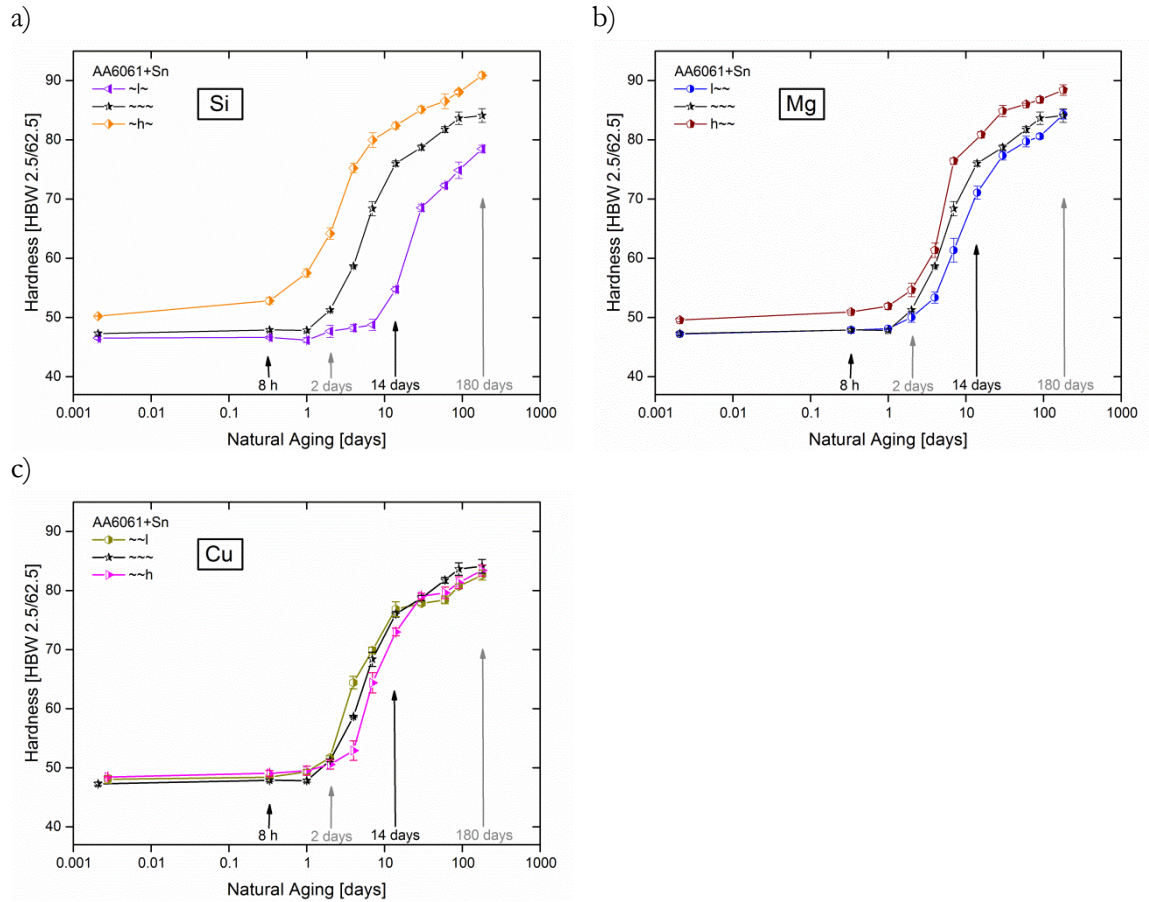
Figure 2. Influence of a) Si, b) Mg and c) Cu on NA kinetics in AA6061 with ~95 at. ppm of Sn after annealing at 570 °C.

4.3.3 Thermodynamic Calculations

Figure 3 shows for all tested alloys the calculated Sn-solubility curves in fcc Al dependent on temperature. In order to always exceed maximum solubility, a Sn amount of 0.1 wt.% was used for the calculations.

For alloys with low Mg-, Si- and Cu-content (no. 1 and 2 in **Table 1**) a maximum of ~60 at. ppm Sn-solubility can be observed at 570 °C. With decreasing temperature a rapid decline in the maximum dissolved Sn-amount is perceived.

Figure 3b shows the effect of Si-variation in Sn-added AA6061. The average alloy no. 3 (Mg 0.87, Si 0.72 and Cu 0.30, all in wt.%) also exhibits its maximum Sn-solubility at 570 °C. At the same temperature higher Si-content results in increased Sn-solubility. Significantly lower amounts dissolve in the alloy with low Si-content.

The Mg-influence at 570 °C shown in Figure 3c indicates lower Sn-solubility for higher Mg concentrations but smaller differences for medium and low content compared to the impact of Si. With decreasing temperature the Sn-solubility decreases.

With regard to Cu, the thermodynamic calculations between ~0.20 and ~0.38 wt.% do not suggest any influence on the Sn-solubility limit below the maximum at 570 °C.
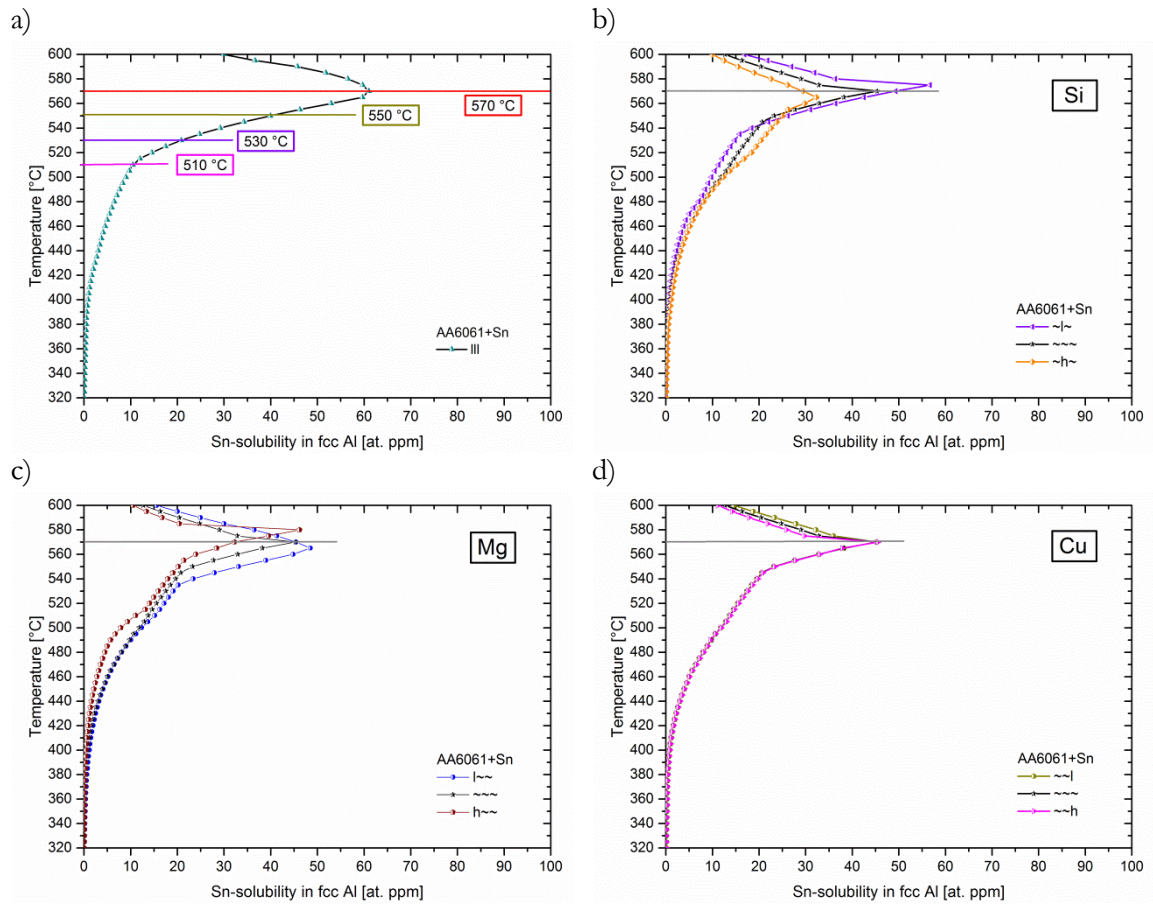
Figure 3. Thermodynamic calculation of the solubility of Sn in the Al matrix. The influence of a) solution treatment temperature and b) Si-, c) Mg-, d) Cu-content in AA6061 is shown.

4.4 Discussion

The present investigation demonstrates that various processing parameters like the solution treatment temperature as well as alloy composition can have significant influence on the effect of Sn on NA kinetics. The suppressive effect of Sn on NA kinetics decreases with decreasing annealing temperature. This goes along with the results from thermodynamic calculations using CALPHAD software, which indicate lower Sn-solubility in the fcc Al matrix with decreasing temperature.

Variations in chemical composition can always occur in industrially produced alloys, due to variations in production or unavoidable macro segregations which form during casting [12]. To estimate the influence of the main alloying elements Si, Mg and Cu on the suppression of NA, high and low concentrations were compared to a reference alloy with medium contents of these elements. Decreasing Si in Sn-added AA6061 by 0.2 wt.% delayed hardening by orders of magnitude, i.e. from 8 h to about 7 days. Note that such strong effect on NA kinetics is known for Sn addition to Al-Mg-Si alloys [8], but not for conventional variations of the main alloying

elements in the margins of commercial alloys [13]. The variation of Mg and Cu showed only small effects on NA. Thermodynamic calculations indicate that Si strongly reduces the solid solution content of Sn in fcc Al. Furthermore, a smaller effect of Mg and almost no effect of Cu was found from the theoretical investigation of the solubility of Sn, which was supported by the experimental results.

As expected from results presented in reference [8], which states that for Sn additions above the solubility limit no further retardation of hardening is achievable, an alloy containing Sn beyond that level, i.e. 430 at. ppm in **Figure 1**a, preserves the as-quenched hardness for about 14 days of NA. Sn-contents below the solubility limit (like 70 at. ppm in **Figure 1**b) exhibit an earlier hardness increase (e.g. here after about 4 days of RT storage). In general, from experiments and calculations it can be stated that higher amounts of Sn dissolved in fcc Al lead to a stronger suppression of NA.

To quantify the retarding effect of Sn on NA in AA6061 we recently proposed a retardation factor R (Equation 1) using DFT-computed vacancy-Sn binding energies and thermodynamic modeling [8]. This factor mainly takes into account that any diffusional processes at a given temperature are controlled by a residual untrapped vacancy concentration. The link between the calculated Sn-solubility values (Figure 2) and the suppression of NA (Figure 1) can be easily established by looking at Equation 1, where c_{Sn} is the concentration of Sn in fcc Al, ΔE_{SV} is the solute-vacancy binding energy and k is Boltzmann's constant [8].

$$R = 1 + 12c_{Sn}(e^{\Delta E_{SV}/kT}) \tag{1}$$

For the SHT applied, it is assumed that the total amount of dissolved Sn at SHT, which complies with the calculated equilibrium level (Figure 3), is quenched-in resulting in c_{Sn} at RT. The linear dependence of the retardation factor R on c_{Sn} can be used to understand experimental results. Reduction in c_{Sn} at RT due to decreasing annealing temperature can explain why the effect of Sn on kinetics is reduced for alloys 1 and 2 (70 or 430 at. ppm Sn) compared to NA after 570 °C. Comparable conclusions can be drawn with regard to the Si-influence. Less Si means higher c_{Sn} at 570 °C resulting in retardation of hardening during RT storage. For Mg, although less pronounced, the same trend applies. Cu-variation does not seem to change c_{Sn} at any temperature, which might explain the negligible effect on kinetics.

With the help of thermodynamic calculations it is possible to shed more light upon the reasons why rising annealing temperature and also varying chemical composition changes the retarding effect of Sn on NA kinetics dramatically.

The following conclusions can be made:

- Increasing the solution treatment temperature raises the quenched-in concentrations of Sn dissolved in the fcc Al matrix resulting in an increased delay in natural aging.
- Variations of the main alloying elements Si, Mg and Cu affect the Sn-solubility and hence the impact of Sn additions on natural aging kinetics.

In general a careful design of solution treatment and alloy composition is necessary when a modification of natural aging kinetics is intended by minute addition of Sn to Al-Mg-Si alloys.

Acknowledgements

References

1.   F. Ostermann, *Anwendungstechnologie Aluminium*, 2nd ed. (Springer, 2007).

2.   S. Pogatscher, H. Antrekowitsch, H. Leitner, T. Ebner, and P. Uggowitzer, "Mechanisms controlling the artificial aging of Al-Mg-Si Alloys," Acta Materialia **59**, 3352–3363 (2011).

3.   J. Banhart, C. Chang, Z. Liang, N. Wanderka, M. Lay, and A. Hill, "Natural aging in Al-Mg-Si alloys - A process of unexpected complexity," Advanced Engineering Materials **12**, 559–571 (2010).

4.   A. Ried, P. Schwellinger, and H. Bichsel, "Untersuchungen über den Zwischenlagerungseffekt bei AlMgSi-Legierungen," Aluminium **53**, 595–599 (1977).

5.   I. Kováćs, J. Lendvai, and E. Nagy, "The mechanism of clustering in supersaturated solid solutions of A1-Mg2Si alloys," Acta Metallurgica **20**, 975–983 (1972).

6.   H. Zandbergen, S. Andersen, and J. Jansen, "Structure determination of Mg5Si6:particles in Al by dynamic electron diffraction studies," Science **277**, 1221–1225 (1997).

7. S. Pogatscher, H. Antrekowitsch, H. Leitner, D. Pöschmann, Z. Zhang, and P. Uggowitzer, "Influence of interrupted quenching on artificial aging of Al-Mg-Si alloys," Acta Materialia **60**, 4496–4505 (2012).

8. S. Pogatscher, H. Antrekowitsch, M. Werinos, F. Moszner, S. Gerstl, M. F. Francis, W. A. Curtin, J. F. Löffler, and P. J. Uggowitzer, "Diffusion on Demand to Control Precipitation Aging: Application to Al-Mg-Si Alloys," Phys. Rev. Lett. **112**, 225701–225705 (2014).

9. I. J. Polmear, "Role of Trace Elements in Aged Aluminium-Alloys," Materials Science Forum **13-14**, 195–214 (1987).

10. S. Pogatscher, M. Werinos, and Antrekowitsch, H. and Uggowitzer, P.J., "The role of vacancies in the aging of Al-Mg-Si alloys," Materials Science Forum, 1008–1013 (2014).

11. C. Bale, P. Chartrand, S. Degterov, G. Eriksson, K. Hack, R. Ben Mahfoud, J. Melançon, A. Pelton, and S. Petersen, "FactSage thermochemical software and databases," Calphad: Computer Coupling of Phase Diagrams and Thermochemistry **26**, 189–228 (2002).

12. S. Pogatscher, H. Antrekowitsch, and P. Uggowitzer, "Interdependent effect of chemical composition and thermal history on artificial aging of AA6061," Acta Materialia **60**, 5545–5554 (2012).

13. S. Hirth, G. Marshall, S. Court, and D. Lloyd, "Effects of Si on the aging behaviour and formability of aluminium alloys based on AA6016," Materials Science and Engineering A **319-321**, 452–456 (2001).

5 INFLUENCE OF ALLOY PRODUCTION HISTORY

For the previous studies presented in the preceding chapters the used materials were gravity mould-cast and rolled in laboratory. For the transfer of the trace element effect to industrial scale production, a confirmation that industrially wrought sheets or plates behave comparably was therefore pending. The present study investigated the influence of the production route of AA6061 with and without Sn addition for two different solution treatment temperatures, and with two different combinations of Mg-, Si- and Cu-content.

Influence of Alloy Production History on Natural Aging of AA6061 Modified with Sn[*]

Although Al-Mg-Si alloys are widely used in cast, wrought and extruded shapes, the processes leading to the negative effect of natural pre-aging on artificial aging are still not fully understood. Finding a way to avoid this phenomenon of 6xxx series aluminum alloys has been subject of numerous research studies. Recently it has been shown that minute additions of Sn suppress and/or reduce this effect. Sn retards the hardness increase during natural aging and also enhances artificial aging kinetics and maximum hardness. As these previous studies used material gravity mould-cast in laboratory, a confirmation that wrought sheets or plates behave comparably is pending. The present study investigates the influence of the production route of AA6061 with and without Sn additions, and with two different combinations of Mg-, Si- and Cu-content.

5.1   Introduction

Most commercial Al-Mg-Si alloys are subject to the negative effect of natural aging (n.a.) on artificial aging. This adverse effect appears within minutes of room temperature (RT) storage after quenching from solution treatment temperatures (STT) $\sim$530 °C [1,2]. By subsequent heat treating at temperatures of commonly 150 to 180 °C, natural aging significantly retards hardening kinetics and reduces the achievable strength [3–6]. Due to this characteristic property, alloy development of 6xxx series aluminium alloys is of major interest for alloy producers and their customers in the automotive, shipbuilding, architecture, and aviation industries. Thus many researches have addressed this problem [1,6–9]. Still, the exact microstructural processes leading to this effect are not fully understood.

Recent research improved the understanding of the negative effect and attributed its origin to the clustering of Mg and Si at ambient temperatures after quenching from STT [6]. These n.a. clusters are assumed to trap quenched-in vacancies and are known to dissolve slowly during subsequent artificial aging. Thus, clusters act as stable vacancy prisons and retard further hardening, as the nucleation of the major hardening phase β´´ [10] depends on the during dissolution of clusters released vacancies [11].

Based on the idea to avoid this detrimental cluster formation at RT, further research revealed that trace additions of the element Sn to the alloy AA6061 could suppress n.a. for > 2 weeks

after a solution heat treatment (SHT) at 570 °C and water-quenching to RT [12–15]. This can be explained by the high solute-vacancy binding energy of Sn (~0.3 eV [12]), because of which quenched-in vacancies are preferentially trapped in Sn-vacancy pairs leaving fewer vacancies in the matrix for the diffusion of Mg and Si-atoms. Consequently, cluster formation is slowed down and n.a. is retarded for orders of magnitude.

For alloy development and possible application of the Sn-effect in industrial production, also the influences of temperature and composition are of importance. It has been found that a careful design of solution treatment and alloy composition is necessary when a modification of n.a. kinetics is intended by trace additions of Sn to Al-Mg-Si alloys [12,13]. Variation of the Sn-content in the alloy AA6061 revealed that retardation of n.a. linearly depends on the concentration of Sn in fcc Al c_{Sn} [12]. Atom probe tomography investigations showed that maximum retardation of n.a. kinetics is achievable by Sn-additions at the solubility limit at STT (~100 at. ppm Sn at 570 °C in AA6061 [12]). Accordingly, investigations of STTs in the range of 510 °C to 570 °C revealed a later onset of n.a.-hardening at higher STT [13]. An increasing c_{Sn} at higher STT (confirmed by thermodynamic calculations using the CALPHAD approach) can explain why the effect of Sn on n.a. kinetics is increased. Investigations of the influence of the main alloying elements Mg, Si and Cu on Sn-solubility demonstrate a significant effect of Si-content [13]. Variation of the Si-content from 0.6 wt.% to 0.8 wt.% in AA6061 reduces c_{Sn} for the STT of 570 °C and thus the RT stability of the alloy. Variation of the Mg- and Cu-content, however, results in only small effects on n.a. kinetics. All above-mentioned studies have been carried out on gravity mould-cast material produced and rolled in laboratory-scale equipment.

In product development processes, however, the transition of laboratory experiments on material produced at small scale to experiments on industrially produced material is always a critical factor. In this study identical heat treatment procedures are applied to as-rolled sheets or plates from AMAG rolling GmbH to illustrate the comparability of the aging behaviour to gravity mould-cast material.

5.2   Experimental

The AA6061 alloys 1 (Sn-added), 2 (Sn-free), 5 (Sn-added) and 6 (Sn-free) were supplied by AMAG rolling GmbH. Whereas alloys 1 and 2 were provided in the form of wrought, as-rolled plates (plate thickness ~27 mm), alloys 5 and 6 were supplied in the form of wrought, as-rolled sheet (sheet thickness ~3 mm). Their composition is given in Table 1.

Alloy 4 (Sn-free, Table 1) was prepared by melting an industrially produced AA6061 alloy followed by gravity mould-casting. Alloys 3 and 7 (Table 1) were produced from an AA6061 base alloy which contained Mg 0.80, Si 0.59, Cu 0.21, Fe 0.47, Cr 0.15, Mn 0.12, Zn 0.05 and Ti 0.04, all in wt.%, as well as ~95 at. ppm Sn which complies with the solubility limit in alloy 3 at 570 °C (see introduction). The base alloy was casted by the Austrian Institute of Technology (AIT) in Ranshofen (Austria) using a continuous vertical chill caster in laboratory scale. To obtain the composition of alloys 3 and 7 in Table 1, the base alloy was re-melted and Mg, Si and Cu were added accordingly. After alloying, Ar gas purging was applied to reduce the hydrogen content before the alloys were gravity mould-cast to small slabs (150 × 90 × 35 mm^3). After cutting and homogenization, hot rolling to sheets was conducted in laboratory scale from 20 to 4.2 mm thickness. To check the chemical composition, optical emission spectrometry (SPECTROMAXx from SPECTRO) was performed on the final plates using an appropriate calibration sample as standard.

Solution heat treatment of hardness test samples was performed in a circulating air furnace (Nabertherm N60/85 SHA) at different temperatures (530 °C or 570 °C) for 20 min. Subsequent quenching was carried out in water at RT (25 °C) and samples were kept in a Peltier-cooled incubator (IPP from Memmert) at RT for n.a..

Compared to the AA6061 alloys numbered 1-4 with low concentrations of Mg, Si and Cu (l: low), alloys 5-7 are intended to depict the different n.a. behaviour of AA6061 specimens with average Mg-, Si- and Cu-contents (~: average).

Table 1: Composition and production history of alloys (Al in balance)
(ind. = industrial, lab. = laboratory, r. = rolled)

Alloy	Symbol MgSiCu	Material	Sn [at.ppm]	Sn [wt.%]	Mg [wt.%]	Si [wt.%]	Cu [wt.%]	Fe [wt.%]	Mn [wt.%]	Cr [wt.%]	Zn [wt.%]	Ti [wt.%]
1	lll	ind. plate	89	**0.039**	0.76	0.55	0.217	0.455	0.109	0.135	0.046	0.059
2	lll	ind. plate	10	0.0045	0.79	0.59	0.216	0.455	0.107	0.143	0.049	0.069
3	lll	lab.-cast+r.	95	**0.042**	0.78	0.61	0.210	0.493	0.119	0.154	0.045	0.040
4	lll	lab.-cast+r.	6	0.0026	0.81	0.62	0.220	0.485	0.111	0.146	0.059	0.081
5	~~~	ind. sheet	88	**0.039**	0.92	0.72	0.323	0.478	0.140	0.268	0.039	0.085
6	~~~	ind. sheet	5	0.0021	0.91	0.72	0.260	0.450	0.130	0.190	0.050	0.060
7	~~~	lab.-cast+r.	95	**0.041**	0.87	0.72	0.300	0.510	0.118	0.148	0.045	0.041

Brinell hardness measurements (HBW 2.5/62.5) were carried out using an EMCO-Test M4 unit. A maximum standard deviation of 2.0 HBW was achieved.

5.3 Results

Figure 1 depicts the n.a. behaviour of the plate alloys no. 1 and 2 with low concentrations of Mg, Si and Cu (Table 1) and the influence of STT. Starting from the as-quenched hardness of ~49-50 HBW, the Sn-free alloy no. 2 shows similar hardening kinetics after SHT at 530 °C and 570 °C: Shortly after quenching hardening starts, it is followed by a steeper logarithmic hardness increase after ~3 h of n.a. and another slower, but still continuous increase till 180 days at RT.

The Sn-added plate alloy 1, in contrast, shows a significant influence of STT on n.a. kinetics (Figure 1). After annealing at 570 °C the alloy preserves the as-quenched hardness of ~48 HBW for ~14 days and reaches ~71 HBW after 180 days at RT. After SHT at 530 °C the initial hardness increase is preserved for ~1 day followed by a steep logarithmic increase and another slower hardening after ~30 days until 180 days.
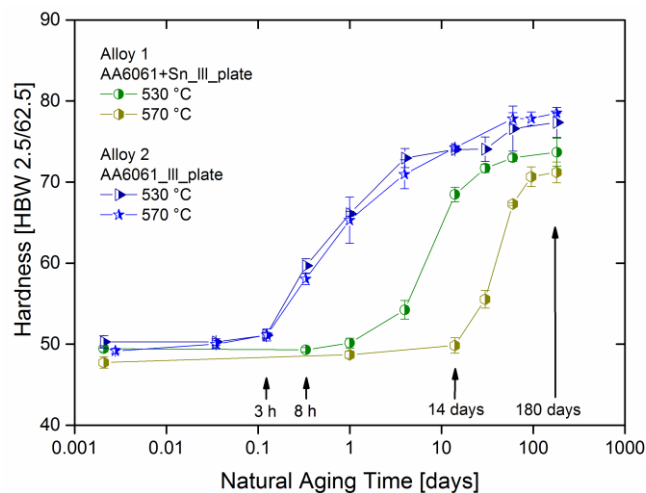
Figure 1: Natural aging (n.a.) kinetics of plate alloys 1 and 2 (see Table 1) after solution heat treatment (SHT) at 530 °C or 570 °C. The Sn-free alloy 1 doesn't show an influence of solution treatment temperature (STT) whereas the Sn-added variant shows an earlier onset of hardening at lower STT.

Figure 2 compares the n.a. behaviour of the plate alloys 1 and 2 (see also Figure 1) with the n.a. kinetics of the gravity mould-cast alloys 3 and 4 of comparable composition (Table 1) after a SHT at 530 °C. After quenching, the gravity mould-cast alloy 3 with Sn-addition starts softer (~45 HBW) than the plate alloy no. 1 (~49 HBW). Thereafter, alloy 3 shows the onset of hardening after ~1 day at RT followed by a steep logarithmic hardness increase. The alloy reaches similar hardness as the plate alloy 1 after ~4 days after which both alloys, plate and gravity mould-castd, show comparable n.a. kinetics as well as similar hardness values.

The Sn-free alloy 4 produced by gravity mould-casting shows about the same as-quenched hardness as the Sn-added variant no. 3 (Figure 2). Compared to the Sn-free plate alloy 2, alloy 4

shows faster initial hardening, thus after ~0.125 days (3 h) both alloys exhibit similar hardness followed by comparable aging kinetics until 180 days. The same comparison between n.a. kinetics of industrial plate and laboratory scale produced material as described before for SHT at 530 °C applies for n.a. after 570 °C (not depicted).
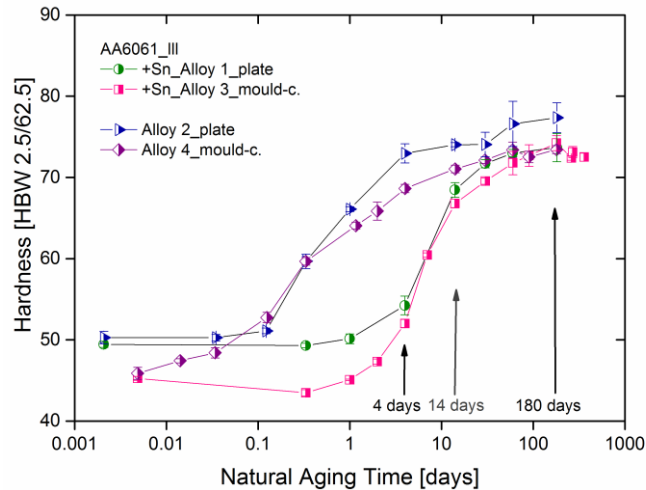
Figure 2: Comparison of n.a. kinetics of plate alloys 1 and 2 to gravity mould-cast alloys 3 and 4 after SHT at 530 °C.

Figure 3 shows the influence of Sn-addition and STT on n.a. kinetics of the sheet alloys no. 5 and 6 with average concentrations of Mg, Si and Cu (Table 1). Comparable to the Sn-free plate alloy 2 (Figure 1), Sn-free sheet material (alloy 6) exhibits similar hardening kinetics for the STTs 530 °C and 570 °C. Unlike alloy 2 with low Mg-, Si- and Cu-content (Figure 1), samples of alloy 6 annealed at 530 °C exhibit lower hardness values than after SHT at 570 °C.

Sn-added sheet material (alloy 5) preserves the as-quenched hardness after both STTs (530 °C and 570 °C) until ~1 day of n.a. (Figure 3). Thereafter, n.a. after SHT at 530 °C shows slightly faster hardening kinetics than a SHT at 570 °C until ~4 days, followed by a lower gradient and similar hardness as the Sn-free variant after annealing at the same STT.

The Sn-added AA6061 plate material with average concentrations of Mg, Si and Cu shows the same trend as sheet material with regard to slightly faster n.a. kinetics after the onset of hardening (~1 day) and SHT at 530 °C than after annealing at 570 °C (not depicted, compare Figure 3).
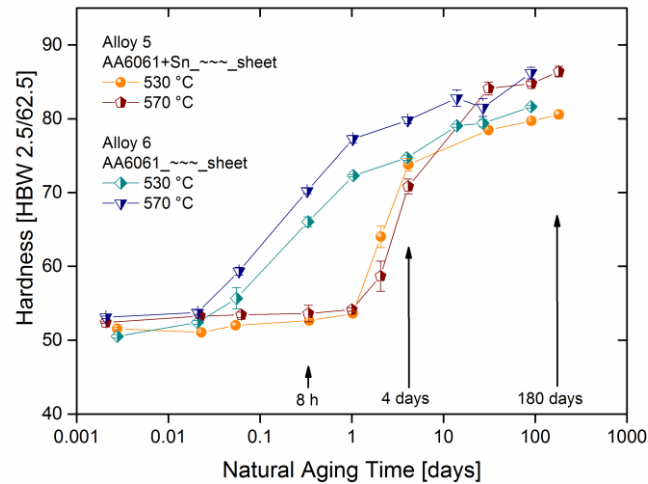
Figure 3: Comparison of n.a. kinetics of sheet alloys 5 (Sn-added) and 6 (Sn-free) after SHT at 530 °C or 570 °C.

Figure 4 compares the n.a. behaviour of the Sn-added sheet alloy 5 with the gravity mould-cast alloy 7 of comparable composition (see Table 1). As found for alloys no. 1 and 3 in Figure 2, also alloy 7, produced in laboratory, shows lower as-quenched hardness values than the industrially produced sheet material: ~46 HBW versus ~52 HBW after quenching from 530 °C (Figure 4a) and ~47 HBW versus ~52 HBW after 570 °C (Figure 4b). Upon SHT at 530 °C (Figure 4a), alloy 7 starts hardening after ~8 h and reaches similar hardness as the sheet alloy after ~1 day. Then both alloys, sheet and gravity mould-cast, exhibit comparable n.a. kinetics as well as similar hardness values. After SHT at 570 °C (Figure 4b) both alloys, sheet and gravity mould-cast, show the initial hardness increase after ~1 day followed by similar n.a. kinetics and comparable hardness ~90 days later.

a)

b)
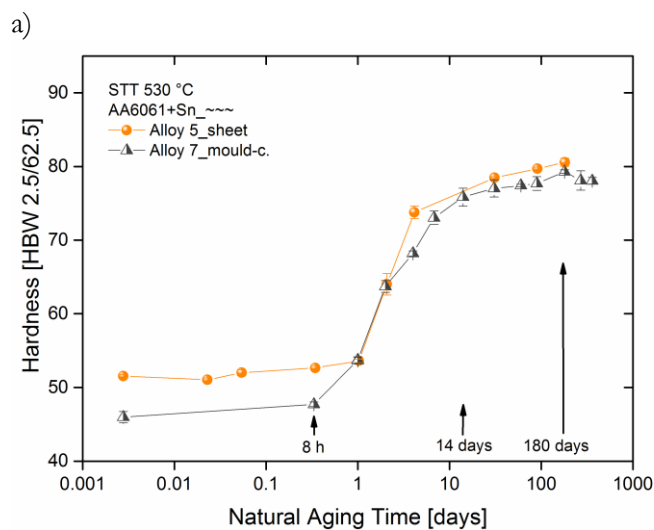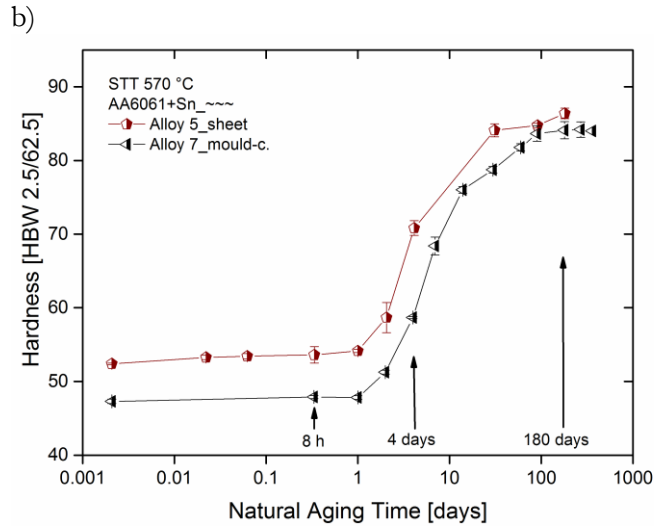
Figure 4: Comparison of n.a. kinetics of Sn-added sheet alloy 5 and gravity mould-cast alloy 7 of comparable composition after (a) SHT at 530 °C or (b) 570 °C.

5.3   Discussion and Conclusion

The present investigation compares n.a. kinetics of AA6061 material produced in laboratory (gravity mould-cast) and in industry (sheet or plate material of comparable composition as the gravity mould-cast alloys). Comparable to the Sn-added gravity mould-cast material, investigated in previous studies [13,14], industrially produced plates (Figure 1) and sheets (Figure 3) show a significant influence of STT and composition. Maximum Sn-solubility after quenching from STT is supposed to be obtained for alloys 1 and 3, i.e. ~100 at. ppm at 570 °C in AA6061 [12] with low Mg-, Si- and Cu-content (Table 1, see introduction). Thus alloy 1 achieves a maximum retardation of n.a. of ~14 days after a SHT at 570 °C (Figure 1). At lower STTs (530 °C in Figures 1 and 3), less Sn is dissolved in fcc Al at the beginning of n.a. and thus the suppressive effect of Sn on n.a. kinetics decreases.

As shown in Figure 3, the Sn-added sheet alloy 5 (average concentrations of Mg, Si and Cu) shows a smaller influence of STT than plate alloy no. 1 with low Mg-, Si- and Cu-content (Figure 1; same for alloy 3, not depicted). This is a side effect and can be explained by the difference of Si-content in alloy 1 (0.6 wt.%) and alloy 5 (0.7 wt.%): An increase in Si-content reduces the solubility of Sn c_{Sn} at STT and thus the RT stability of the alloy. Sn-free AA6061 alloys, in contrast, do not show an influence of STT on n.a. kinetics, independently of the production history or Si-content (investigated between 530 °C and 570 °C, see Figures 1 and 3).

A more detailed comparison of n.a. behaviour of Sn-added AA6061 alloys produced industrially or in laboratory, reveals a lower as-quenched hardness of gravity mould-cast

material independently of the STT (Figures 2 and 4). The hardness difference remains constant until the onset of hardening of the gravity mould-cast alloy. Thereafter an assimilation of hardening kinetics and hardness values prevails. Several circumstances may be responsible for this behaviour: i) during industrial rolling, sheets and plates reach higher degrees of deformation than the investigated gravity mould-cast sheets rolled in laboratory. Higher degrees of deformation can cause smaller fragmented intermetallic phases in production material, which may contribute to higher initial hardness values slightly. ii) Industrial rolling causes different texture of grains.

The following conclusions can be made:

- The suppressive effect of Sn on natural aging kinetics of the alloy AA6061 is comparable for industrially produced material and material produced in laboratory with comparable composition.
- Sn-free alloys, in contrast to Sn-added alloys with the same concentrations of Mg-, Si- and Cu, do not show an influence of solution treatment temperature (STT) on natural aging kinetics for the STTs investigated.

Acknowledgments

References

1. J. Banhart, C. Chang, Z. Liang, N. Wanderka, M. Lay, and A. Hill, "Natural aging in Al-Mg-Si alloys - A process of unexpected complexity," Advanced Engineering Materials **12**, 559–571 (2010).
2. I. Kovaćs, J. Lendvai, and E. Nagy, "The mechanism of clustering in supersaturated solid solutions of A1-Mg$_2$Si alloys," Acta Metallurgica **20**, 975–983 (1972).
3. F. Ostermann, *Anwendungstechnologie Aluminium*, 2nd ed. (Springer, 2007).
4. Brenner, P., Kostron, H., "Über die Vergütung der Aluminium–Magnesium–Silizium–Legierungen (Pantal). Einfluß einer Raumtemperaturlagerung auf die folgende Warmaushärtung - Abhängigkeit der Aushärtung von der Höhe des Magnesium- und

Siliziumgehaltes sowie von Kupferzusätzen," Zeitschrift für Metallkunde **4**, 89–97 (1939).

5. A. Ried, P. Schwellinger, and H. Bichsel, "Untersuchungen über den Zwischenlagerungseffekt bei AlMgSi-Legierungen," Aluminium **53**, 595–599 (1977).

6. S. Pogatscher, H. Antrekowitsch, H. Leitner, T. Ebner, and P. Uggowitzer, "Mechanisms controlling the artificial aging of Al-Mg-Si Alloys," Acta Materialia **59**, 3352–3363 (2011).

7. C. Marioara, S. Andersen, J. Jansen, and H. Zandbergen, "The influence of temperature and storage time at RT on nucleation of the β″ phase in a 6082 Al-Mg-Si alloy," Acta Materialia **51**, 789–796 (2003).

8. J. Banhart, M. Lay, C. Chang, and A. Hill, "Kinetics of natural aging in Al-Mg-Si alloys studied by positron annihilation lifetime spectroscopy," Physical Review B **83**, 014101 (2011).

9. S. Esmaeili and D. Lloyd, "Modeling of precipitation hardening in pre-aged AlMgSi(Cu) alloys," Acta Materialia **53**, 5257–5271 (2005).

10. H. Zandbergen, S. Andersen, and J. Jansen, "Structure determination of Mg_5Si_6:particles in Al by dynamic electron diffraction studies," Science **277**, 1221–1225 (1997).

11. S. Pogatscher, H. Antrekowitsch, H. Leitner, D. Pöschmann, Z. Zhang, and P. Uggowitzer, "Influence of interrupted quenching on artificial aging of Al-Mg-Si alloys," Acta Materialia **60**, 4496–4505 (2012).

12. S. Pogatscher, H. Antrekowitsch, M. Werinos, F. Moszner, S. Gerstl, M. F. Francis, W. A. Curtin, J. F. Löffler, and P. J. Uggowitzer, "Diffusion on Demand to Control Precipitation Aging: Application to Al-Mg-Si Alloys," Phys. Rev. Lett. **112**, 225701–225705 (2014).

13. M. Werinos, H. Antrekowitsch, W. Fragner, T. Ebner, P. Uggowitzer, and S. Pogatscher, "Influence of Sn-solubility on suppression of natural aging in an AA6061 aluminum alloy.," in *Proceedings of MS&T14. Materials Science & Technology 2014* (2014), pp. 1283–1290.

14. M. Werinos, H. Antrekowitsch, W. Fragner, T. Ebner, P. Uggowitzer, and S. Pogatscher, "Influence of temperature on natural aging kinetics of AA6061 modified with Sn," (Paper presented at TMS 2015, Orlando, USA, 2015).

15. M. Werinos, H. Antrekowitsch, F. Moszner, P. J. Uggowitzer, and S. Pogatscher, *Ultrafast artificial aging of Al-Mg-Si alloys* (in preparation, 2015).

6 TRACE ELEMENT ASSISTED CONTROL OF NATRUAL AGING

The previous chapters showed the negligible influence of the production route on the achievable suppression of natural aging with and without Sn addition whereas the solution treatment temperature and the Mg, Si and Cu content show a significant influence. This chapter goes one step further and describes a design strategy to control natural aging in the course of which also the effect of a combined trace element addition of Sn and indium (In) is explored. The effects of Mg, Si and Cu content on natural aging kinetics are interpreted via their influence on the Sn solubility and clustering mechanisms. Theoretical considerations suggest that the reduction of the free excess vacancy concentration by Sn is most important for early Si clustering and thus explains the significant effect of Si addition. Cu is believed to show a similar, but weaker effect as Sn whereas Mg lowers the quenchable Sn solubility only. Application of the proposed design strategy led to the development of a new Sn-added Al–Mg–Si alloy that shows suppression of natural aging for > 6 months and significant artificial aging potential.

Design strategy for controlled natural aging in Al–Mg–Si alloys[*]

This study presents a design strategy for Al–Mg–Si alloys to control natural aging. Recently, trace addition of Sn was shown to suppress natural aging for up to two weeks, which was explained by the strong trapping of vacancies to Sn atoms. Here we explore the effect of solution treatment temperature, the combination of trace elements such as Sn and In, and the composition of main hardening elements Mg, Si and Cu on natural aging. The results are discussed based on the dissolvable amount of trace elements and their effect on diffusion retardation, and solute clustering mechanisms in Al–Mg–Si alloys. Thermodynamic calculations using the CALPHAD approach show that maximum retardation of natural aging is achievable at the highest trace element solubility, which exists at significantly different solution treatment temperatures for Sn or In. The effects of Mg, Si and Cu content on natural aging kinetics are interpreted via their influence on the Sn solubility and clustering mechanisms. It is proposed that Sn additions reduce the concentration of excess vacancies, which is most important for early Si clustering, and that the effect of Cu is comparable to the effect of Sn, but less pronounced. Based on the investigated parameter space, a design concept is proposed and an Al–Mg–Si alloy showing suppression of natural aging for > 6 months and significant artificial aging potential is demonstrated.
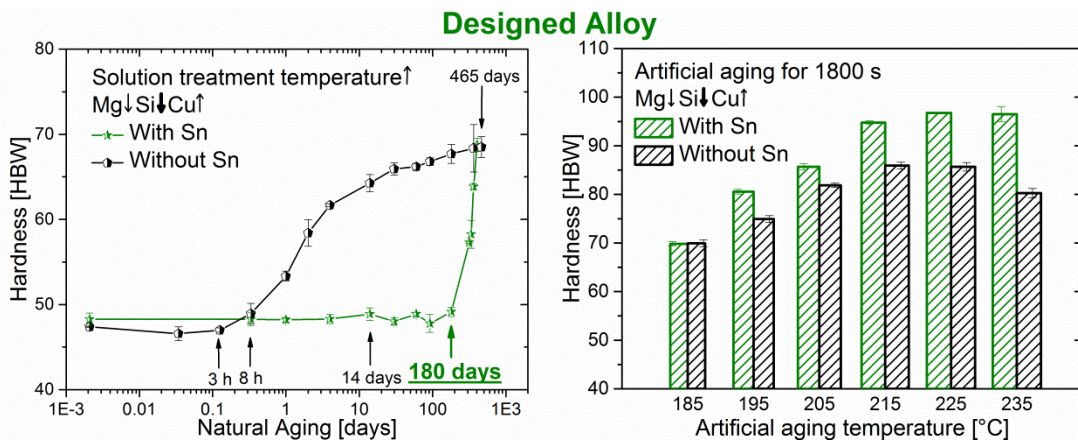
6.1   Introduction

Age hardenable Al–Mg–Si alloys (6xxx-series) are widely used in the transport, automotive, shipbuilding, and aviation industry [1–3]. Aluminum allows lightweight construction for

---

improved fuel efficiency and reduced CO_2-emissions. 6xxx-series alloys are especially attractive as they combine good formability with medium to high strength after age hardening, good corrosion resistance, and weldability. In the automotive industry, for example, they are used as outer skin alloys, for non-decorative inner parts, and structural or crash components with individual property criteria [1–5]. Yet, the ever-growing demand to increase formability and strength for more complex parts of lower weight drives the alloy development considerably [4–7].

The delivery of semi-finished products mostly occurs after quenching to enable forming operations at low strength prior to the final heat treatment to gain high strength [4,8–10]. During natural aging (n.a.), which starts directly after quenching from solution heat treatment, the material hardness increases due to solute clustering of Mg- and Si-atoms [11–15]. This generates two problems for the transportation industry: first, dynamic hardening during n.a. reduces formability [4]; second, clustering results in a negative effect of n.a. on subsequent artificial aging (a.a.) [12,13,16–18]. The transportation industry, however, requires several months of stable formability combined with good a.a. performance so as to obtain reproducibility of designs that have increasing complexity [4,10]. Hence, pre-aging treatments have been developed to improve a.a. and to achieve a relatively "stable" material state [8,10,19–22]. Pre-aging treatments, however, result in undesired hardness increase [10].

This study presents a novel design strategy for 6xxx-alloys to achieve maximal suppression of n.a. hardening after quenching while still achieving a potential for significant a.a. The study builds on recent research showing that trace tin (Sn) addition to the alloy AA6061 can suppress n.a. for 2 weeks and simultaneously improve the a.a. potential [23–25]. Here, detailed investigation of the effects of solution treatment temperature and Mg, Si and Cu content in alloys, with and without trace element additions, leads to a designed Al–Mg–Si alloy showing n.a. stability for more than 6 months.

6.2 Methods

Table 1 shows the alloys studied here. Alloys 1-13 were produced at the laboratory scale starting from AA6061 base alloys. After re-melting, pure Mg, Si, Cu, Sn or Sn+In were added to the base alloys to obtain the compositions listed in Table 1. Ar gas purging was applied to reduce the hydrogen content before the alloys were cast to slabs. After cutting and homogenization, hot rolling was conducted. To check the chemical composition of the final sheets, optical emission spectrometry and, for In, inductively coupled plasma mass spectroscopy, were used. Alloys 14 and 15 with and without Sn addition were industrially

produced and supplied by AMAG rolling GmbH in the form of wrought plates. Note that all chemical compositions in Table 1 are near to commercial AA6061 alloys.

Table 1: Composition of alloys (Al in balance)

Alloy	Symbol MgSiCu	Sn [at.ppm]	Sn [wt.%]	In [wt.%]	Mg [wt.%]	Si [wt.%]	Cu [wt.%]	Fe [wt.%]	Mn [wt.%]	Cr [wt.%]	Zn [wt.%]	Ti [wt.%]
1	↓↓↓	430	0.188		0.82	0.63	0.232	0.59	0.111	0.147	0.059	0.079
2	↓↓↓	96	0.042		0.78	0.61	0.210	0.493	0.119	0.154	0.045	0.040
3	↓↓↓	70	0.030		0.79	0.58	0.213	0.482	0.11	0.147	0.057	0.088
4	↓↓↓	6	0.0026		0.81	0.62	0.220	0.485	0.111	0.146	0.059	0.081
5	~~~	94	0.041		0.87	0.72	0.300	0.510	0.118	0.148	0.045	0.041
6	↑~~	94	0.041		0.96	0.71	0.288	0.456	0.116	0.147	0.044	0.043
7	↓~~	96	0.042		0.77	0.73	0.298	0.462	0.117	0.148	0.045	0.042
8	~↑~	91	0.040		0.85	0.83	0.287	0.449	0.116	0.147	0.045	0.043
9	~↓~	94	0.041		0.86	0.61	0.245	0.456	0.116	0.148	0.045	0.042
10	~~↑	91	0.040		0.84	0.70	0.379	0.443	0.115	0.150	0.043	0.043
11	~~↓	89	0.039		0.86	0.74	0.203	0.476	0.116	0.151	0.045	0.044
12	↓↓↓	98	0.043	0.039	0.78	0.62	0.211	0.5	0.118	0.152	0.045	0.039
13	~~~	91	0.040	0.04	0.84	0.71	0.245	0.447	0.115	0.150	0.043	0.044
14	↓↓↑	96	0.042		0.78	0.434	0.357	0.455	0.109	0.136	0.047	0.056
15	↓↓↑	5	0.002		0.76	0.411	0.355	0.452	0.109	0.138	0.045	0.053

Solution heat treatment of hardness test samples was performed in a circulating air furnace (Nabertherm N60/85 SHA) at temperatures between 510-570 °C for 1.2×10^3 s. Subsequent quenching was carried out in water at room temperature and, for n.a., samples were kept in a Peltier-cooled incubator IPP (Memmert) at 25 °C. Artificial aging was undertaken in an oil bath.

Brinell hardness measurements (HBW 2.5/62.5) were carried out using an EMCO-Test M4 unit. A maximum standard deviation of 2.0 HBW was achieved.

Thermodynamic calculations of the alloys were performed using FactSage™ 6.4 software [26,27] together with the FACT FTlite light alloy database (2014). For the equilibrium calculations the alloy compositions according to Table 1 were entered and all possible phases selected from the databases. Data of phases and their stabilities, compositions and element solubility were calculated between 320 °C and 600 °C.

6.3 Results

6.3.1 Influence of solution treatment temperature

Figures 1 and 2 show the effect of solution treatment temperature on n.a. kinetics of alloys 1-3 containing 430, 96 and 70 at. ppm Sn, respectively, and alloy 4 (Table 1). Alloy 4 represents the "Sn-free" reference alloy with low Mg, Si and Cu content (↓: low, symbol: ↓↓↓) and commercial amounts of impurity elements (compare ref. [23]). A solution heat treatment at 570 °C is compared to 550 °C, 530 °C and 510 °C. After annealing at 570 °C, the alloys containing 430 and 96 at. ppm Sn preserve the as-quenched hardness for ~14 days (Fig. 1a). The alloy with 70 at. ppm Sn starts hardening after more than 4 days (Fig. 1b). At lower solution treatment temperatures hardening starts earlier, followed by a steep logarithmic increase in hardening. Between 530 °C and 570 °C, all alloys reach comparable hardness maxima, which is in contrast to a lower peak hardness after annealing at 510 °C.
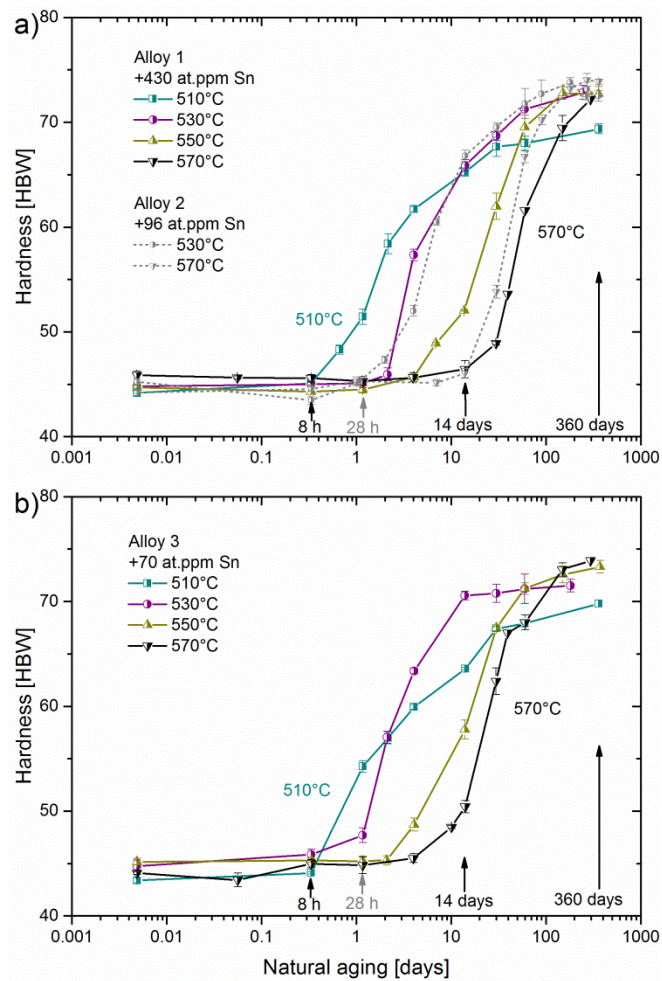
Fig. 1. Influence of solution treatment temperature (570-510 °C) on natural aging kinetics of Sn-added Al–Mg–Si alloys containing a) 430, 96 or b) 70 at. ppm Sn. For all alloys hardening starts earlier at lower solution treatment temperatures.
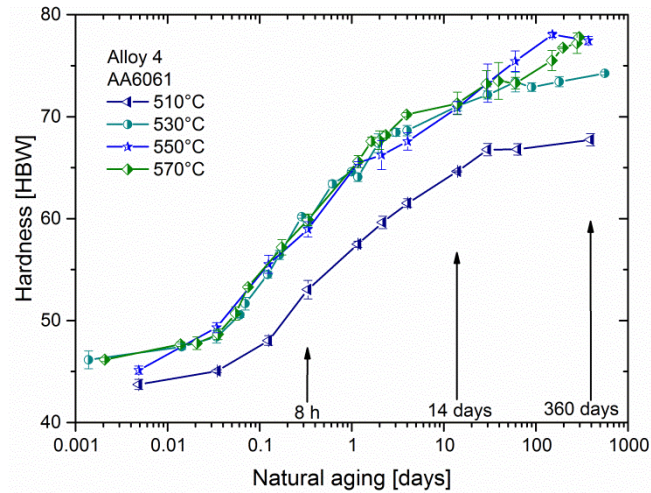
Fig. 2: Influence of solution treatment temperature (570-510 °C) on natural aging kinetics of a commercial, "Sn-free" Al–Mg–Si alloy. The alloy shows similar hardening kinetics for the solutions treatment temperatures investigated.

The "Sn-free" reference alloy 4 starts hardening within minutes and exhibits similar kinetics after all solution treatment temperatures (Fig. 2). Between 530 °C and 570 °C, hardness values are similar. After annealing at 510 °C, in contrast, the alloy shows ~5-8 HBW lower hardness until 360 days. The final hardness maxima, however, are comparable to the Sn-added alloys 1-3 after same heat treatments.

6.3.2 Addition of In as a second trace element

To elucidate the effect of combined Sn and In addition on n.a. kinetics (Fig. 3), alloys 12 (symbol: ↓↓↓) and 13 (symbol: ~~~) with low or average Mg, Si and Cu content contain ~0.04 wt.% In (~100 at. ppm, Table 1) in addition to ~0.04 wt.% Sn. Figure 3 shows the n.a. curves after annealing at 530 °C and 570 °C. The In-added low-alloyed alloy starts hardening after ~14 days nearly independent of solution treatment temperature. The In-added average alloy shows slightly retarded hardening kinetics after 530 °C compared to annealing at 570 °C.
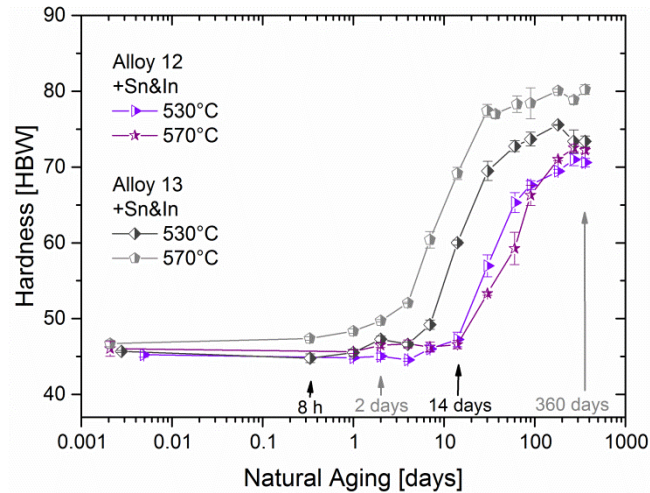
Fig. 3. Natural aging (n.a.) kinetics of two different Sn- and In-added Al–Mg–Si alloys (Tab. 1), annealed at 530 °C and 570 °C. The alloys only show small differences in their hardening kinetics for the solutions treatment temperatures investigated.

6.3.3 Influence of Mg, Si and Cu content

To evaluate the influence of Mg, Si and Cu on n.a. kinetics for alloys with Sn addition, Fig. 4-6 compare the average alloy 5 (symbol: ~~~; for Mg Si Cu), with alloys containing ~0.1 wt.% higher (↑: high) or lower (↓: low) concentrations of the corresponding element (Table 1). After annealing at 570 °C (Fig. 4a-6a) the average alloy starts hardening after ~1 day; after 530 °C (Fig. 4b-6b) n.a. starts earlier. Alloys 8 (symbol: ~↑~) and 9 (symbol: ~↓~) with high or low Si content demonstrate a significant influence of Si on hardening kinetics (Fig. 4). After both solution treatment temperatures, a higher Si content (0.83 wt.%) results in earlier hardening than the average alloy. With lower Si content (0.61 wt.%) hardening is retarded, starting after ~7 days after annealing at 570 °C (Fig. 4a). For Mg-variation (Fig. 5, alloys 6 and 7), a weaker effect on n.a. kinetics is found, although the trend is similar to Si: a lower Mg content produces slightly retarded n.a. hardening and vice versa. Cu variations (Fig. 6) show a general tendency to marginally retard hardening with increasing Cu content.

Further, for the alloy with high Si content, significantly higher initial hardness values are measured after annealing at 570 °C. The same applies for high Mg content, but less pronounced as compared to Si. For Cu variations, no significant shift of the initial hardness is seen.
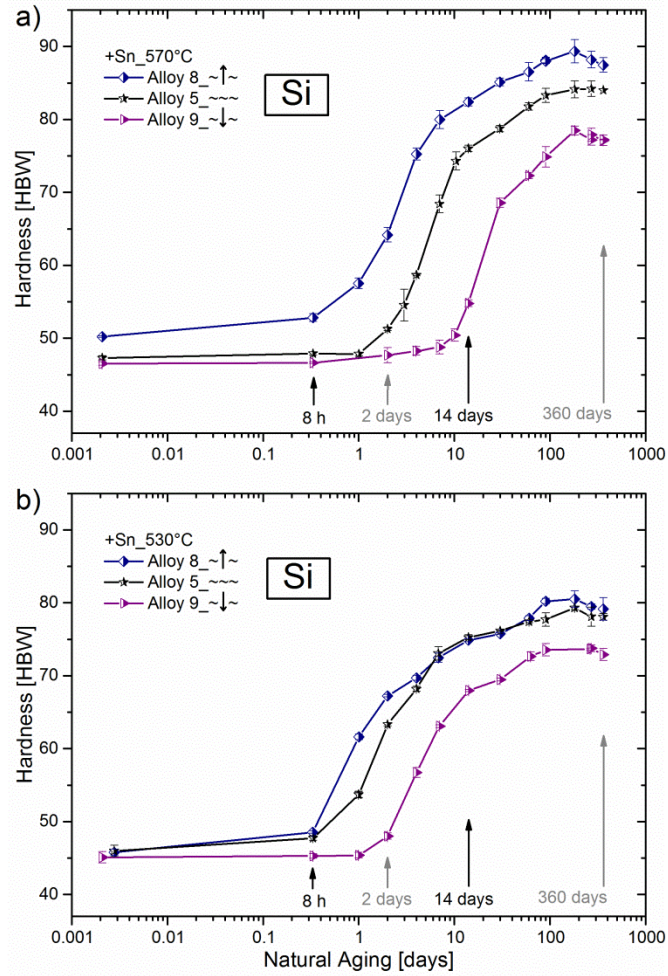
Fig. 4. Influence of Si content on natural aging kinetics of Sn-added Al–Mg–Si alloys annealed at a) 570 °C or b) 530 °C. An alloy with average Mg, Si and Cu content (symbol: ~~~) is compared to alloys with high (↑) or low (↓) Si content (Tab. 1). With lower Si content hardening starts delayed.
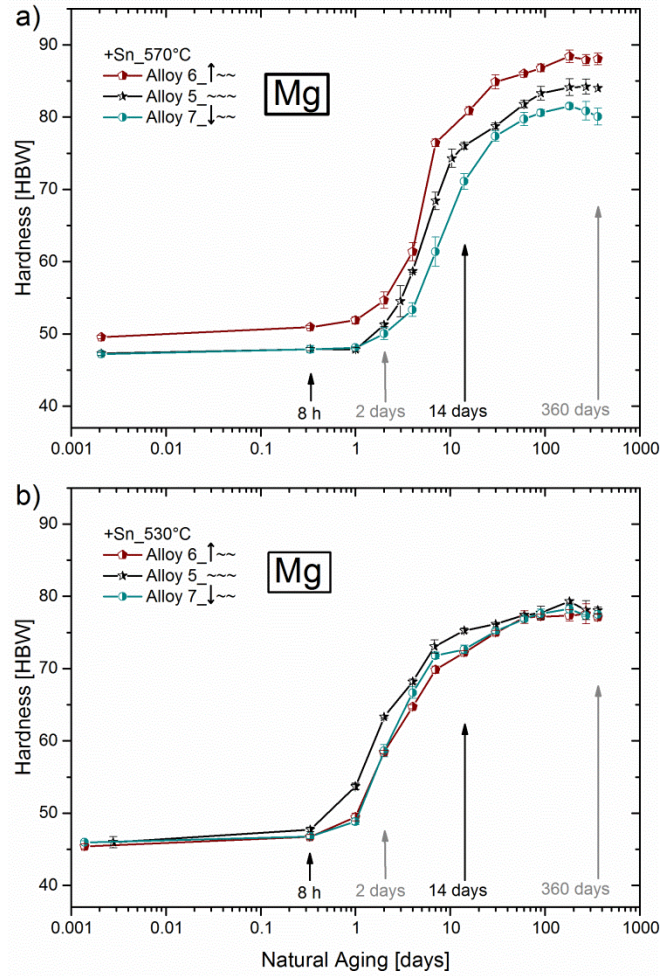
Fig. 5. Influence of Mg content on natural aging kinetics of Sn-added Al–Mg–Si alloys annealed at a) 570 °C or b) 530 °C. An alloy with average Mg, Si and Cu content (symbol: ~~~) is compared to alloys with high (↑) or low (↓) Mg content (Tab. 1). The effect of Mg is not pronounced at 530 °C, but hardening starts delayed for a lower Mg content at 570 °C.
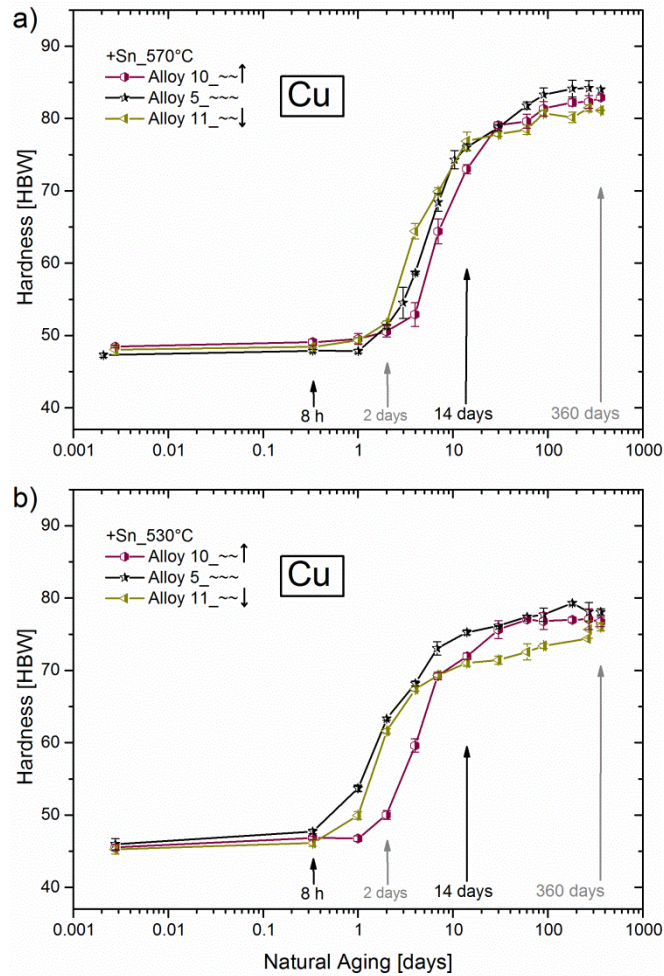
Fig. 6. Influence of Cu content on natural aging kinetics of Sn-added Al–Mg–Si alloys annealed at a) 570 °C or b) 530 °C. An alloy with average Mg, Si and Cu content (symbol: ~~~) is compared to alloys with high (↑) or low (↓) Cu content (Tab. 1). The results show a general tendency to marginally retarded hardening with increasing Cu content.

6.3.4 Thermodynamic calculations

The thermodynamic calculations in Fig. 7 show the temperature-dependent Sn solubility in the fcc Al matrix between 320 °C and 600 °C for alloys 1, 3 and 14 (Table 1). The low alloyed alloys with 430 and 70 at. ppm Sn show the maximum solubility of Sn at 570 °C (Fig. 7). At lower temperature the solubility decreases. Similar values were calculated for alloy 2, but for the sake of clarity not shown in Fig. 7. The same trend applies for alloy 14, but at 570 °C it exhibits a higher Sn solubility.
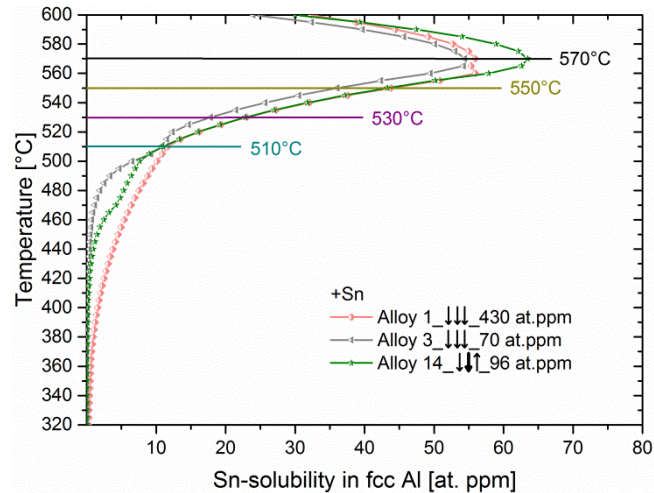
Fig. 7. Calculated temperature dependency of the Sn solubility in fcc Al in Al–Mg–Si alloys containing low Mg, Si and Cu content (symbol: ↓↓↓) or low Mg, very low Si and high Cu content (symbol: ↓↓↑).

For combined Sn and In addition, the thermodynamic calculations in Fig. 8 show two contrary effects of the Sn and In solubility for alloys 12 and 13, with low and average Mg, Si and Cu content, respectively. The higher the Sn solubility, the lower the solubility of In and vice versa, because with decreasing temperature, the In solubility increases.

To evaluate the influence of Si, Mg and Cu on Sn solubility, Figs. 9a-c compare the thermodynamic calculation of the average alloy 5 to alloys 6-11 with varied element contents. According to the calculations, Si addition (in blue) significantly reduces the Sn solubility at temperatures above ~550 °C and below 530 °C (Fig. 9a). An opposite effect is found for lower Si content (in pink). Similar to Si, Fig. 9b indicates a lower Sn solubility for higher Mg concentrations. For Cu variations, the thermodynamic calculations between 0.20 and 0.38 wt.% Cu do not suggest any influence on the Sn solubility (Fig. 9c).

6.4 Discussion

The results showed that n.a. kinetics of the Sn-added Al–Mg–Si alloys is significantly influenced by the Sn content, the solution treatment temperature applied, the Mg, Si and Cu content and additional trace elements.

6.4.1 Solution treatment temperature

The n.a. results of alloys 1-3 with 430, 96 and 70 at. ppm Sn in Fig. 1 showed after solution heat treatments between 570 °C and 510 °C earlier hardening with decreasing temperature. In contrast, the n.a. kinetics of the "Sn-free" reference alloy 4 showed no dependence on solution treatment temperature (Fig. 2). The lower hardness level of the alloy after annealing at 510 °C

is supposed to result from the reduced Mg and Si solubility at this temperature in fcc Al, because of the solvus temperature of Mg₂Si being >510 °C (not depicted). The same applies for the lower peak hardness of alloys 1-3 at 510 °C. The other results can be interpreted with the Sn solubility calculations in Fig. 7.

For the solution heat treatments applied, it is assumed that the total amount of Sn dissolved at the solution treatment temperature is quenched-in, resulting in a concentration of Sn in fcc Al c_{Sn} at room temperature. This implies that the maximum quenchable c_{Sn} is limited by the Sn solubility at a given solution treatment temperature. According to the calculations in Fig. 7, at lower temperature the Sn solubility decreases, which reduces c_{Sn} at room temperature. To quantify the retardation of n.a. hardening at temperature T due to Sn additions, we recently proposed a retardation factor R [23] which shows a linear dependency on c_{Sn},

$$R = 1 + 12c_{Sn}(e^{\Delta E_{SV}/kT}) \tag{1}$$

Where ΔE_{SV} is the solute-vacancy binding energy and k the Boltzmann's constant. Thus the link between the influence of solution treatment temperature on retardation of n.a. hardening (Fig. 1) and the calculated temperature-dependency of the Sn solubility (Fig. 7) can be easily established. A lower quenched-in c_{Sn} at room temperature with decreasing solution treatment temperature explains why alloys 1, 2 and 3 start hardening earlier (Fig. 1). Thus the calculated Sn solubility values are expected to give accurate trends, if not absolute values.

The Sn solubility at 570 °C for alloys 1-3 was calculated to be ~55 at. ppm. From this calculation one would expect no difference in hardening retardation since the Sn content of all alloys is above this value. However, the 70 at. ppm Sn alloy starts hardening earlier than the 96 and 430 at. ppm Sn alloys (compare Fig. 1a and 1b). Alloy 2 with 96 at. ppm and alloy 3 with 430 at. ppm Sn, on the other hand, start hardening at nearly the same time. From this observation we assume that the real Sn solubility of alloys 1-3 is higher than the calculated 55 at. ppm, namely >70 ppm but ≦100 at. ppm. Indeed, the Sn solubility in an AA6061 alloy containing a Mg, Si and Cu content comparable to alloys 1-3 was experimentally found to be ~100 at. ppm after annealing at 570 °C [23]. Consequently, it is assumed that the 96 and 430 at. ppm Sn alloys generate comparable quenched-in c_{Sn}, which explains the similar hardening kinetics (Fig. 1a). Based on these results, the Sn content in alloys 5-14 was adjusted at ~100 at. ppm.

6.4.2 Additional trace elements

Equation 1 predicts that the retardation of n.a. hardening also depends on the strong Sn-vacancy binding energy ΔE_{SV} (~0.24-0.3 eV [23,28,29]). The Sn addition is envisioned to result

in trapping of excess vacancies, which reduces the amount of untrapped vacancies in the Al matrix that control diffusional processes. Consequently, any diffusional processes, like clustering, are slowed down [23]. Yet, this favorable trapping of excess vacancies is limited by the Sn solubility at the solution treatment temperature (section 4.1). Therefore a second element with strong solute-vacancy binding energy, if soluble in fcc Al, is expected to increase the effect of Sn on n.a. kinetics.

To evaluate the effect of combined trace element addition, a diffusion retardation factor R for two different types of trace elements is required. The thermodynamic model assumes two types of dilute solutes dissolved in fcc Al after quenching, with the solute concentrations much higher than the total quenched-in vacancy concentration at the effective quench temperature T_Q [30], $c_S^{(1)}$ and $c_S^{(2)} \gg c_V^{tot}(T_Q)$. During quenching, some excess vacancies are trapped in solute-vacancy pairs at the beginning of n.a. at temperature T (solute-divacancy arrangements, or similar, types of configuration are assumed to be negligible). Only the residual untrapped vacancy concentration $c_V(T)$ is present to control any vacancy-mediated diffusional processes. Thus, n.a. hardening is retarded by a factor $R = c_V^{tot}(T_Q)/c_V(T)$. Following the lines of the derivation in ref. [23] and with the solute-vacancy binding energies ΔE_{SV} of each solute type denoted with a superscript, the retardation factor is

$$R = \frac{c_V(T_Q)}{c_V(T)} = \frac{1 + 12c_S^{(1)}(e^{\Delta E_{SV}^{(1)}/kT}) + 12c_S^{(2)}(e^{\Delta E_{SV}^{(2)}/kT})}{1 + 12c_S^{(1)}(e^{\Delta E_{SV}^{(1)}/kT_Q}) + 12c_S^{(2)}(e^{\Delta E_{SV}^{(2)}/kT_Q})} \tag{2}$$

For sufficient high T_Q, the denominator approaches 1 and can be neglected. Thus, the retardation factor for combined trace element addition is approximately

$$R = 1 + 12c_S^{(1)}(e^{\Delta E_{SV}^{(1)}/kT}) + 12c_S^{(2)}(e^{\Delta E_{SV}^{(2)}/kT}) \tag{3}$$

According to Eq. 3, In fulfills both preconditions to be effective in the retardation of n.a. hardening: (i) it shows a strong solute-vacancy binding energy of ~0.20 eV [28] and (ii) thermodynamic calculations indicate a reasonable solubility in fcc Al (see Fig. 8).

Compared to the solely Sn-added alloys 2 and 5 of comparable composition, the In-added alloys 12 and 13 with low or average Mg, Si and Cu content show significantly retarded n.a. hardening after annealing at 530 °C, while n.a. kinetics after 570 °C are only reduced slightly (compare Fig. 3 to alloy 2 in Fig. 1a and alloy 5 in Fig. 4-6). This can be explained by the trend toward increasing In solubility at lower solution treatment temperatures (Fig. 8). It is concluded that the effect of trace elements on retardation of n.a. hardening can be expanded to a broad

solution treatment temperature range by a combination of Sn and In additions. However, this effect is limited by the mutual influences on element solubility as shown in Fig. 8.
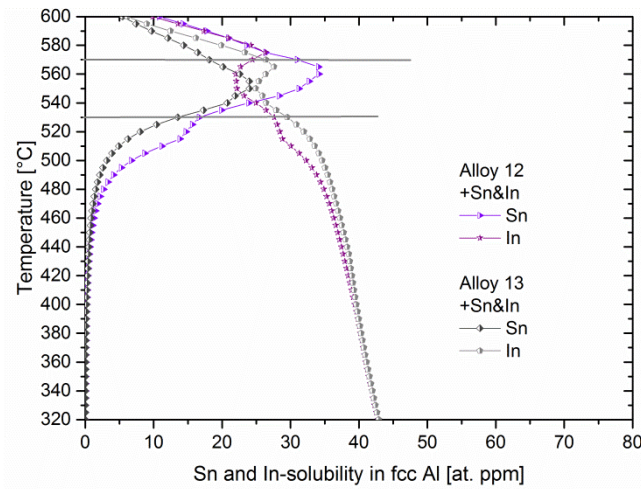
Fig. 8. Calculated temperature dependency of the Sn and In solubility in fcc Al in two different Sn- and In-added Al–Mg–Si alloys (Tab. 1).

6.4.3 Influence of Mg, Si and Cu content and mechanisms

The influence of Mg, Si and Cu content on n.a. kinetics in Fig. 4-6 can be interpreted with the Sn solubility curves in Fig. 9 and considering clustering mechanisms in Al–Mg–Si alloys.

According to Fig. 9a, an increase in Si content reduces the Sn solubility at the solution treatment temperatures investigated and thus reduces c_{Sn}. According to Eq. 1, the reduction of c_{Sn} at 570 °C by a factor of ~1.8 should increase n.a. kinetics by the same factor. The ratio of hardening onset times in Fig. 4a is, however, ~20, decreasing from ~7 days (alloy 9) to ~8 h (alloy 8). Although the computed values of c_{Sn} might be not totally accurate, it is not expected that the error of the thermodynamic calculations is sufficient to account for the observed differences. Thus the lower c_{Sn} only partly explains the observed earlier n.a. hardening for higher Si content (Fig. 4).
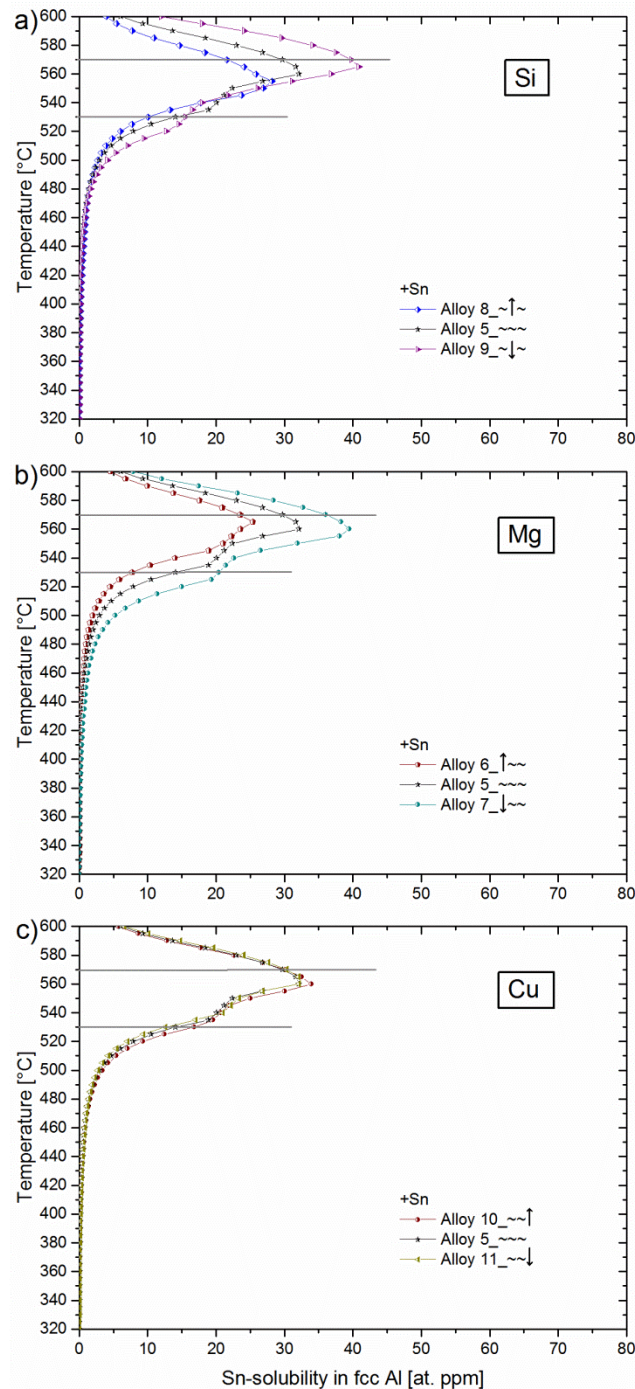
Fig. 9. Influence of the a) Si, b) Mg or c) Cu content on the calculated Sn solubility in fcc Al in Al–Mg–Si alloys. For the nomenclature see Tab. 1 and Fig. 4-6.

We compare our findings with the latest research on n.a. clustering in Sn-free Al–Mg–Si alloys. At the beginning of n.a., clustering is dominated by solute-vacancy complexes (stage I). In the following clustering stage II, the fraction of vacancy-free clusters continuously increases until these dominate [15]. Both types of clusters are interpreted as predominantly involving Si and result in an increase of electrical resistivity or hardening at an initial rate in stage I and a more rapid increase in stage II [13,14,31,32]. Both linear logarithmic stages are present in the hardening curves in Fig. 1-6. With exception of a recent study by Kim et al. [33], most studies

on n.a. kinetics of Sn-free Al–Mg–Si alloys including the effect of Si show, unfortunately, only results for $\geq$ 60 min n.a. [16,34], so that the first stages are not revealed. The only effect observed is a higher n.a. hardness for alloys with increased Si content. Note that the same effect is observable here for Si variations in Fig. 4. In ref. [33] an earlier onset of n.a. hardening is seen the higher the Si content. All studies, including those focusing on the influence of Si content on a.a. kinetics [16,33–35], interpret the higher n.a. hardness or better a.a. performance of high Si-alloyed Al–Mg–Si alloys (e.g. 6016) as being primarily influenced by the early clustering processes [16] and rapidly forming Si(-rich) clusters [33–35], respectively. A higher Si content can be consequently expected to increase early stage clustering kinetics during n.a. [13,14,31,33,36]. The higher initial hardness for high Si content after annealing at 570 °C (Fig. 4a), in contrast, may be attributed to pre-existing Si clusters formed during quenching. Indirect evidence of faster hardening kinetics at higher Si content is given in ref. [36,37] where a pure Al-Mg-Si alloy is compared to an alloy with Fe and Mn addition. The slower hardening kinetics of the Fe- and Mn-containing alloy is attributed to the formation of intermetallic phases containing Si. This lowers the quenchable Si-concentration in the matrix and thus the rate of clustering [36]. Summing up, these studies support the hypothesis that Si-related clustering controls the beginning of n.a. and its kinetics [13,14,31–33,38]. This implies that, due to the formation of Si-vacancy complexes, early Si clustering is controlled by the availability of quenched-in excess vacancies (compare ref. [31,32]) because during n.a., vacancies detach from unstable solute-vacancy complexes or vacancy-containing clusters to transport further solute atoms to emerging vacancy-free clusters [31,32,39]. With Sn additions, the formation kinetics of vacancy free-clusters is supposed to be slowed down due to the favorable trapping of vacancies in stable Sn-vacancy pairs [23], resulting in a reduction of untrapped vacancies available for Si clustering. Thus two trends may produce the accelerated n.a. kinetics at higher Si content in stages I and II (Fig. 4): first, the lower quenched-in c_{Sn} (Fig. 9a) corresponds to fewer trapped vacancies and thus more untrapped vacancies; second, in alloys with higher Si content the vacancy diffusion distances to nearby Si atoms are reduced for untrapped and detached vacancies (compare ref. [40]). A more detailed analysis of the mechanisms involved is the subject of on-going research.

Only in the later clustering stages diffusion of Mg atoms into the emerging clusters does occur (stage III), causing intermediate hardening rate perceived by a transition range before the slowest hardening rate seen at the end of n.a. (stage IV) [13–15,31]. Thus, Mg is believed not to take part in the early clustering processes in stages I and II. Figure 9b shows that Mg addition reduces the calculated Sn solubility by a factor of 1.5 (at 570 °C) to ~2.6 (at 530 °C), which is, at 570 °C, comparable to the difference in retardation of n.a. hardening (Fig. 5). At lower Mg content, the higher quenched-in c_{Sn} favors the trapping of vacancies by Sn and reduces the

number of untrapped vacancies. This is presumed to reduce Si clustering in stages I and II and the diffusion velocity of Mg atoms by a comparable factor. Consequently, in contrast to the strong direct effect of Si on early clustering, it is believed that Mg shows only a secondary effect by influencing the Sn solubility. The higher initial hardness for high Mg content after annealing at 570 °C (Fig. 5a) is attributed to solid solution strengthening. The reduced n.a. kinetics of the alloy with high Mg content after annealing at 530 °C may result from a combination of effects: Thermodynamic calculations of the Sn-added alloys show for increased Mg and same Si content a constant Si solubility at 570 °C, whereas at 530 °C the Si solubility already decreases the higher the Mg content, assumingly due to Mg$_2$Si-Phase formation. Hence, the lower quenched-in Si concentration may reduce n.a. kinetics while the simultaneously reduced quenched-in c_{Sn} increases n.a. kinetics. For the average alloy with fastest n.a. kinetics one or both effects may contribute weaker.

An increase in Cu content does not influence Sn solubility, but shows a trend toward retardation of n.a. hardening (compare Fig. 5 and 9c). Cu addition to Al–Mg–Si alloys is known to lower the first clustering peak in DSC-measurements that is related to Si clustering in stages I-II and also to reduce early stage n.a. kinetics [36,41–43]. Cu also shows an attractive solute-vacancy binding energy [28,44]. Assuming that Cu stays dissolved in the fcc Al matrix, it may bind vacancies and lower the number of Si-vacancy complexes, which slows down clustering kinetics. This interpretation by ref. [36] is compatible with our interpretation of the effect of Sn on clustering processes in Al–Mg–Si alloys. A higher Cu content may thus add to the effect of Sn in Fig. 5 in some way. But in contrast to Sn, we assume that Cu only weakly immobilizes vacancies, which would explain the weaker effect of Cu on n.a. kinetics.

6.4.4 Design strategy for maximum retardation of natural aging

Based on the knowledge established through the studies reported above, we propose the following design strategy to obtain Al–Mg–Si alloys with considerably reduced n.a. kinetics:

Identification of the solution treatment temperature with maximum solubility of Sn;

Detailed adjustment of the Mg, Si and Cu contents according to their individual effects on the solubility of Sn and on early Si clustering;

Alloying of additional trace elements of high solute-vacancy binding energy.

Step (i) is applicable to any Al–Mg–Si alloy. With thermodynamic calculations of Sn-added alloys, the solution treatment temperature with the highest Sn solubility is computable. For the alloy investigated in this study, this is ~560-570 °C (Fig. 7).

Step (ii) requires understanding of the influence of composition on n.a. kinetics. Compared to the average alloy 5 (Tab. 1), the investigations on alloys within the standards of AA6061 revealed retarded n.a. hardening for low Si- and high Cu-content, and a small effect of Mg on

kinetics (Fig. 3-5). However, Cu addition should be treated with care, to still meet the product requirements on corrosion resistivity [45–47].

Step (iii) expands steps (i) and (ii) with a second trace element of high solute-vacancy binding energy and reasonable solubility in the Al–Mg–Si alloy. A significant retardation of n.a. hardening at low solution treatment temperatures (~530 °C) was found with In addition to Sn-added AA6061 (Fig. 6). For industrial application of In, however, the high metal price needs to be considered.

6.4.5 Designed alloy

In light of the above, we have developed a Sn-added Al–Mg–Si alloy that contains low Mg, very low Si and high Cu content, while remaining within the standards of alloy AA6061 (alloy 14 in Tab. 1, symbol: ↓↓↑). For reference, we have also prepared a similar alloy, alloy 15, containing essentially no Sn additions. Derived from the strategy steps this approach focuses on identifying the maximum suppression of n.a. hardening with trace Sn addition.

The calculations presented in Fig. 7 confirm that the developed alloy shows the highest calculated Sn solubility in fcc Al of all alloys investigated in this study. Figure 10a compares n.a. hardening curves of the designed alloy 14 with the "Sn-free" alloy 15 of comparable composition. The designed alloy shows improved n.a. stability at both solution treatment temperatures, i.e. after annealing at 530 °C hardening starts after 14 days. After a solution heat treatment at 570 °C, the as-quenched alloy 14 is stable for more than 180 days. Thereafter, it takes ~405 days of n.a. until alloy 14 reaches a peak hardness that is similar to that of the "Sn-free" alloy 15. As further shown in Fig. 10a, the "Sn-free" alloy 15 shows comparable hardness values and n.a. kinetics for both solution treatment temperatures investigated. But compared to the "Sn-free" alloy 4 with low Mg, Si and Cu content (Fig. 2), alloy 15 reveals significantly slower hardening kinetics, i.e. it starts hardening only after ~3 h and takes more than 90 days to reach maximum hardness. Consequently, Sn-free Al–Mg–Si alloys within the range of commercial compositions can achieve retarded n.a. hardening for low Si and high Cu content.

For applications of Al–Mg–Si alloys, the a.a. performance for optimum strength in service is also required. Figure 10b shows the a.a. performance of the designed alloy 14 after annealing at 570 °C followed by 3 months of n.a.; results for the "Sn-free" alloy 15 are also shown. During a.a. at 185 °C, the designed alloy 14 starts hardening immediately and reaches a maximum hardness of ~103 HBW. After 1800 s of a.a. the "Sn-free" variant shows similar hardness. The inset to Fig. 10b compares the a.a. results after 1800 s to higher a.a. temperatures, i.e. 195 °C, 205 °C, 215 °C, 225 °C and 235 °C. Here, the designed alloy shows the greatest increase in hardness of up to ~97 HBW, which can be explained by unconventional fast a.a. kinetics of Sn-added Al–Mg–Si alloys found at high a.a. temperatures (ref. [24]).
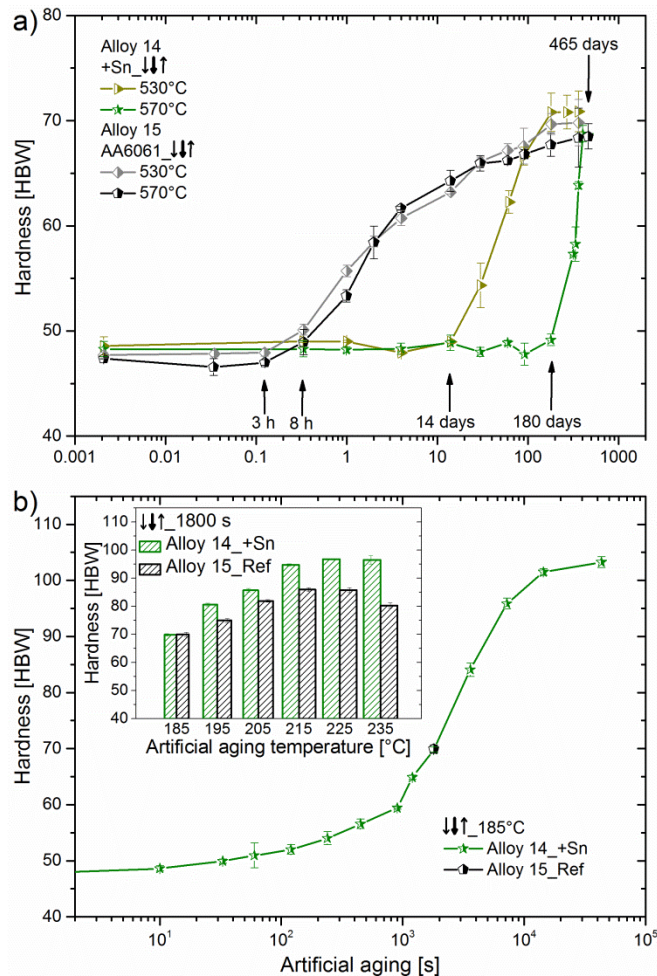
Fig. 10. Aging potential of the designed, Sn-added Al–Mg–Si alloy containing low Mg, very low Si and high Cu content (symbol: ↓↓↑); results for the "Sn-free" reference alloy are also shown. a) Natural aging (n.a.) kinetics after annealing at 530 °C and 570 °C where after annealing at 570 °C, the designed alloy is stable for >180 days. b) Artificial aging (a.a.) after annealing at 570 °C followed by 3 months of n.a. where the designed alloy shows a significant a.a. potential.

6.4 Conclusions

The objective of this study was to develop a design strategy to reduce natural aging (n.a.) kinetics of Al–Mg–Si alloys while still achieving a significant artificial aging (a.a.) potential. Through an extensive study across a range of composition space, we have found that

- The addition of trace elements with high solute-vacancy binding energy and reasonable solubility in the Al matrix retards diffusional processes during n.a.

- For maximum retardation of n.a. hardening with trace Sn addition, the application of a high solution treatment temperature is necessary to obtain the maximum quenchable Sn solubility.

- The influences of Mg, Si and Cu content are explained via their effect on Sn solubility and individual effect on clustering. Si increases n.a. clustering kinetics and lowers the quenchable Sn solubility. Cu retards n.a. hardening, but does not influence the Sn solubility and is therefore believed to show a similar, but weaker effect as Sn. Mg lowers the quenchable Sn solubility only.

- Application of a new design strategy has led to the development of a new Sn-added Al–Mg–Si alloy that shows n.a. stability of more than 6 months and a significant a.a. potential.

Overall, the new design strategy and underlying aging mechanisms have the potential to trigger the development of new industrial Al–Mg–Si alloys in general, and especially in the field of transportation industries that have a demand for highly formable materials.

Acknowledgements

References

[1]   Polmear IJ. Light alloys: From traditional alloys to nanocrystals. 4th ed. Oxford, Burlington, MA: Elsevier/Butterworth-Heinemann; 2006.

[2]   Ostermann F. Anwendungstechnologie Aluminium. 3rd ed. Berlin, Heidelberg: Springer Berlin Heidelberg; 2014.

[3]   Kammer C. Aluminium-Taschenbuch. 16th ed. Düsseldorf: Aluminium-Verl; 2002.

[4]   Prillhofer R, Rank G, Berneder J, Antrekowitsch H, Uggowitzer PJ, Pogatscher S. Materials 2014;7:5047–68.

[5]   Hirsch J. Transactions of Nonferrous Metals Society of China (English Edition) 2014;24:1995–2002.

[6]   Hirsch J. Materials Transactions 2011;52:818–24.

[7]   Hirsch J. Materials Forum 2004;28:15–23.

[8]   Abouarkoub A, Thompson GE, Zhou X, Hashimoto T, Scamans G. Metallurgical and Materials Transactions A 2015:1–14.

[9]   Berneder L, Prillhofer R, Enser J, Grohmann T. TMS Light Metals 2014:177–82.

[10]   Birol Y. Materials Science and Engineering A 2005;391:175–80.

[11]   Panseri C, Federighi T. Journal of the Institute of Metals 1966;94:99–105.

[12]   Kovaćs I, Lendvai J, Nagy E. Acta Metallurgica 1972;20:975–83.

[13]   Banhart J, Chang C, Liang Z, Wanderka N, Lay M, Hill A. Advanced Engineering Materials 2010;12:559–71.

[14]   Banhart J, Lay M, Chang C, Hill A. Physical Review B 2011;83:14101.

[15]   Liu M, Čížek J, Chang C, Banhart J. Acta Materialia 2015;91:355–64.

[16]   Brenner, P., Kostron, H. Zeitschrift für Metallkunde 1939;4:89–97.

[17]   Ried A, Schwellinger P, Bichsel H. Aluminium 1977;53:595–9.

[18]   Pogatscher S, Antrekowitsch H, Leitner H, Ebner T, Uggowitzer P. Acta Materialia 2011;59:3352–63.

[19]   Yan Y, Liang ZQ, Banhart J. Materials Science Forum 2014;794-796:903–8.

[20]   Miao W, Laughlin D. Journal of Materials Science Letters 2000;19:201–3.

[21]   Shen C. Journal of Materials Science and Technology 2011;27:205–12.

[22]   Cao L, Rometsch PA, Zhong H, Muddle BC. Materials Science Forum 2010;654-656:918–21.

[23]   Pogatscher S, Antrekowitsch H, Werinos M, Moszner F, Gerstl S, Francis MF, Curtin WA et al. Physical Review Letters 2014;112:225701–5.

[24]   Werinos M, Antrekowitsch H, Kozeschnik E, Ebner T, Moszner F, Löffler JF, Uggowitzer PJ et al. Scripta Materialia 2016;112:148–51.

[25]   Werinos M, Antrekowitsch H, Fragner W, Ebner T, Uggowitzer PJ, Pogatscher S. Influence of Alloy Production History on Natural Aging of AA6061 Modified with Sn, in: GDMB (Ed.). Proceedings of European Metallurgical Conference (EMC) 2015. Clausthal-Zellerfeld: GDMB Verlag GmbH; 2015. p. 303–310.

[26]   Bale C, Chartrand P, Degterov S, Eriksson G, Hack K, Ben Mahfoud R, Melançon J et al. Calphad: Computer Coupling of Phase Diagrams and Thermochemistry 2002;26:189–228.

[27]   Bale C, Bélisle E, Chartrand P, Decterov S, Eriksson G, Hack K, Jung I et al. Calphad: Computer Coupling of Phase Diagrams and Thermochemistry 2009;33:295–311.

[28]   Wolverton C. Acta Materialia 2007;55:5867–72.

[29]   Simonovic D, Sluiter M. Physical Review B - Condensed Matter and Materials Physics 2009;79.

[30]   Fischer F, Svoboda J, Appel F, Kozeschnik E. Acta Materialia 2011;59:3463–72.

[31]   Chang C, Liang Z, Schmidt E, Banhart J. International Journal of Materials Research 2012;103:955–61.

[32]   Chang C, Banhart J. Metallurgical and Materials Transactions A: Physical Metallurgy and Materials Science 2011;42:1960–4.

[33]   Kim S, Kim J, Tezuka H, Kobayashi E, Sato T. Materials Transactions 2013;54:297–303.

[34]   Hirth SM, Marshall GJ, Court SA, Lloyd DJ. Materials Science and Engineering A 2001;319-321:452–6.

[35]   Gupta A, Lloyd D, Court S. Materials Science and Engineering A 2001;316:11–7.

[36]   Liang Z. Clustering and Precipitation in Al-Mg-Si Alloys. PhD thesis. Berlin; 2012.

[37]   Liang Z, Chang C., Wanderka N., Banhart J., Hirsch J. The Effect of Fe, Mn and Trace Elements on Precipitation in Al-Mg-Si Alloy, in: Proceedings of the 12th International Conference on Aluminium Alloys. p. 492–497.

[38]   Zandbergen MW, Xu Q, Cerezo A, Smith G. Acta Materialia 2015;101:136–48.

[39]   Zurob H, Seyedrezai H. Scripta Materialia 2009;61:141–4.

[40]   Torsaeter M, Hasting H, Lefebvre W, Marioara C, Walmsley J, Andersen S, Holmestad R. Journal of Applied Physics 2010;108:073527-1 - 073527-9.

[41]   Liang Z, Chang C, Banhart J, Hirsch J. The effect of Cu and Cr on clustering and precipitation in Al–Mg–Si alloys., in: ICAA13: 13th International Conference on Aluminum Alloys: John Wiley & Sons, Inc; 2012. p. 1125–1130.

[42]   Zandbergen MW, Cerezo A, Smith G. Acta Materialia 2015;101:149–58.

[43]   Kim J, Kobayashi E, Sato T. Materials Transactions 2015;56:1771–80.

[44]   Mantina M, Wang Y, Chen L, Liu Z, Wolverton C. Acta Materialia 2009;57:4102–8.

[45]   Svenningsen G, Larsen MH, Walmsley J, Nordlien JH, Nisancioglu K. Corrosion Science 2006;48:1528–43.

[46]   Wang Zb, Li H, Miao F, Sun W, Fang B, Song R, Zheng Z. Materials Science and Engineering A 2014;590:267–73.

[47]   Svenningsen G, Larsen M, Nordlien J, Nisancioglu K. Corrosion Science 2006;48:3969–87.

7 EFFECT OF STORAGE TEMPERATURE

The design strategy for controlled natural aging in Al-Mg-Si alloys presented in the previous chapter takes account of processing parameters controllable during the individual production steps. A maybe more difficult to control parameter is the storage temperature of solution heat treated material before the final artificial aging step, which is investigated in the next study. Two different AA6061 alloys with and without trace Sn addition show a strong dependence of natural aging hardening kinetics on temperature. As Sn suppresses the negative effect due to controlled buffering of quenched-in excess vacancies at low temperatures, the study evaluates and analyses the buffering performance of Sn in the temperature range between 5 and 45 °C.

Influence of Temperature on Natural Aging Kinetics of AA6061 Modified with Sn[*]

Al-Mg-Si alloys are widely used in cast, wrought and extruded form. A characteristic property of these alloys is the negative effect of natural pre-aging at room temperature on artificial aging. Minor additions of Sn suppress the adverse effect of room temperature aging due to controlled buffering of quenched-in excess vacancies at low temperatures. In this study we evaluate the buffering performance of Sn in the temperature range between 5 and 45 °C. This is investigated for two Sn-added AA6061 alloys with systematic variation in their Mg-, Si- and Cu-content, for comparison the natural aging kinetics of a Sn-free alloy is studied. In general a strong dependence of hardening kinetics on temperature and on chemical composition is observed. Results of aging kinetics are discussed in terms of common clustering theories and the temperature dependent trapping effect of Sn on excess vacancies.

7.1   Introduction

Today numerous age hardenable Al-Mg-Si alloys are used as structural materials in cast, wrought, rolled or extruded form in the automotive, shipbuilding, architecture, and aviation industry [1–4]. Rich alloys like AA6061 show a strong adverse influence of natural aging (NA) on subsequent artificial aging (AA). This negative effect appears within minutes of room temperature (RT) storage after quenching from solution treatment temperatures (STT) ~800 K [4,5]. During AA at commonly 150 to 180 °C, NA retards the hardening kinetics by an order of magnitude and reduces the achievable strength. Since discovered 75 years ago [6] many researchers have addressed this problem [2,4,7,8]. Still, the exact mechanisms remain unsolved. Recently, the origin of the negative effect on AA has been linked to the clustering processes at RT [2]. The simple concept assumes that clusters formed during NA act as traps for quenched-in thermal vacancies during AA. Largely dependent on the thermal stability of these clusters, vacancies may be released and become mobile again. Due to the slow dissolution kinetics of these clusters at typical AA temperatures, clusters act as stable vacancy prisons during AA. Hence, a reduced contribution of quenched-in vacancies to diffusion during the nucleation of the major hardening phase β" [9] can explain the negative effect of NA on AA [10].

Recently we presented a concept which avoids the formation of clusters at RT by adding trace amounts of the element Sn to the alloy AA6061 leading to the suppression of hardening during

---

NA for > 2 weeks after a solution heat treatment (SHT) at 570 °C and water-quenching to RT [3,11]. Without Sn, NA starts already after several minutes. The slowdown of NA kinetics is achievable in principle by suppressing vacancy diffusion at RT while allowing such diffusion during processing at elevated temperature (e.g. AA) [3]. Sn exhibits a high binding energy ΔE_{SV} to vacancies of 0.24 eV (calculated for Sn-vacancy pairs using quantum DFT [3]).

This results in trapping of vacancies in preferably Sn-vacancy pairs which strongly retards the formation of clusters. Thus, temporary suppression of NA at RT is achieved.

Further research revealed an influence of STT and composition on the achievable retardation of age hardening during NA [11]. To quantify the retarding effect of Sn on NA in AA6061 we proposed the retardation factor $R = 1 + 12c_{Sn}(e^{\Delta E_{SV}/kT})$ (Equation 1, [3]) which is also useful to understand the influence of STT and composition. c_{Sn} is the concentration of Sn in fcc Al, k is Boltzmann's constant. The Sn-vacancy pairs, formed during or after quenching from STT to RT, buffer vacancies during NA, which leaves fewer untrapped vacancies available for diffusion of other alloying atoms such as Mg or Si. Thus NA kinetics is slowed down through the reduction of mobile vacancies in the matrix. Investigation of STTs in the range of 570 °C to 510 °C, revealed an earlier onset of NA-hardening at lower STT [11]. As obvious from Equation 1, the retardation of NA depends linearly on c_{Sn}. For the STT applied, it is assumed that the total amount of solute Sn dissolved in fcc Al at STT complies with the equilibrium level. A significant reduction of c_{Sn} due to decreasing solubility at lower STT can explain why the effect of Sn on NA kinetics is reduced. A similar effect on c_{Sn} was found for a variation of the Si-content [11]. Confirmed by thermodynamic calculations, an increasing Si-content from 0.6 wt.% to 0.8 wt.% in AA6061 reduces c_{Sn} at the annealing temperature of 570 °C and thus the RT stability of the alloy. A small variation of the Mg- and Cu-content showed only small effects on NA kinetics. Atom probe tomography measurements revealed a maximum Sn-solubility of ~100 at. ppm after quenching from 570 °C for the AA6061 alloy investigated in Ref. [3] (alloy 2 in Table 1). For Sn additions above this solubility limit no further retardation of hardening is achievable. Sn-contents below the solubility limit exhibit an earlier onset of hardening [3].

The present work investigates the influence of varying NA temperature on kinetics using hardness measurements. Seyedrezai et al. [12] studied this phenomenon between -20 and 50 °C for the alloy Al-0.5%Mg-1%Si applying electrical resistivity measurements and positron annihilation spectroscopy. The authors identified three stages of clustering indicated by three extended periods of time, over which the resistivity increases linearly with the logarithm of time. At higher NA temperatures, i.e. 20 °C and 50 °C, only the last two stages have been observed during the aging times investigated. Applying the cross-cut technique, the evaluation of the activation energy of clustering Q for the second stage revealed ~45 kJ/mol [12], which is

interpreted to be related to the energy of migration of a Mg-vacancy pair with ~49 kJ/mol [13]. By computing the approximate diffusion distances of solutes for the transition from stage II to III using migration activation energies of Mg and Si, they obtained constant diffusion distances. Thus, the transition from stage II to III is associated to be related to the impingement of the solute fields around clusters [12]. Further, Seyedrezai et al. [12] found a relatively small influence of a change in the STT on NA kinetics and thus on the activation energy Q. This was interpreted as a confirmation that the mechanism of clustering remains unchanged. According to [14,15] this can be explained by finding that the temperature at which the vacancy concentration is frozen in, is generally much lower than the STT.

Here we show a significant influence of not only the NA temperature, but also an effect of the STT on NA kinetics with and without Sn-addition in a commercial AA6061 alloy. An estimation of the effective activation energy of clustering Q indicates a significant influence of Sn-addition.

7.2 Experimental

Alloy 1 (Table 1) was prepared by melting an industrially produced AA6061 alloy followed by die-casting. Alloys 2 and 3 (Table 1) were produced from an AA6061 base alloy, already containing ~95 at. ppm Sn (as well as Mg 0.80, Si 0.59, Cu 0.21, Fe 0.47, Cr 0.15, Mn 0.12, Zn 0.05 and Ti 0.04, all in wt.%), which was produced by the Austrian Institute of Technology (AIT) in Ranshofen (Austria) using a continuous caster in laboratory scale. The Sn content of 95 at. ppm complies with the solubility limit in alloy 2 at 570 °C (see introduction). To obtain the compositions listed in Table 1, the base alloy was re-melted and Mg, Si and Cu were added accordingly. After alloying, Ar gas purging was applied to reduce the hydrogen content before the alloys were cast to slabs (150 × 90 × 35 mm³). After cutting and homogenization, hot rolling from 20 to 4.2 mm thickness was conducted. To check the chemical composition, optical emission spectrometry (SPECTROMAXx from SPECTRO) was performed on the final plates using an appropriate calibration sample for Al-Mg-Si alloys as standard (Mg 0.85, Si 1.00, Cu 0.08, in wt.%). Hardness test samples (17 × 10 × 4 mm³) were solution heat treated in a circulating air furnace (Nabertherm N60/85 SHA) at different temperatures (530 °C or 570 °C) for 20 min. Subsequent quenching was carried out in water at RT and samples were kept in two Peltier-cooled incubators (IPP from Memmert) at RT (25 °C) or 45 °C for NA. Samples naturally aged at 5 °C were kept in a refrigerator.

Alloy 1 in Table 1 represents the almost Sn-free reference alloy with low Mg-, Si- and Cu-content (l: low) and commercial amounts of trace elements (see also [3]). Apart from a Sn-content of ~95 at. ppm, alloy 2 is comparable to alloy 1. Alloy 3 with average Mg-, Si- and Cu-

amounts (~: average) is intended to reveal the influence of these main alloying elements on the Sn-solubility (compare [11]).

Table 1: Composition of alloys

Alloy	Symbol MgSiCu	Sn [at.ppm]	Sn [wt.%]	Mg [wt.%]	Si [wt.%]	Cu [wt.%]	Al
1	lll	6	0.0026	0.81	0.62	0.220	Bal.
2	lll	95	0.042	0.78	0.61	0.210	Bal.
3	~~~	95	0.041	0.87	0.72	0.300	Bal.

Brinell hardness measurements (HBW 2.5/62.5) were carried out using an EMCO-Test M4 unit. A maximum standard deviation of 1.8 HBW was achieved.

7.3 Results

7.3.1 Hardness measurement

The hardening curves of alloy 2 at 25 °C (Figure 1a and Figure 1b) show comparable NA kinetics as previously studied for Sn-added AA6061 alloys in [3] or [11] which, apart from higher Sn-content above the solubility limit, exhibit a similar composition. After a SHT at 530 °C (Figure 1a) the alloy preserves the as-quenched hardness of ~45.3 HBW for more than 86.4 ks. Starting before 172.8 ks (2 days) of NA at 25 °C the alloy shows a constant logarithmic hardness increase until 14 days of NA followed by another steady increase in hardness with lower gradient. NA at 5 °C significantly decreases hardening kinetics of alloy 2, i.e. hardening starts after ~14 days and the constant hardness increase ends after ~90 days. Fastest kinetics is perceived for aging at 45 °C. A steady rise in hardness could be interpolated between 8 h and 4 days.

After a SHT at 570 °C alloy 2 (Figure 1b) starts hardening after ~14 days of NA at 25 °C followed by a steady logarithmic increase until ~90 days. A third stage of lower gradient follows. For aging at 5 °C after ~130 days the onset of hardening can be observed. Fastest kinetics is again perceived for aging at 45 °C with linear hardening between less than 2 days and ~30 days and also followed by a third stage.
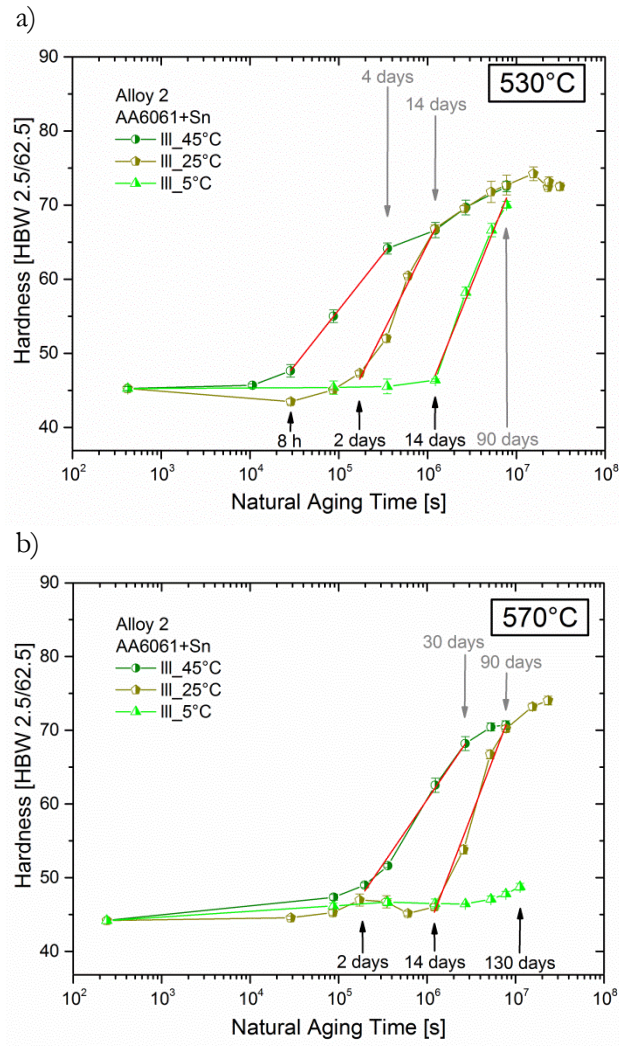
Figure 1: Influence of NA temperatures on hardening kinetics of alloy 2 after a SHT at a) 530°C and b) 570°C.

As can be seen in Figure 2 for both STTs (530 and 570 °C) and for each NA temperature (5 °C, 25 °C and 45 °C), alloy 3 exhibits faster kinetics than alloy 2 (Figure 1). For aging at 45 °C after a SHT at 530 °C (Figure 2a) three subsequent logarithmic gradients are perceived. Following the as-quenched hardness of ~46 HBW, the second stage lies between 3 h and 2 days. For aging at RT, hardening starts after ~8 h and slows down after ~14 days. At 5 °C linear hardening occurs between ~2 days and less than 60 days. After a SHT at 570 °C, NA at 45 °C leads to a linear logarithmic increase between 8 h and 4 days. During RT aging, stage II starts before 2 days and ends after ~14 days. At 5 °C the second stage is perceived between ~14 and ~133 days.

a)

b)
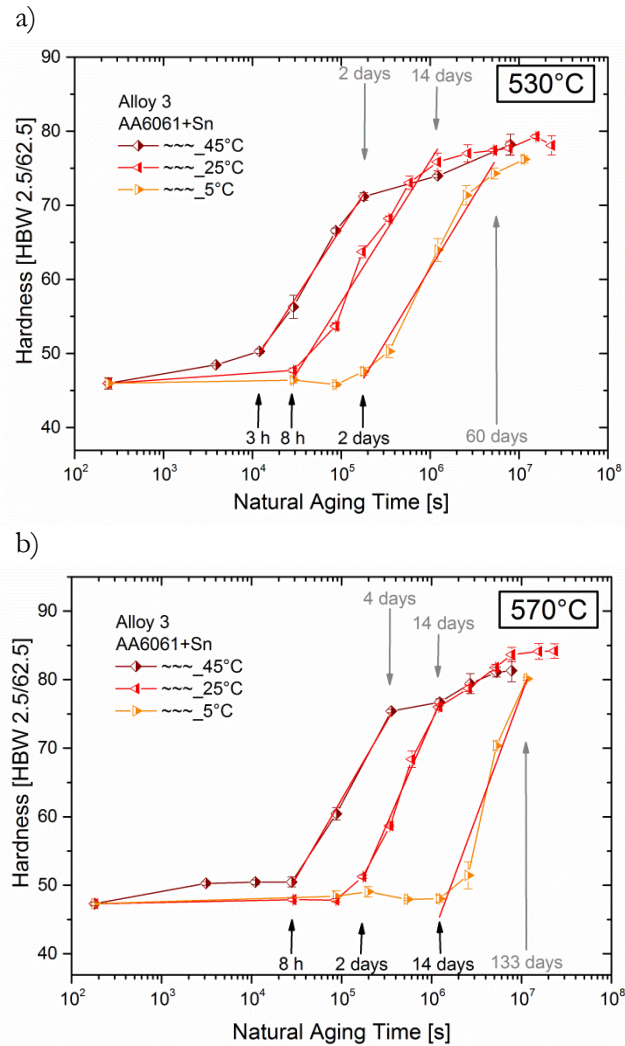
Figure 2: Influence of NA temperatures on hardening kinetics of alloy 3 after a SHT at a) 530°C and b) 570°C.

Figure 3 depicts the influence of NA temperature as well as STT on hardening kinetics of the Sn-free reference alloy 1. For 530 °C (Figure 3a) and 570 °C (Figure 3b) STT and similar NA temperatures the logarithmic hardness increase periods occur in similar aging times. At 5 °C hardening starts after ~3 h and slows down after ~14 days. At 25 °C three distinct stages are observed, the second one between 50 min and ~4 days. For aging at 45 °C only two different hardening gradients are measured. A fast logarithmic hardness increase starts at ~7 min and slows down after ~1 day, i.e. an earlier stage I of hardening is not observed at the aging times investigated.
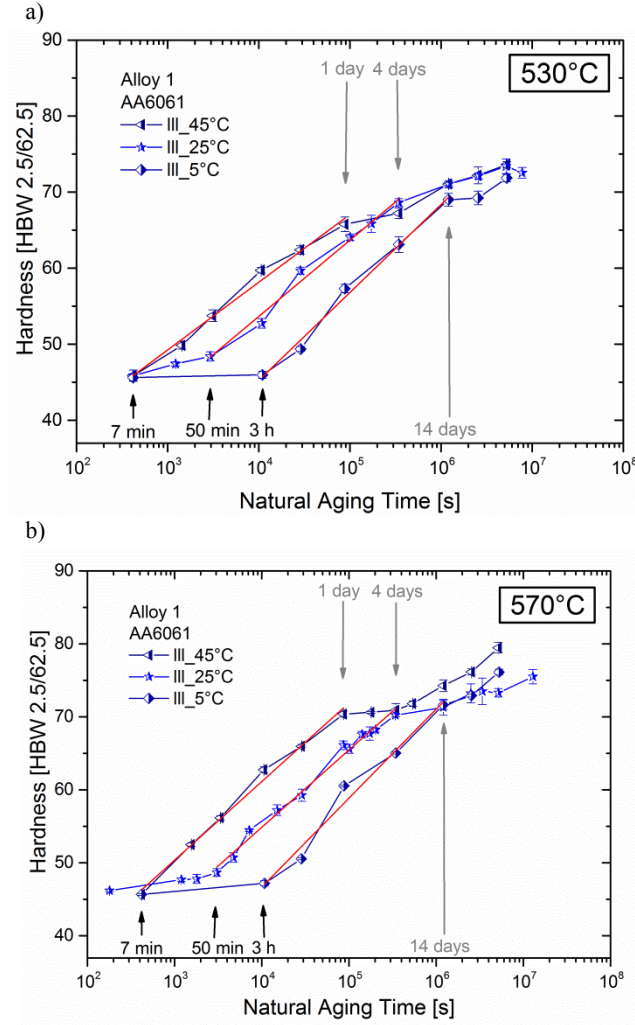
Figure 3: Influence of NA temperatures on hardening kinetics of alloy 1 after a SHT at a) 530°C and b) 570°C.

7.3.2 Effective activation energy calculation

Effective activation energies of clustering Q are calculated using the cross-cut method as derived from Guo et at. [16] for hardness measurements and used in [12] and [17] for resistivity measurements in Al alloys. According to [16] the hardness H can be expressed by the formula $H = (K_0 \, exp^{(-Q/RT)} t)^n$ (Equation 2) for the clustering processes investigated. K_0 signifies the pre-exponential term in the Arrhenius expression for the temperature dependent rate constant K (for the full equation see [16]) and R is the gas constant. Taking the natural logarithm of both sides and assuming that n is constant leads to $\ln 1/t = -Q/RT - \ln \Delta H_0 /n + \ln K_0$ (Equation 3). Thus the effective activation energy of clustering Q can be obtained by plotting $\ln 1/t$ versus $1/T$, where t is the time to reach a constant increase in hardness ΔH_0 at a temperature T [16]. The slope equals $-Q/R$ (see Equation 3). Preconditions for using this method are a coherent precipitate strengthening mechanism, spherical precipitates and that

aging does not proceed beyond the early stage [16]. For the calculations in the present publication, fits have been applied for the second stage of linear logarithmic hardening (Figure 1 and Figure 3) as shown in [12]. The times t for the Arrhenius plot in Figure 4 are read at the same hardness value of the different curves for 5 °C, 25 °C and 45 °C. As for the calculations all curves need to be in stage II the corresponding onsets of hardening have been chosen.
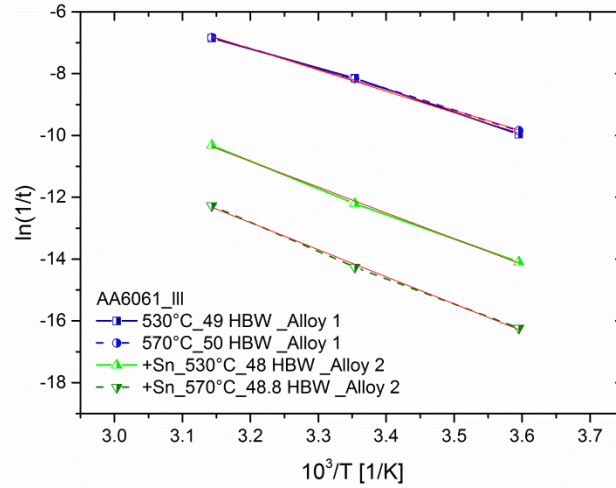
Figure 4: $\ln 1/t$ versus $1/T$ plots for the onset of hardening in stage II. The slope of the straight line equals $-Q/R$.

To evaluate the influence of Sn on the effective activation energy of clustering Q, Table 2 shows the calculated Q values obtained for alloys 1 and 2 at the onset of hardening in stage II (see Figure 1 and Figure 3). While for alloy 1 similar activation energies Q are obtained for a SHT at 530 and 570 °C, Sn-addition leads to significantly higher values at both STTs.

Table 2: Effective activation energy of clustering Q for alloys 1 and 2 at a STT of 530 and 570 °C

Alloy	Symbol	Sn	STT	H_{Onset}	Q
	MgSiCu	[at. ppm]	[°C]	[HBW]	[kJ/mol]
1	lll	6	530	49	57.4
1	lll	6	570	50	55.4
2	lll	95	530	48	69.3
2	lll	95	570	48.8	72.8

7.4 Discussion

The present investigation demonstrates that besides the STT and alloy composition also the NA temperature can have significant influence on the effect of Sn on NA kinetics of AA6061. Due to decreasing Sn-solubility c_{Sn} at lower STT, less Sn is dissolved in fcc Al at the beginning of NA and thus the suppressive effect of Sn on NA kinetics decreases with decreasing STT. Maximum Sn-solubility (~100 at. ppm, see introduction) is obtained for alloy 2 at 570 °C and

thus maximum retardation of NA is achieved (Figure 1b). The same effect of a lower c_{Sn} applies for the higher Si-containing alloy 3 (see [11]). Variation of the NA temperature between 5 °C and 45 °C reveals slower hardening kinetics with lower temperatures, which applies for the Sn-free reference alloy 1 as well as the Sn-added alloys 2 and 3. Calculations of effective activation energies of clustering Q for alloys 1 and 2 (Table 2) reveal significant higher values for the Sn-added material.

As found by Seyedrezai et al. [12] for resistivity measurements in an Al-0.5%Mg-1%Si alloy, also for age hardening curves during NA of AA6061 with and without Sn up to three stages of linear logarithmic hardening are perceived (Figure 1 to Figure 3). In contrast to alloy 1, stage I lasts for the Sn added alloys 2 and 3 for a long period of time. This can be explained by atom probe tomography measurements performed in [3]: Before the onset of hardening in stage II, Sn added alloys show random distributions of the solute atoms in the Al matrix and thus no clusters can contribute to the hardness until this time of NA.

As discussed in the introduction, Seyedrezai et al. [12] observed only a slight influence of the STT (525 °C and 560 °C) on kinetics of clustering, which was expressed also by comparable activation energies Q. For alloy 1, the calculated effective activation energies Q at the onset of stage II after a SHT at 530 °C and 570 °C (Table 2) are also comparable. Although the actual values differ slightly from the Q values obtained by Seyedrezai et al., they remain in the range of activation energies reported in literature (~53.5 kJ/mol found by Gaber et al. [18]). Furthermore, a possible influence of the alloy composition on Q cannot be excluded.

In the following possible reasons for the significantly higher Q values for the Sn-added alloy 2 compared to the Sn-free alloy 1 are discussed (Table 2). As shown in the introduction, Sn reduces the amount of vacancies in the matrix available for diffusional processes of other alloying elements (like Mg or Si) due to the formation of Sn-vacancy pairs. Thus, clusters of stage II form at a much slower rate than in alloys without Sn. The higher Q values for alloy 2 let assume a direct influence of Sn on clustering kinetics. Thermally activated release of vacancies from Sn-vacancy complexes with increasing temperature may give an additional contribution to Q (which is normally attributed to the migration of solutes barrier only) associated with the Sn-vacancy binding energy. Besides this, another possible explanation may be an additional thermally activated contribution of the migration for Sn-vacancy pairs or small complexes to the effective activation energy of clustering Q.

7.5 Conclusions

The objective of this study was to analyze the influence of varying NA temperatures between 5 and 45 °C and two STTs (530 °C and 570 °C) on NA hardening kinetics for a Sn-free commercial Al-Mg-Si alloy compared to two Sn-added alloys containing different Mg-, Si- and Cu-amounts.

Up to three different stages of hardening could be observed for the alloys investigated. For the commercial, Sn-free, variant stage I is not observed at 45 °C, but might occur at shorter times than investigated.

For the commercial alloy and both STTs, comparable effective activation energies of clustering Q are calculated at the onset of hardening during NA.

Sn-addition results in higher activation energy values of clustering Q than obtained for the Sn-free reference alloy. Additional contributions from the migration energy for the migration of Sn-vacancy pairs or a thermally activated release of vacancies are assumed as possible explanations for this effect.

Acknowledgment

References

1. F. Ostermann, *Anwendungstechnologie Aluminium*, 2nd ed. (Springer, 2007).
2. S. Pogatscher, H. Antrekowitsch, H. Leitner, T. Ebner, and P. Uggowitzer, "Mechanisms controlling the artificial aging of Al-Mg-Si Alloys," Acta Materialia **59**, 3352–3363 (2011).
3. S. Pogatscher, H. Antrekowitsch, M. Werinos, F. Moszner, S. Gerstl, M. F. Francis, W. A. Curtin, J. F. Löffler, and P. J. Uggowitzer, "Diffusion on Demand to Control Precipitation Aging: Application to Al-Mg-Si Alloys," Phys. Rev. Lett. **112**, 225701–225705 (2014).

4.   J. Banhart, C. Chang, Z. Liang, N. Wanderka, M. Lay, and A. Hill, "Natural aging in Al-Mg-Si alloys - A process of unexpected complexity," Advanced Engineering Materials **12**, 559–571 (2010).

5.   I. Kovaćs, J. Lendvai, and E. Nagy, "The mechanism of clustering in supersaturated solid solutions of A1-Mg$_2$Si alloys," Acta Metallurgica **20**, 975–983 (1972).

6.   Brenner, P., Kostron, H., "Über die Vergütung der Aluminium–Magnesium–Silizium–Legierungen (Pantal)," Zeitschrift für Metallkunde **4**, 89–97 (1939).

7.   J. Banhart, M. Lay, C. Chang, and A. Hill, "Kinetics of natural aging in Al-Mg-Si alloys studied by positron annihilation lifetime spectroscopy," Physical Review B **83**, 014101 (2011).

8.   S. Esmaeili and D. Lloyd, "Modeling of precipitation hardening in pre-aged AlMgSi(Cu) alloys," Acta Materialia **53**, 5257–5271 (2005).

9.   H. Zandbergen, S. Andersen, and J. Jansen, "Structure determination of Mg$_5$Si$_6$:particles in Al by dynamic electron diffraction studies," Science **277**, 1221–1225 (1997).

10. S. Pogatscher, H. Antrekowitsch, H. Leitner, D. Pöschmann, Z. Zhang, and P. Uggowitzer, "Influence of interrupted quenching on artificial aging of Al-Mg-Si alloys," Acta Materialia **60**, 4496–4505 (2012).

11. M. Werinos, H. Antrekowitsch, W. Fragner, T. Ebner, P. Uggowitzer, and S. Pogatscher, *Influence of Sn-solubility on suppression of natural aging in an AA6061 aluminum alloy.* (Paper presented at MS&T '14, Pittsburgh, USA, 2014).

12. H. Seyedrezai, D. Grebennikov, P. Mascher, and H. Zurob, "Study of the early stages of clustering in Al-Mg-Si alloys using the electrical resistivity measurements," Materials Science and Engineering A **525**, 186–191 (2009).

13. R. C. Picu and D. Zhang, "Atomistic study of pipe diffusion in Al-Mg alloys," Acta Materialia **52**, 161–171 (2004).

14. S. Pogatscher, E. Kozeschnik, H. Antrekowitsch, M. Werinos, S. Gerstl, J. F. Löffler, and P. Uggowitzer, "Process-controlled suppression of natural aging in an Al-Mg-Si alloy," Scripta Materialia **89**, 53–56 (2014).

15. S. Pogatscher, M. Werinos, and Antrekowitsch, H. and Uggowitzer, P.J., "The role of vacancies in the aging of Al-Mg-Si alloys," Materials Science Forum **794-796**, 1008–1013 (2014).

16. Z. Guo, W. Sha, and E. A. Wilson, "Modelling of precipitation kinetics and age hardening of Fe-12Ni-6Mn maraging type alloy," Materials Science and Technology **18**, 377–382 (2002).

17.   A. Juhász, I. Kovács, J. Lendvai, and P. Tasnádi, "Initial clustering after quenching in AlZnMg alloys," Journal of Materials Science **20**, 624–629 (1985).

18.   A. Gaber, K. Matsuda, Z. Yong, T. Kawabata, A. M. Ali, and S. Ikeno, "DSC and HRTEM Study of Precipitation in Al-Mg-Si-Cu Alloys," Materials Forum **28**, 402–405 (2004).

8   MECHANISMS CONTROLLING (NATURAL) AGING

In this chapter a concise review of natural aging phenomena and its effect on artificial aging is used to refine suggestions of underlying mechanisms. With this in-depth analysis of recent literature and therefrom-generated new cross-links and the refined overall mechanistic picture of natural aging our results for prolonged natural aging at different temperatures for > 500 days of commercial and trace element added alloys can be interpreted. A strong dependence of natural aging hardening kinetics on the storage temperature was measured for various AA6061 alloys. For the Sn- and Sn+In-added alloys an additional contribution of a thermally activated vacancy release from Sn- and In-vacancy pairs is assumed. The trapping of quenched-in excess vacancies by Sn and/or In is interpreted to decrease the cluster number density during natural aging while increasing the cluster size. Furthermore it could be interpreted from differential scanning calorimetry (DSC) measurements and artificial aging curves that prolonged natural aging up to years increasingly retards artificial aging kinetics due to slower cluster dissolution kinetics and slower preferential growth of β'' needles. The reachable strength though strongly depends on the ratio and size of less hardenable coarse preferentially grown β'' needles and increasing amount of fine re-precipitated β'' needles.

Hardening of Al–Mg–Si alloys: Effect of trace elements and prolonged natural aging[*]

The first part of this study provides a concise review of natural aging in Al–Mg–Si alloys and its effect on artificial aging, and the second gives insights into prolonged natural aging at different temperatures for > 500 days of commercial and trace element added alloys. Together, the two parts improve the picture of underlying mechanisms and refine suggestions regarding the five stages of natural aging. Trace Sn- or Sn+In-added alloys show a trend towards higher activation energies of clustering, and a higher temperature dependency of natural aging in stage II than commercial alloys. This is explained by the additional contribution of a thermally activated vacancy release from Sn- and In-vacancy pairs. The authors' interpretation of natural aging hardening suggests that Sn and In additions decrease cluster number density while increasing cluster size, producing more pronounced hardness increase during stage II of natural aging. Prolonged natural aging over a period of years increasingly retards artificial aging kinetics, which is interpreted according to increasingly slower cluster dissolution kinetics and slower preferential growth of β´´ needles. It is suggested that the reachable strength depends strongly on the ratio and size of less hardenable coarse β´´ needles, preferentially grown, and the number of fine re-precipitated β´´ needles. Artificial aging after prolonged natural aging at 45 °C beneficially influences the artificial aging peak hardness due to a lower density of larger clusters than that at lower natural aging temperatures.

8.1 Introduction

Although age-hardenable Al–Mg–Si alloys (6xxx series) were developed in the 1920s, the exact mechanisms controlling natural aging (n.a.) and the latter's effect on artificial aging (a.a.) are still not fully understood. The following presents a concise review of the most unclear phenomena. The description shows that n.a.. clustering processes occur in distinct temporal stages that are associated with characteristic alloy behavior, but also that the duration and kinetics of these stages depend on chemical composition and heat treatment history. Together with a comparison to findings regarding Al–Mg and Al–Si alloys and an analysis of clustering theories based on solute-vacancy interaction, we suggest a refined overall mechanistic picture of n.a. Our in-depth analysis of recent literature and the connections we have drawn enable us

to better understand the effect of n.a. temperature and prolonged storage on Al–Mg–Si alloys with and without trace element additions.

8.1.1 Natural aging in 6xxx series alloys

8.1.1.1 Five stages of clustering

Figure 1 summarizes schematically the five stages of n.a. clustering introduced by Banhart et al. [1,2]. Most of the mechanisms suggested were derived from hardness, electrical resistivity (ϱ), differential scanning calorimetry (DSC) and positron annihilation data (PALS).

In stage 0 the initial decrease in the average positron lifetime τ_{av} after quenching from solution treatment temperature (s.t.t.) is attributed to the first clustering stage 0 and the predominant annihilation of positrons in vacancy-related defects, i.e. quenched-in excess vacancies ($\square_{ex}$) or solute-vacancy complexes [3]. The decrease is faster and ends at a lower τ_{av} the higher the Mg content, and can be observed only in alloys of limited Mg content < 0.6 at.% [2]. The subsequent short stage I is characterized by a nearly constant τ_{av}, which is pronounced only for alloys with a Mg/Si ratio close to 1. These alloys alone also show a small DSC clustering peak C0 in stage I as seen in Fig. 1 [2,4]. In stage I an initial (low) logarithmic electrical resistivity increase ϱ and hardness increase are followed by a fast increase in stage II. The decomposition of the τ_{av} into positron lifetimes at defined locations τ_i shows that in a lean alloy ~5 min after quenching 80-85% of the positron signal accounts for vacancy-related defects and the remainder for vacancy-free solute clusters [3]. This suggests that solute clustering sets in even during quenching. In stage II the τ_{av} decreases to a minimum as the signal for vacancy-free solute clusters with lower lifetime increases up to ~70% [3]. The increasing number of vacancy-free solute clusters generates the clustering reaction C1 in DSC (Fig. 1), which we interpret as predominantly involving Si [4]. We attribute the re-increase of the τ_{av} in stage III to continuous Mg-addition to pre-formed solute clusters [2]. Stage III is further characterized by an intermediate logarithmic electrical resistivity and hardness increase and the DSC clustering reaction C2, which may already start around the end of stage II [2]. With time, the positron signal of vacancy-related defects can no longer be separated, i.e. vacancy-free solute clusters dominate [3]. With increasing Mg-content the τ_{av} in stage III increases faster and the transition to stage IV, in which the τ_{av} drops again, occurs earlier. Stage IV is accompanied by another slow-down of the hardness and resistivity increase [2]. While for the Si-rich alloy in ref. [5,6] hardness hardly increases at all in 1.5 years, in other alloys a significant non-linear hardness increase is observed in stage IV [5,7] (Figs. 1 and 3a). Possible mechanisms here are a coarsening or ordering and zone formation on the part of cluster C2 [2].

Liang et al. [8] reported on three clustering peaks in an Si-rich alloy which was also investigated by PALS in ref. [2]. As the clustering reaction C1 has already terminated after the end of stage

II (compare Fig. 1), cluster C1 is weakly observed during a subsequent DSC measurement. Cluster C2 is observed until the end of stage III [2]. For a DSC measurement after stage IV another peak is observed [8] which is interpreted here as a possible C3 peak only observable in Si-rich alloys with a Mg/Si ratio of << 1 [9]. DSC data analysis indicates that the clustering process C1 resembles "cluster formation", while C2 and C3 resemble "cluster growth" [8].
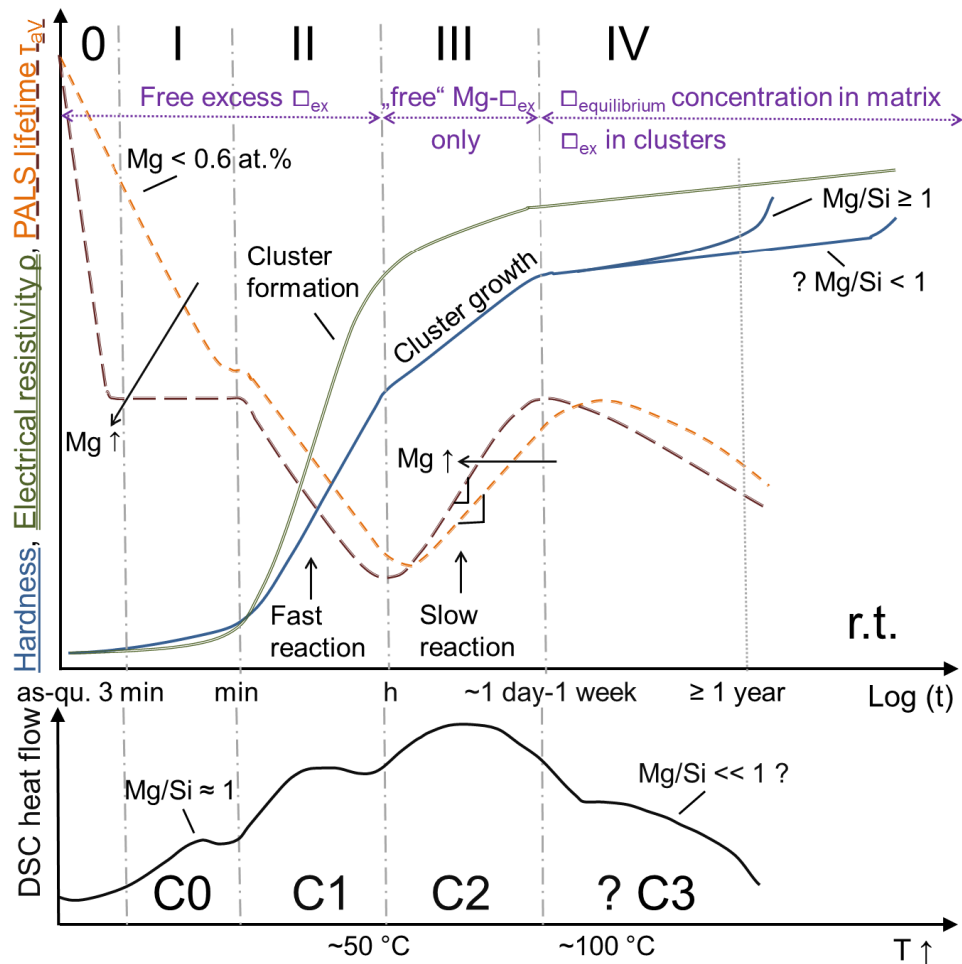
Fig. 1. Schematic representation of the five stages of natural aging (n.a.) clustering and suggestions regarding the mechanisms involved. Comparison of hardness, electrical resistivity ϱ and average positron lifetime τ_{av} evolution at room temperature (r.t.) to differential scanning calorimetry (DSC) results. Note that cluster peaks obtained by linear heating reflect the same clusters formed with increasing n.a. time. Partly reproduced from ref. [2].

8.1.1.2 Influence of trace elements

The wish to control n.a. kinetics and the negative effect on a.a. is of major importance for the Al manufacturing industry. The positive effect of trace elements such as Sn and In on temporary suppression of n.a. is known for Al-Cu alloys [10,11], but only a few recent investigations address Al–Mg–Si alloys [12–16]. Our group recently presented a design strategy [17] which involves fine-tuning the alloy composition with respect to the Mg, Si, Cu and trace

element content. N.a. could be suppressed for more than 6 months while retaining a significant a.a. potential [17], which is explained by the strong trapping of quenched-in excess vacancies in stable Sn-vacancy pairs [12–15,18]. This suppresses the formation of clusters during n.a. which act as relative stable vacancy prisons and reduce the a.a. potential [19]. The precondition for achieving the maximum trace element effect is the quenching in of the maximum concentration of dissolved Sn atoms, i.e. (i) a high s.t.t. for maximum Sn solubility, (ii) a Sn content > solubility limit and (iii) a controlled content of Mg and Si. The interpretation of the effect of trace elements on n.a. hardening and kinetics is used in this paper to generate a better understanding of the processes underlying n.a..

8.1.1.3 Dependence on the Mg, Si and Cu content and the (Mg+Cu)/Si ratio

The duration of each clustering stage is not fixed, because it depends on the chemical composition, the heat treatment history, and trace elements [7,20]. Yet direct observations are challenging, and even the highest resolution characterization methods such as atom probe tomography (APT) operate at their limits [1,20,21].

Nevertheless, APT studies showed that direct pre-aging at 100 °C [22,23] or 80 °C [6] of Mg-rich [22,23] or Si-rich [6,22] alloys produces clusters with an Mg/Si ratio of ~1, a composition close to that of elongated precipitates formed during a.a., as shown by ref. [24]. For n.a. (< 80 °C) the situation is different: Torsæter et al. [22] found that the composition of clusters is closer to the alloy composition. In an Si-rich alloy, Zandbergen et al. [6] observed clusters with an average Mg/Si ratio of ~0.66 partitioned into 98% of Mg,Si co-clusters and < 2% Si-only clusters after 100 min of n.a.. No Mg-only clusters were observed. Because a slower hardness increase follows soon after 100 min (see also Fig. 1), their alloy was near the end of clustering stage II. This requires a diffusion distance for clustering of ~2 nm [6]. As the estimated Mg or Si equilibrium diffusion distances are much shorter [6] quenched-in excess vacancies are necessary for early-stage cluster formation and growth (Fig. 1) [6,20,25]. Attributed to the greater intrinsic Si diffusivity with respect to Mg [6,26] and the attractive Si-vacancy binding energy E_b [6,10,26,27], Si clusters have been speculated to form even during or directly after quenching [6]. Note that with decreasing temperature the ratio of the Si and Mg equilibrium diffusivity D_{Si}/D_{Mg} increases [6,26], i.e. at r.t. $D_{Si} > D_{Mg} > D_{Cu}$ [26]. Generally, Si-related clustering is assumed to control the beginning of n.a. and its kinetics [1,2,4,6,9,28–31], which is driven by (i) the availability of quenched-in excess vacancies [17] and (ii) by Si attraction to, but Mg repulsion from, locally strained areas for stress-relief [31]. The Si-rich clusters observed with APT grow further at a slow rate in stage III [6]. This suggests that, at least at r.t., some excess vacancies persist as solute-vacancy pairs [6]: only after weeks in stage IV the growth rate decreases to a very low (equilibrium) value (Fig 1). Higher Si content causes earlier transitions

I-II and II-III [9,17,29,32] (Fig. 2a), higher n.a. hardness [9,17,33,34] (Fig. 2a), a better a.a. performance [35,36] and, for Si-rich alloys, a persistent low cluster Mg/Si ratio which is also attributed to the greater intrinsic Si diffusivity with respect to Mg [6]. This accords with decreasing DSC peak temperatures of clusters C1 (stage II) and C2 (stage III), signifying an increasing formation rate of Si-rich clusters [9]. With increasing Si content, free vacancies and vacancies that detach from unstable initial solute-vacancy complexes [3] need to diffuse over shorter distances to nearby Si atoms to transport these to the vacancy-free clusters [4,17,22,28,37] in stage II (Fig. 1) [3].

The increase in the τ_{av} in stage III (Fig. 1) is attributed to Mg diffusion to pre-formed solute clusters [2,3]. Mg is believed not to have a part in the early stage I and II clustering process [17]. This suggestion is supported by comparable stage I-II transition times for increasing Mg content, with the exception of very lean alloys, but earlier stage II-III and III-IV transitions times measured by electrical resistivity (Fig. 2b) [9] and PALS (Fig. 1) [2]. The latter fits to only negligibly decreasing C1 DSC peak temperatures, but significantly decreasing C2 peak temperatures [9]. According to ref. [31] a cluster needs to be enriched enough in Mg to possess a nucleation barrier and to become stabilized in size, which reduces the cluster energy and is the precondition for survival and growth during a.a..
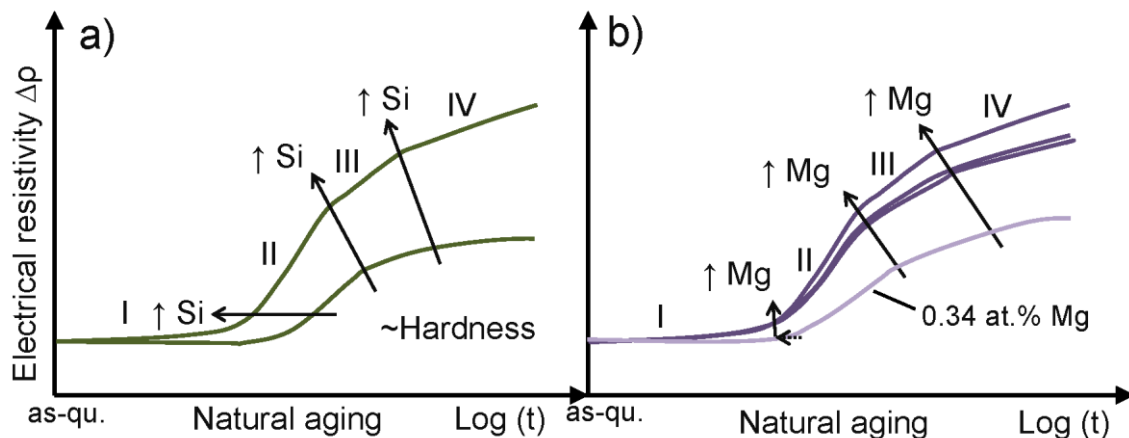
Fig. 2. Schematic dependence of natural aging kinetics on a) Si content and b) Mg content. With increasing Si content all transition times occur earlier; with increasing Mg content stage I-II transition times are similar (except for very lean alloys). Reproduced from ref. [9].

The highest formation rates, i.e. lowest peak temperatures in DSC, for cluster C1 are obtained for Mg/Si ≈ 1.0 alloys and for cluster C2 for Mg/Si ≈ 1.0-1.5 alloys. Generally Mg/Si ≈ 1 alloys generate the greatest C1 and C2 heat effect [9,28], i.e. the largest cluster volume fractions, and greatest total electrical resistivity change in stage IV, i.e. the highest cluster number densities [9]. Note that some authors (e.g. ref. [9,23]) have a different interpretation of

and notation for DSC clusters, but we refer to the notation of Chang et al. [4,28] throughout (see Fig. 1).

Cu addition to Al–Mg–Si alloys retards n.a. hardening in stages I and II (Fig. 3a) [5,7,17] and lowers the first DSC clustering peak C1 (Fig. 1) [8,29], which seems comparable to the Sn effect [17]: due to its attractive solute-vacancy binding energy [10,26] quenched-in dissolved Cu atoms may bind vacancies and lower the number of untrapped vacancies available for Si clustering [29]. In contrast to Sn, we assume that Cu immobilizes vacancies only weakly, which may explain the weaker effect on n.a. kinetics [17].

Ref. [7] posits that the repulsive interaction between Cu and Si atoms [38] interrupts the agglomeration of Si atoms and that Cu preferably incorporates into clusters with Mg atoms around the middle stage (stage III) due to an attractive interaction with Mg [38]. APT measurements in ref. [5] are interpreted comparably: after 1 week of n.a. a nearly Cu-free (Si-rich) reference alloy shows an (Mg+Cu)/Si ratio in clusters of 0.66, whereas the Cu-rich alloy shows a ratio of 1.08. The latter composition is much closer to subsequent a.a. precipitates, which explains the lower negative effect on a.a. [5]. Because Mg is ~12% larger than Al [26,39,40], Si is ~2.2-3.8% smaller [26,39,40] and Cu is ~10.2-10.7% smaller [26,39,40], an optimum Cu/Mg ratio minimizes the strain energy caused by the differences in atomic sizes in the Al host and also reduces the need for vacancy incorporation to relieve stresses [5]. This makes clusters less efficient vacancy traps and more stable [5]. Hence, more untrapped vacancies can transport more solute atoms [5], which enhances the cluster growth rate and, as shown in Fig. 3a, causes a higher increase in n.a. hardness in stages III and IV than a nearly Cu-free alloy [5,7].
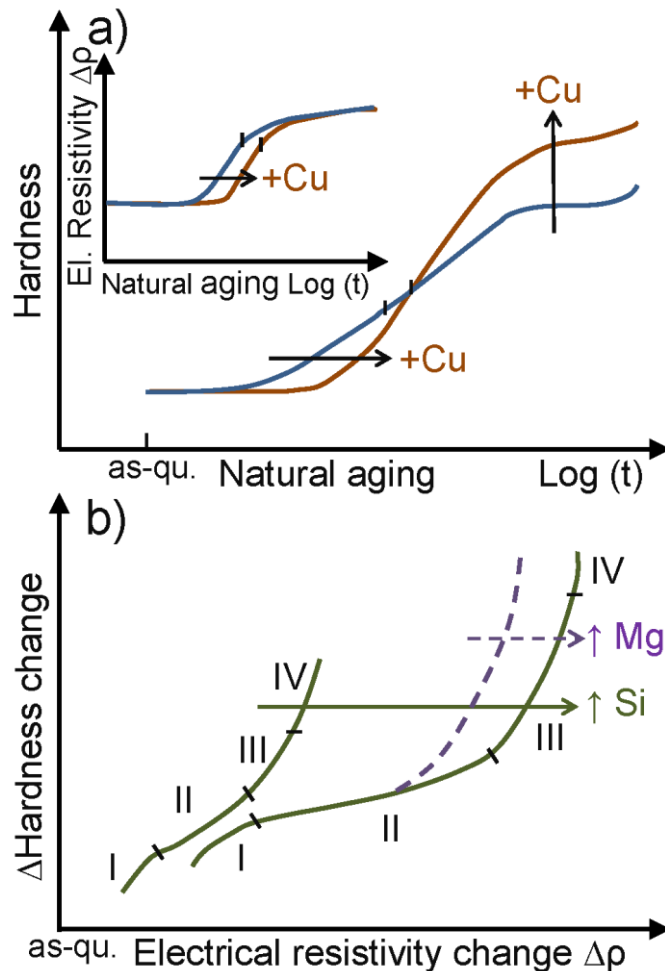
Fig. 3. Comparison of hardness and electrical resistivity change $\Delta\varrho$ for a) the influence of Cu addition on natural aging kinetics; and b) for Si or Mg addition. Hardness mainly correlates with cluster size, while the $\Delta\varrho$ mainly correlate with cluster density. Reproduced from ref. [7] (a) and [9] (b).

8.1.1.4 Comparison of hardness and electrical resistivity measurements

Figure 3b illustrates schematically that after an initial hardness and electrical resistivity increase in stage I, the resistivity in stage II changes more significantly than hardness which is more pronounced with increasing Si (or Mg) content [9]. In stages III (and IV), however, the hardness increase dominates [9]. For stage II this is connected with marginal cluster growth but a high increase in cluster number density, which fits the simulations in ref. [31], and for stages III and IV with cluster growth (nearly) with no change in the cluster number density [9]. Thus electrical resistivity is mainly affected by cluster number density [7,9] and only to a lower degree by cluster size [37], whereas hardness predominantly correlates with cluster size, presumably due to coherency strengthening [41] (Fig. 1 and 4a). Thus, as the cluster number density in stage III is reported to remain constant [37], it is mainly the enhanced cluster growth rate of Cu-added alloys in stages III and IV which causes the greater hardness (increase) compared to a Cu-free alloy [5] (Fig. 3a). Because DSC analysis of Cu-added alloys suggests the formation of

a lower cluster number density in stage II [8], it is reasonable that the reported stage II-III transition occurs at slightly lower electrical resistivity values. With constant cluster number density in stage III the resistivity only increases due to cluster growth until the stage III-IV transition [37], and finally reaches resistivity values comparable to those of the nearly Cu-free alloy.
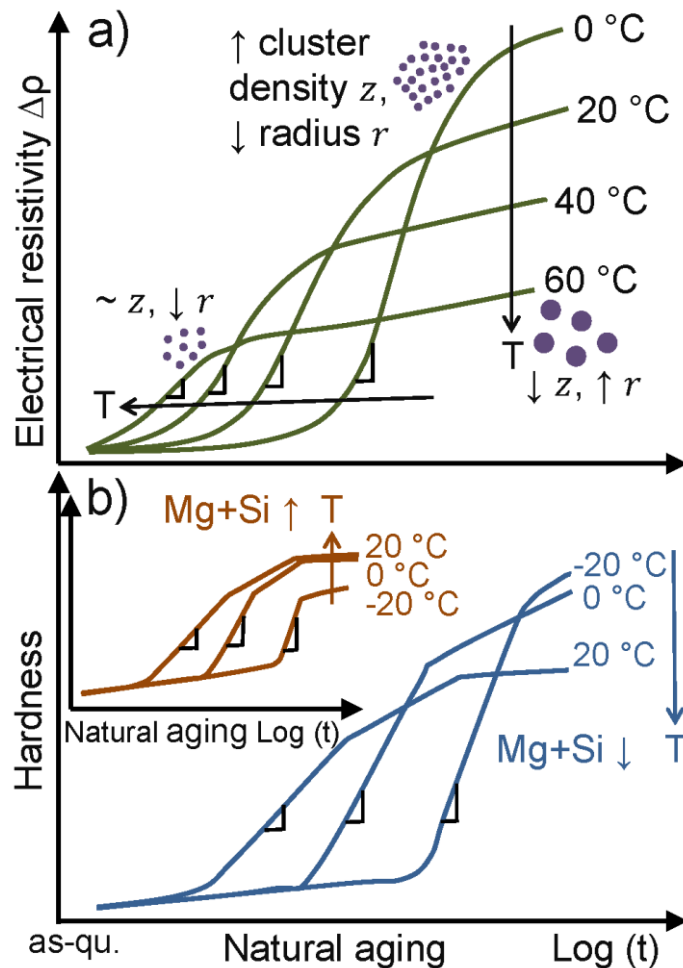
Fig. 4. a) Schematic dependence of clustering kinetics and attainable long-term electrical resistivity change ($\Delta\varrho$) on natural aging (n.a.) temperature. Whereas the cluster density z decreases with n.a. time, the radius r increases. b) Schematic dependence of hardness on n.a. temperature and Mg+Si content. Reproduced from ref. [42,43]

8.1.1.5 Influence of natural aging temperature

As shown schematically in Fig. 4, with decreasing temperature (< 80 °C) clustering stages are retarded and transition times delayed [2,42–46], while in stage II a sharper logarithmic hardness [43] and electrical resistivity [42,43] increase are perceived. At high temperatures, the total resistivity reached after sufficiently long n.a. times (Fig. 4a) becomes lower independently of the alloy composition [42,43]. This is interpretable with the concept of ideal clustering [42]. As shown schematically for aging at 60 °C in Fig. 4a for clusters with simplified identical radii the

number density of clusters z decreases with increasing cluster radius r [42]. As further shown schematically for 60 °C and 0 °C, at lower temperature and for constant radius r the density of clusters increases [42]. Røyset [43] concluded the same.

For low Mg+Si content in lean alloys, the hardness in Fig. 4b decreases with rising temperature, whereas alloys with high Mg+Si content show increasing long-term hardness [43]. Because hardness predominantly correlates with cluster size (Fig. 3b), this is explainable according to (i) increasing cluster size with increasing temperature in alloys with high Mg+Si content and (ii) small and thus less hardenable clusters in lean alloys with increasing cluster density at lower temperatures [42,43].

8.1.1.6 Comparison to findings for Al–Mg and Al–Si alloys

A "permanent" increase in r.t. electrical resistivity in Al–Mg alloys after a fast quench from s.t.t. to ≤ 100 °C [47] is explained by a suppression of vacancy annihilation at r.t. due to Mg atoms trapping vacancies. Above ~0.1 at.% Mg content the permanent increase increases further only marginally. A recovery of the permanent (r.t.) increase occurs between ~80-120 °C; this is attributed to Mg-vacancy pairs that acquire higher mobility, or to Mg atoms releasing vacancies. Note that for Al–Mg–Si alloys, Chang [4] concludes that the formation of pre-aging clusters (at this temperature) which show a Mg/Si ratio of ~1 [6,22,23] is assisted by the increased density or mobility of vacancies.

Nishimura [48] investigated clustering using muon spin relaxation. Muons show higher defect binding energies than do positrons. The as-quenched features of binary alloys seem to be reflected in the Al–Mg–Si alloy: A slight decrease in muon trapping rates between an as-quenched and an Al–Mg sample n.a. for 13 days is attributed to the persistent presence of Mg-vacancy "clusters" (compare Fig. 1, stage III). For Al–Si, by contrast, a large muon trapping rate after ~15 min of n.a. disappeared after 12 days of n.a., which indicates initial Si-vacancy "clusters" that disappear with time. Liu et. al [3] also report that in Al–Mg alloys vacancies remain separate entities throughout aging, and are probably attached to and stabilized by Mg atoms.

8.1.2 Mechanistic descriptions of clustering

Because limited atomic mobility at low-temperature aging suppresses long-range diffusion, at r.t. only local rearrangement of solutes seems possible [22]. Depending on the solute number and distance, agglomerated clusters form that follow the alloy composition and achieve energy reduction by forming favorable, neighbor-neighbor bonds, which make them hard to dissolve [22]. Diffusion over longer distances during pre-aging at ~80-120 °C generates more stable cluster configurations, both electronically and elastically [22,24]. Unlike at r.t., during pre-aging

clusters slowly grow into spheroidal precipitates. These are referred to as GP zones in literature, but they have also been reported not to be phases distinct from clusters from a chemical or morphological perspective [6].

In sum, the mobility, i.e. diffusivity, of atoms depends on (i) temperature, (ii) vacancy concentration around a solute and (iii) the degree of matrix strain [10,22,31]. Factor (ii) depends on the quenching rate from s.t.t. [25] and the trace element content of Cu or (e.g.) Sn [17].

The initial cluster composition depends on (i) the relative intrinsic diffusivities of solute species [6]; (ii) the relative strength of solute-vacancy interactions during n.a. [6]; (iii) solute attraction of Si to locally strained areas for stress-relieve followed by cluster stabilization through Mg addition due to the formation of favorable neighbor-neighbor bonds between Mg and Si [31]; and (iv) the availability of solutes and vacancies which control the arrival rate of solutes to a cluster [5,17].

8.1.2.1 Theories of clustering based on solute-vacancy interaction

The quantitative interaction between clusters and vacancies can be simplified with a binding energy $E_{b,cluster}$ [49]. If $E_{b,cluster}$ is zero, vacancies would cross clusters without interaction and diffuse until elimination at sinks as it would happen in pure Al. For high attractive (positive) $E_{b,cluster}$, a vacancy is permanently trapped and eliminated from the matrix in a short time. In the general case of intermediate $E_{b,cluster}$ a vacancy is trapped temporarily, so that after the initial "fast-reaction" (stage II) in which clusters form and grow due to a high concentration of excess vacancies ($\square_{ex}$), the clustering reaction slows down until most vacancies are trapped [49]; compare Fig. 1. A transition to a "slow-reaction" (stages III/IV; Fig. 1) is expected in which the equilibrium vacancy ($\square_{equilibrium}$) concentration in the matrix controls the slow growth of the initially still small clusters by establishing an equilibrium between vacancies reaching and evaporating from clusters. The transition is sharper the higher the $E_{b,cluster}$, which also increases with cluster size. These theoretical considerations by Federighi and Thomas [49] can be compared with the growth model of solute clusters proposed by Zurob et al. [37].

Zurob [37] defined the binding energy E_b as the probability of dissociation of a solute-vacancy complex, which is $\propto \exp(-\frac{E_b}{kT})$ (Eq. 1, k is Boltzmann's constant). For positive E_b, "cluster formation" starts with quenched-in excess vacancies ($\square_{ex}$, stages 0-I in Fig. 1) which form migrating solute-vacancy complexes with limited lifetimes. During this period other solute atoms join until the complex is more stable and migrates sluggishly. Finally a stationary cluster exists, and for further "cluster growth" the vacancy needs to escape with a number of jumps x proportional to the number of neighboring solute cluster atoms n. The probability is roughly

$\propto \exp(-\frac{\alpha n E_b}{kT})$ (Eq. 2, α is a constant). This can explain the formation of vacancy-free clusters at the transition to stage II (Fig. 1). The escaped vacancy forms a new solute-vacancy complex which, depending on E_b, either evolves into a new cluster or joins an existing cluster. In either case the finally trapped vacancy needs to escape for further cluster growth [37] since the vacancy concentration has been estimated to ~1/100 of the average solute concentration [4,28].

8.1.2.2 Activation energy calculations

Activation energies Q for cluster formation have been derived using transition times between stages [2,43,46,50] or DSC analysis [8,28]. Chang et al. [28] calculated the Q change for increasing DSC cluster volume fractions C1 (stage II) and C2 (stage III, Fig. 1). Mg/Si ≈ 1 alloys show, compared to Si-rich or Mg-rich alloys, lowest (initial) Q values for C1 and C2 while the Q values increase for increasing cluster volume fractions [28]. The low Q values for Mg/Si ≈ 1 alloys may be associated with attractive equilibrium Mg-Si interaction energies [28,38] as Si-Si and Mg-Mg atoms repel each other in super-saturated Al [38]. N.a. clustering, however, is a kinetic process affected by several factors that have been discussed in the previous sections. Three effects may contribute to the effective Q of cluster C1: (i) the availability of Si atoms for continuous cluster formation, (ii) the vacancy escape from stationary Si-vacancy clusters, and (iii) the arrival rate of Si atoms for subsequent (marginal) cluster growth. The effective Q of clusters C2 in stage III may be dominated by the arrival rate of slow Mg atoms to pre-formed clusters, i.e. (i) the Mg content and (ii) the low Mg diffusivity.

8.1.3 Overall mechanistic picture of natural aging

Based on the literature review the following picture of the five stages of n.a. clustering is suggested (see Fig. 1).

Stage 0: Quenched-in excess vacancies □$_{ex}$ come into contact and interact with solute atoms controlled by the strength of solute-vacancy interaction and the solute diffusivity. Therefore the as-quenched positron signal is dominated by vacancy-related defects, i.e. free vacancies and solute-vacancy complexes in addition to a smaller signal of vacancy-free clusters which presumably formed during the quench [3,30]. Coincidence Doppler broadening spectroscopy measurements in ref. [30] indicate the initial existence of Si-vacancy complexes, while muons also indicate the additional initial existence of Mg-vacancy complexes [48]. For the initial positron lifetime decrease with increasing Mg content (Fig. 1) there seems to be no final explanation. It is possible that Mg promotes the formation of vacancy-free Mg,Si clusters during the quench due to larger high temperature diffusivity [47], which results in a lower initial positron lifetime.

Stage I: In view of the clustering theory proposed by Zurob et al. [37] the authors suggest that migrating Si-vacancy complexes evolve to sluggish and stationary vacancy-containing Si clusters due to (i) the high diffusivity of Si ($D_{Si} > D_{Mg} > D_{Cu}$ [26]), (ii) the attractive Si-vacancy E_b [10,26,27] and attractive Si-vacancy interaction energy [38] which support solute-vacancy pair formation and (iii) attraction of Si atoms to locally strained areas for stress-relief (from which Mg atoms are repelled) [31]. For further cluster growth the vacancy needs to escape, leaving a vacancy-free Si cluster behind. This initiates the transition to stage II, and due to shorter diffusion distances occurs earlier with increasing Si content (Fig. 2). Slow Mg-vacancy pairs do not take part.

Stage II: The formation of new vacancy-containing Si clusters prevails and accompanies continuous formation of vacancy-free Si clusters; at higher Si content more vacancy-containing and vacancy-free clusters are formed (Fig. 3b). During this "fast reaction", Si clusters grow marginally. Later in stage II, slowly migrating Mg-vacancy pairs start to join and stabilize pre-formed vacancy-free clusters due to an attractive Mg-Si interaction energy [38]. Mg inclusion reduces the cluster energy and increases the vacancy $E_{b,cluster}$ of clusters because vacancy incorporation relieves stresses. Finally, they may become a "vacancy-prison" [19], i.e. excess vacancies $\square_{ex}$ can no longer escape and Si cluster formation ends, which defines the transition to stage III. For Cu-containing alloys, combined Mg and Cu inclusion occurs.

Stage III: Vacancies not trapped in clusters exist solely as Mg-vacancy pairs, which continue to join pre-formed clusters and cause cluster growth. An equilibrium between free structural vacancies reaching and evaporating from clusters is established ("slow reaction"). At the transition to stage IV, all Mg-vacancy pairs are incorporated in clusters.

Stage IV: During stage IV the equilibrium vacancy concentration in the matrix controls further cluster growth. Over time coarsening sets in, i.e. growing clusters join each other and the cluster number density decreases. Slower cluster growth in Si-rich alloys may retard or suppress coarsening (Fig. 1).

8.1.4 Influences of natural aging on artificial aging

8.1.4.1 Negative effect: dependency on Mg/Si ratio and Mg+Si content

The negative effect of n.a. signifies retarded a.a. kinetics and lower maximum strength than is reachable during a.a. started directly after quenching from s.t.t, due to a reduced number density of precipitates [1,19,22,33,44,51]. This is observed in alloys with a total content of Mg+Si > 1 wt.% [22,36,52], whereas commercially less relevant alloys with Mg+Si < 1 wt.% show a higher reachable strength than without n.a. [20,43,53,54]. The severity of the negative effect depends on the composition of pre-formed clusters or phases [22,36]. Whereas Mg/Si ratios of n.a. clusters resemble the alloy composition [6,22], positive pre-aging clusters ($\geq$ 80

°C) favor a narrower Mg/Si distribution and Mg/Si-ratios of ~1 similar to a.a. precipitates with a composition close to $(Al+Mg)_5Si_6$ [24,55] for the peak hardening phase β´´ [6], as predicted by ref. [24]. Hence, from agglomerated metastable n.a. clusters with compositions that differ significantly from a Mg/Si ratio of 1, more stable a.a. precipitates form with difficulty [6,22]. Si-rich clusters, for example, first need to dissolve or change chemistry to a Mg/Si ratio of ≥ 1 with Mg enrichment before a structural change into elongated precipitates [6,24]. Acquisition of the critical length and composition close to $Mg_2Si_2Al_7$ required to stabilize the cluster in size is only possible during pre-aging (≥ 80 °C), and is the precondition for survival and growth during a.a. [24,31]. The high $E_{b,cluster}$ of vacancies to n.a. clusters and the reduced solute super-saturation also retard growth kinetics [6,19].

Tao et al. [36] investigated alloys with a total high Mg+Si and Cu content and Mg/Si ratios of 0.5, 1 and 2 (in wt.%). Until ~1 week n.a. (end of clustering stage III, Fig. 1) the Mg/Si ≈ 1 alloy reaches the highest and the Mg-rich alloy medium a.a. peak hardness followed by a significant hardness decrease for longer n.a. times in stage IV; see Fig. 5. Deep cluster dissolution peaks in DSC in both alloys after 2 weeks n.a. (stage IV) indicate unstable n.a. clusters that dissolve slowly, which is more pronounced for the Mg-rich alloy [36]. In combination with TEM analysis of the peak aged condition the hardness decrease in stage IV can be explained by a coarsening of the a.a. microstructure due to preferential growth of a few stable n.a. clusters, while slowly re-precipitated solutes produce small precipitates [36]. For Si-rich alloys, in contrast, the DSC signal only shows limited cluster dissolution and no coarsening in TEM after increasing n.a. times, i.e. the majority of β´´ precipitates grow synchronously from stable (Si-rich) clusters [36] after Mg enrichment to an Mg/Si ratio of ≥ 1 [6]. Therefore, for increasing n.a. times no significant decrease in the reachable peak hardness during a.a. (Fig. 5) is observed [36]. After various n.a. times Si-rich alloys show the fastest, Mg/Si ≈ 1 alloys medium, and Mg-rich alloys the slowest a.a. kinetics [36]. For the Si-rich alloy, the authors suggest that fast Mg-enrichment of stable Si-rich clusters and the sudden synchronous growth to a fine scale microstructure generates the fastest kinetics. During a.a. after n.a. to stages III and IV in alloys richer in Mg, a few larger clusters show a slow preferential growth to a.a. precipitates, but most slowly dissolve and re-precipitate to small β´´ needles, producing a coarse microstructure.
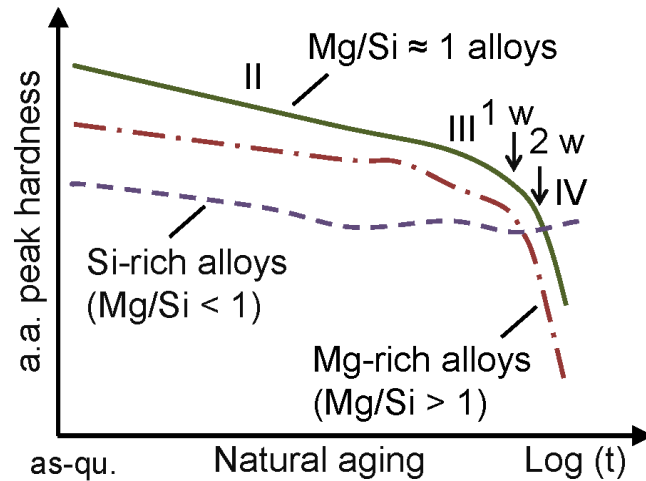
Fig. 5. Schematic evolution of the reachable artificial aging (a.a.) peak hardness after increasing natural aging time for Mg-rich, Si-rich and Mg/Si ≈ 1 alloys. Reproduced from ref. [36].

8.1.4.2 Negative effect: dependency on the clustering stage

The negative effect depends not only on the Mg/Si ratio of the alloy (Fig. 5), but also on the n.a. clustering stage (Fig. 6), because the cluster composition evolves with time, starting from Si(-rich) clusters in the initial stage [2,4,6,7,28,31]. Zandbergen et al. [6] found that very small clusters present after short n.a. times of < 20 min (i.e. Si-vacancy complexes in stage I) still generate relatively fast a.a. kinetics because some transform to spheroidal or short-elongated precipitates during 30 min a.a., which produces a fine-scaled harder microstructure compared to a.a. after longer n.a. times. Note that Martinsen et al. [52] even found an a.a. hardness increase (36 h at 170 °C) after short n.a. times in stage I followed by a decrease for n.a. times in stage II; see Fig. 6. Kim J. et al [7] systematically investigated the evolution of the negative effect between 1 h (stage II) and 1 year of n.a. in a Cu-free and a Cu-containing Si-rich alloy, and divides n.a. into stages (Fig. 6). The "1st stage" until the end of stage II produces a decrease in the a.a. peak hardness compared to direct a.a. at 170 °C, while the increase in the β´´ peak temperature in DSC (Fig. 6) signifies slower formation kinetics. Kim J. interprets this to mean that the Si-rich clusters formed in this stage are relatively stable but need to adjust their composition for β´´ formation [7]. Note that this conclusion for stage II accords with the fast synchronous growth of Si-rich clusters after Mg-enrichment during a.a. in Si-rich alloys (Mg/Si < 1, Fig. 5) [6,36]. The "middle" stage until the end of stage III shows an increase in the a.a. hardness [7,52] and decrease in the DSC peak temperature to a minimum followed by another increase that continues in the "3rd stage" [7]. Kim J. [7] sees the formation of Mg-Si co-clusters which would be useful for β´´, but are thermally less stable than Si-rich clusters. This positive trend in stage III may be comparable with Mg/Si ≈ 1 alloys which show the highest a.a. peak hardness and medium kinetics for n.a. until stage III; see Fig. 5. Another peak hardness decrease in a 3rd stage (stage IV) is attributed to the formation of Mg-Si co-clusters that

dissolve, while some show preferential growth [7]. Thus, stage IV can be compared to the negative effect of Mg-rich clusters in Mg-rich alloys (Mg/Si > 1, Fig. 5) [36].

For the increasing n.a. time in stage IV Martinson et al. [52] reported, for an Si-rich alloy, a scatter of a.a. hardness which lasts until, after several months to > 1 year, an increase prevails (Fig. 6), which he interprets as a reversal of the negative effect. In ref. [7], however, a.a. hardness curves after n.a. between 1 month and 1 year show significant peak broadening, whereas after only 1 year of n.a. might the a.a. peak hardness indicate a slight increase (Fig. 6).

The review presented above enables us to understand the results described in the following sections. In particular, the in-depth analysis of recent literature regarding early-stage clustering processes and the refined overall mechanistic picture of n.a. (section 1.3) derived here, in combination with the critical analysis of the influence of n.a. on a.a. (section 1.4), are mandatory for understanding the effect of n.a. temperature and prolonged storage in Al–Mg–Si alloys with and without trace element additions.
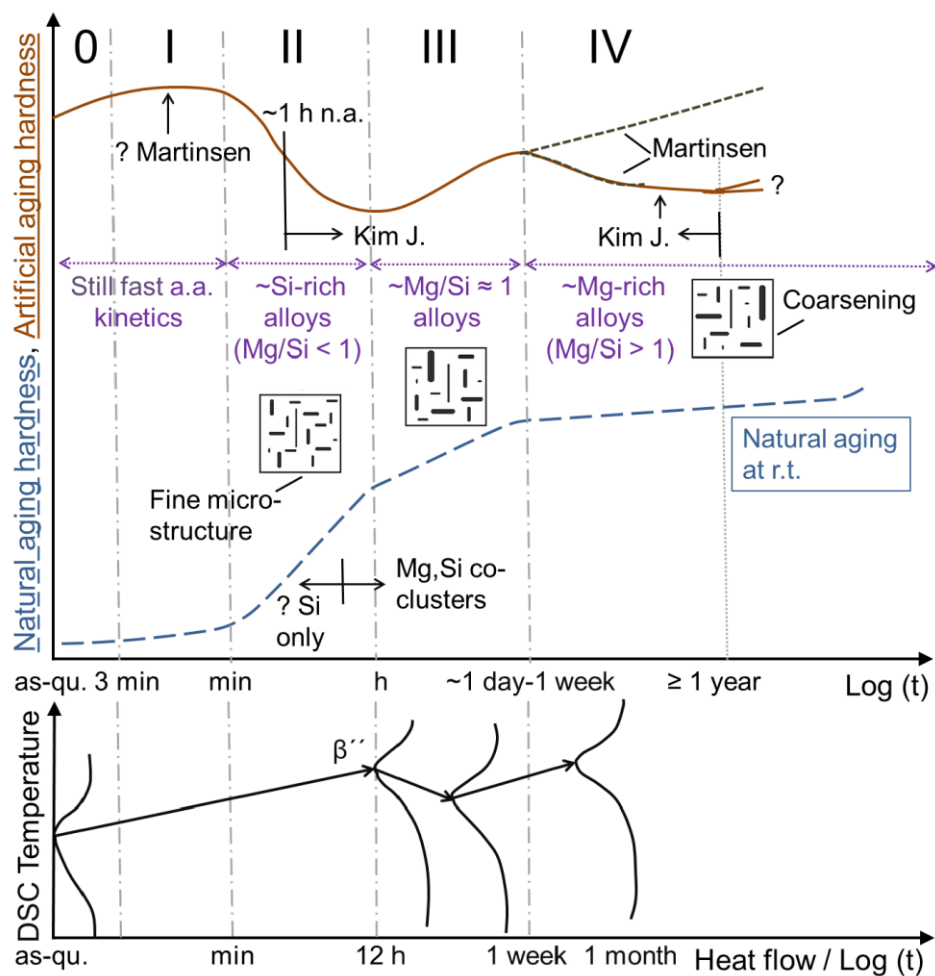

Fig. 6. Schematic dependence of artificial aging (a.a.) on the natural aging (n.a) clustering stage for n.a. at room temperature (r.t.): variation of the reachable a.a. hardness, a.a. microstructure and the a.a. kinetics perceived by the shift of the β´´ peak temperature in DSC. Reproduced from ref. [7,36,52].

2. Methods

Table 1 shows the compositions of the Mg-rich alloys investigated in this study. They were produced on a laboratory scale using a procedure described in [17].

Table 1 Composition of alloys (Al in balance)

Alloy	Sn	In	Mg	Si	Cu	Fe	Mn	Cr	Zn	Ti
	[wt.%]	[wt.%]	[wt.%]	[wt.%]	[wt.%]	[wt.%]	[wt.%]	[wt.%]	[wt.%]	[wt.%]
1	0.0026	-	0.81	0.62	0.220	0.485	0.111	0.146	0.059	0.081
2	0.042	-	0.78	0.61	0.210	0.493	0.119	0.154	0.045	0.040
3	0.043	0.039	0.78	0.62	0.211	0.5	0.118	0.152	0.045	0.039

FactSage™ 6.4 software [56,57] together with the FACT FTlite light alloy database (2014) were used for thermodynamic calculations of alloys 1-3. Table 2 lists the solubility of the main alloying elements at s.t.t. 530 °C and 570 °C (quenched-in). While in alloys 2 and 3 the solubility of Sn decreases at lower s.t.t., the solubility of In increases (compare ref. [17]).

Table 2 Solubility of alloying elements at solution treatment temperatures 530 °C and 570 °C

Alloy	s.t.t.	Sn	In	Mg	Si	Cu	Sn	In	Mg	Si	Cu
	[°C]	[wt.%]	[wt.%]	[wt.%]	[wt.%]	[wt.%]	[at.ppm]	[at.ppm]	[at.%]	[at.%]	[at.%]
1		0.0026	-	0.82	0.34	0.223	6	-	0.91	0.32	0.095
2	530	0.007	-	0.77	0.36	0.215	17	-	0.86	0.35	0.091
3		0.0073	0.0117	0.77	0.37	0.216	17	28	0.86	0.36	0.092
1		0.0026	-	0.82	0.36	0.223	6	-	0.91	0.35	0.095
2	570	0.021	-	0.79	0.39	0.213	49	-	0.88	0.37	0.091
3		0.0136	0.0104	0.78	0.39	0.213	31	24	0.87	0.38	0.091

Solution heat treatment of hardness test samples were performed in a circulating air furnace at 530 °C or 570 °C for 1.2×10^3 s followed by water-quenching to r.t. For n.a. samples were kept at 5 °C, 25 °C and 45 °C in an incubator. Artificial aging was undertaken in an oil bath at 170 °C. Brinell hardness measurements (HBW 2.5/62.5) were performed using an EMCO-Test M4 unit with a maximum standard deviation of 2.0 HBW.

DSC measurements were conducted on a NETZSCH 204 F1 Phoenix with nitrogen gas cooling using samples with ~25 mg and Al pans. The as-quenched samples were inserted less than 2.5 min after water-quenching to r.t. and cooled at 40 K/min to -40 °C with 5 min temperature equalization already employing a nitrogen gas flow of 20 ml/min, and then twice heated to 500 °C, with intermediate cooling, at a rate of 10 K/min. The re-run was used as a base line correction.

8.3 Experimental results

8.3.1 Effect of natural aging temperature

Figures 7-8 show the effect of n.a. temperature (5 °C, 25 °C and 45 °C) on the hardening kinetics of alloys 1-3 after annealing at 530 °C (Fig. 7) or 570 °C (Fig. 8). The data points assigned to clustering stages I, II and III are fitted with straight logarithmic lines. Table 3 lists the transition times as obtained from the intersections and the linear logarithmic increase within stages II and III. The Sn- and Sn+In-added alloys 2 and 3 show a higher final hardness in stage II and a sharper stage II-III transition than the "Sn-free" alloy 1. After annealing at 570 °C, the Sn-added alloy 2 retards hardening kinetics most (Fig. 8b) due to high Sn solubility (Table 2), whereas the Sn+In-added alloy 3 shows similar and slowest n.a. hardening at both s.t.t. due to increasing In and decreasing Sn solubility at lower s.t.t. (Table 2). As can be expected from the temperature dependency of diffusion, for all alloys the retardation factor between n.a. at 5 °C and 25 °C of stage I-II and II-III transition times is significantly higher than the acceleration factor between n.a. at 25 °C and 45 °C (Table 3). For the stage I-II transitions both factors tend to increase with Sn or Sn+In addition. With decreasing n.a. temperature a steeper logarithmic increase k in stage II is observed (Table 3, compare Fig. 4b). Compared to the "Sn-free" alloy 1, the increase for the Sn- and Sn+In-added alloys is steeper; for stage III this trend is less pronounced. A non-linear logarithmic hardening in stage IV can be observed, most pronounced for n.a. at 45 °C of the "Sn-free" alloy 1 and the Sn-added alloy 2 (Figs. 7a,b and 8a,b).
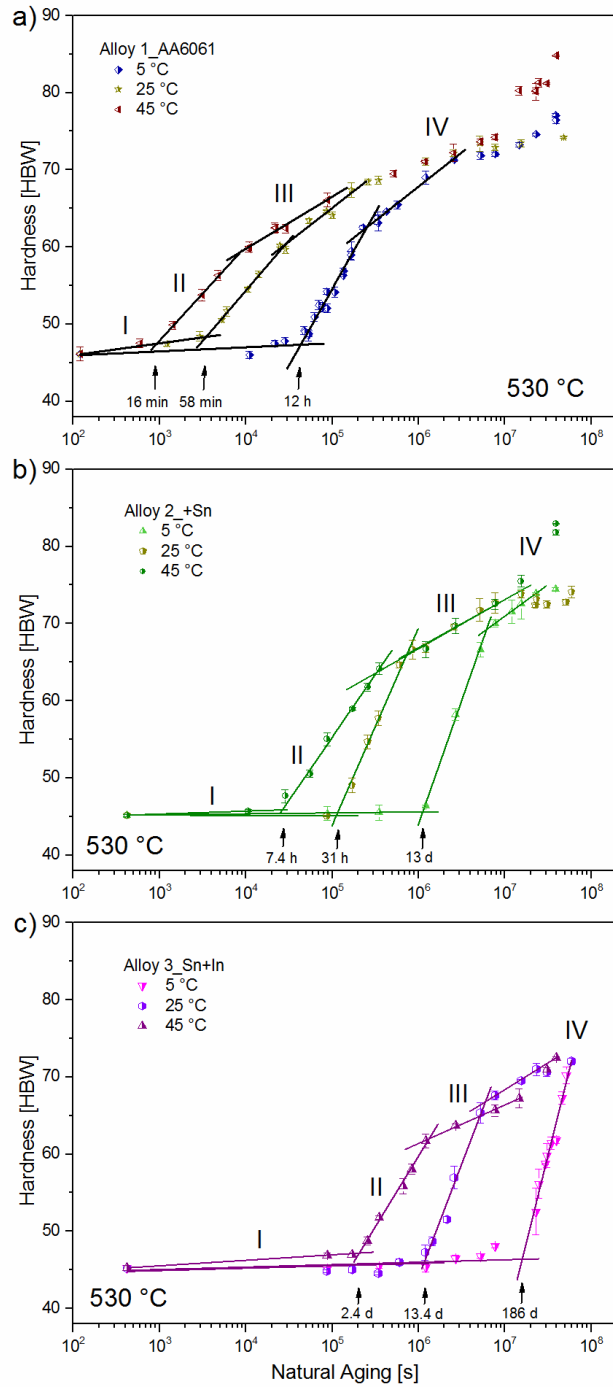
Fig. 7. Effect of natural aging temperature T (5 °C, 25 °C and 45 °C) on hardening kinetics in clustering stages I-IV after an s.t.t. of 530 °C of a) the "Sn-free" alloy 1; b) the Sn-added alloy 2; and c) the Sn+In-added alloy 3.
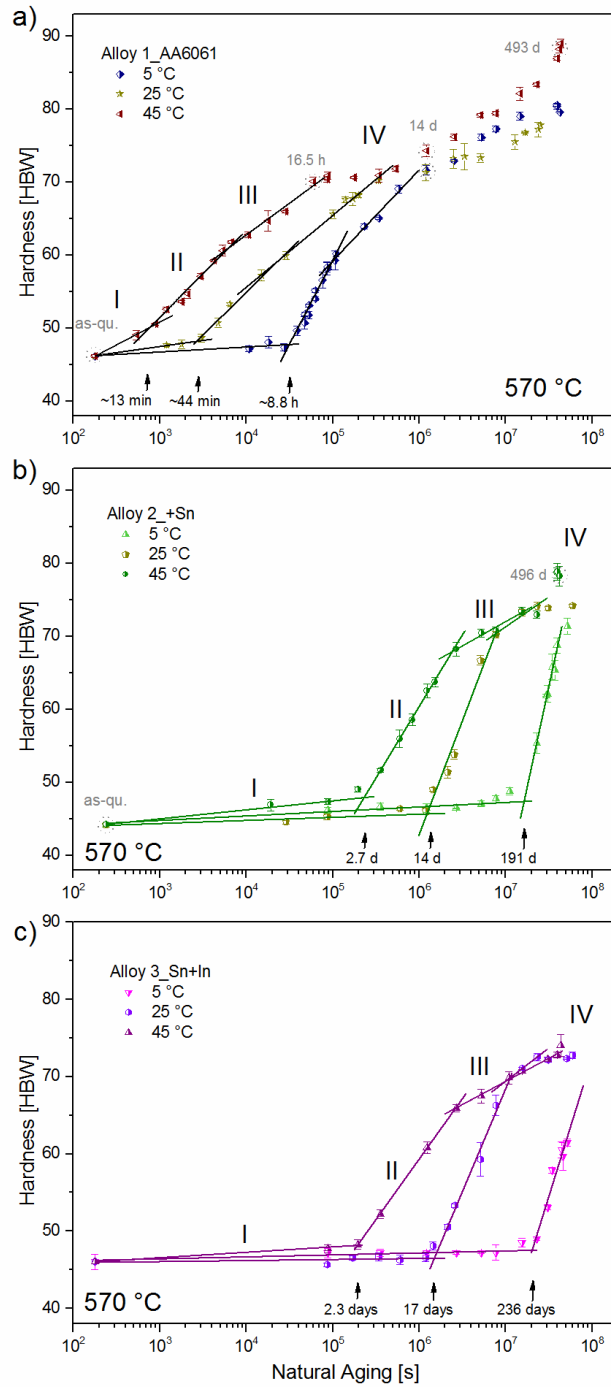
Fig. 8. Effect of natural aging temperature (5 °C, 25 °C and 45 °C) on hardening kinetics in clustering stages I-IV after an s.t.t. of 570 °C of a) the "Sn-free" alloy 1; b) the Sn-added alloy 2; and c) the Sn+In-added alloy 3. The times of DSC measurements (Fig. 10) and/or the initial hardness for subsequent artificial aging (Fig. 11) are marked.

Table 3 Transition times for natural aging (n.a.) at 5 °C, 25 °C or 45 °C between stages I-II and II-III after annealing at 530 °C or 570 °C; retardation factors between 5 °C/25 °C; acceleration factors between 25 °C/45 °C and linear logarithmic increase as fitted in Figs. 7-8.

Alloy	s.t.t.	n.a.	Transition time t [10^3 s]				log increase k	
	[°C]	[°C]	Stage I-II	Factor	Stage II-III	Factor	Stage II	Stage III
1	530	5	43.09	12.4	254.44	8.8	19.7±1.0	8.8±0.5
		25	3.47		28.75		13.1±0.8	8.7±1.1
		45	0.93	3.7	8.70	3.3	12.25±0.5	6.7±0.5
2	530	5	1132	10.0	6214	8.7	32.0±1.5	8.2±0.2
		25	112.9		712.4		25.6±1.6	6.2±0.4
		45	26.46	4.3	331.8	2.1	16.2±0.8	6.4±0.6
3	530	5	16047	13.8	≥ 51829	8.6	45.1±3.6	-
		25	1165		6038		29.4±3.0	7.0±0.7
		45	207.9	5.6	1340	4.5	18.3±0.9	5.0±0.2
1	570	5	31.5	11.8	98.14	4.1	22.9±1.5	12.5±0.6
		25	2.67		23.84		11.7±0.6	9.8±0.3
		45	0.77	3.4	6.31	3.8	11.9±0.7	8.7±0.9
2	570	5	16505	13.2	≥ 39571	5.1	54.9±4.5	-
		25	1244		7691		31.2±2.4	8.2±1.4
		45	232.5	5.4	2445	3.1	19.6±0.7	6.7±0.8
3	570	5	20418	13.3	-	-	36.0±4.5	-
		25	1514		11259		26.6±2.7	8.6± -
		45	195.0	5.4	2670	4.2	15.7±0.2	6.0±0.28

8.3.2 Data analysis

8.3.2.1 Activation energy Q calculation and temperature dependency of stage II

Figure 9a shows activation energy Q results for alloys 1-3 (Table 1) calculated using the stage I-II and II-III transition times t in Table 3 (Note: the slope of $ln(1/t)$ plotted against $1/T$ is Q/R, R is the gas constant [42,46]). Compared to the "Sn-free" alloy 1, for both s.t.t. the value of Q for the stage I-II transition tends to increase with Sn or Sn+In addition and is highest for the Sn+In-added alloy 3 after annealing at 570 °C. At 5 °C this alloy starts hardening only after ~236 days (Fig. 8c).

Within the stages, hardness follows roughly the function $H(t) = k \cdot \ln(t) + H_0$ [1]. For stage II the temperature dependency b of slope $k = f(T)$ can be described with Eq. 1,

$$k = f(T) = A \cdot e^{b \cdot T}$$

(Eq. 1)

where A is a constant. By plotting $ln(k_T)$ against the n.a. temperature T, b is obtained from the slope of the straight line; the results are shown in Fig. 9b. Compared to the "Sn-free" alloy 1, the Sn- and Sn+In-added alloys tend to show a higher temperature dependency in stage II for both s.t.t. as seen for n.a. after annealing at 530 °C.
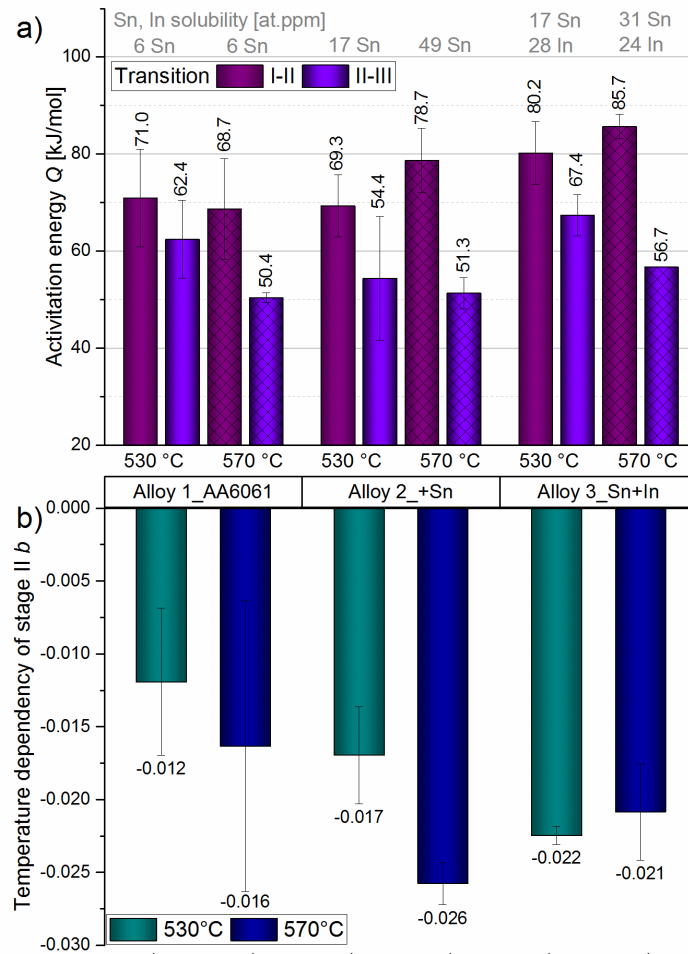
Fig. 9. a) Activation energy of clustering Q results for alloys 1-3 calculated with the stage I-II and II-III transition times (Fig. 7a) and b) temperature dependency b of the increase k in stage II (see text) for s.t.t. of 530 °C or 570 °C. The Sn- and Sn+In-added alloys show a tendency towards higher Q values and temperature dependency b.

8.3.3 Influence of natural aging stage on artificial aging

8.3.3.1 DSC analysis

Figure 10a shows DSC results for the as-quenched "Sn-free" alloy 1 and the Sn-added alloy 2. Sn significantly shifts the cluster peaks, and to a smaller extent, the precipitation peak β´´, to higher temperatures. Sn addition also greatly reduces the total heat flow of stage II cluster C1 and stage III cluster C2 (Fig. 1) compared to the commercial alloy 1, for which the cluster peaks are hardly even separable.

Figure 10b compares DSC measurements of alloy 1 after 16.5 h to 493 days of n.a. at 45 °C (stage IV) and the Sn-added alloy 2 after 496 days at 45 °C; the corresponding alloy hardness is marked in Fig. 8a and 8b. With increasing n.a. time the n.a. cluster dissolution of alloy 1 becomes stronger and a second, earlier endothermic peak appears more pronounced and is accompanied by the retardation of the exothermic precipitation peak β´´. Between 16.5 h

and 14 days the β´´ peak becomes higher, until after 60 days (not depicted) it lowers again and finally divides into a double peak for the 493 days n.a. sample. After 496 days the Sn-added sample in Fig. 10b also shows a deep n.a. cluster dissolution trace with two endothermic peaks and the beginning of a β´´ double peak formation.
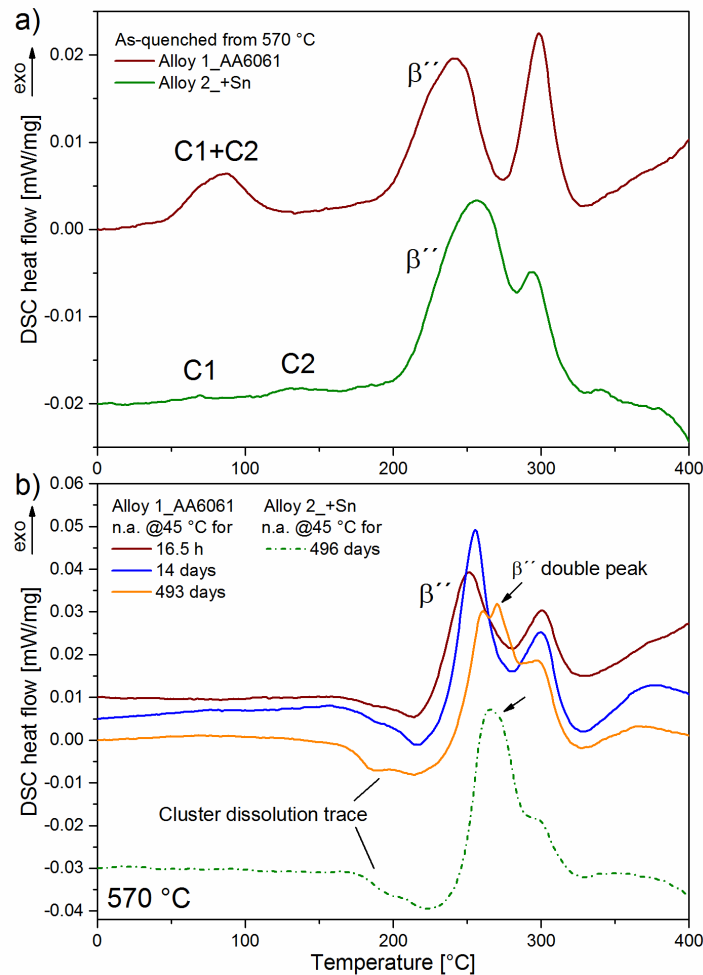

Fig. 10. a) Comparison of as-quenched DSC results for the "Sn-free" alloy 1 to Sn-added alloy 2 after an s.t.t. of 570 °C. Sn reduces the total heat flow of stage II cluster C1 and stage III cluster C2 and shifts the peaks to higher temperatures. b) DSC measurements of alloy 1 and the Sn-added alloy 2 after 16.5 h to 496 days at 45 °C.

8.3.3.2 Artificial aging

Figure 11 shows that direct a.a. (60 s at r.t.) of the "Sn-free" alloy 1 at 170 °C produces the fastest a.a. kinetics ("best case"). Slower a.a. kinetics are achieved after n.a. at 45 °C until the end of stage III for 16.5 h and prolonged n.a. in stage IV with 507 days at 45 °C, whereas the achievable maximum hardness of ~116 HBW after more than 55 h of a.a. is comparable to direct a.a. Although alloy 1 starts with the same n.a. hardness after 14 days at 25 °C, it shows much slower a.a. hardening kinetics and lower maximum hardness (~106 HBW) than after n.a. for 16.5 h at 45 °C.
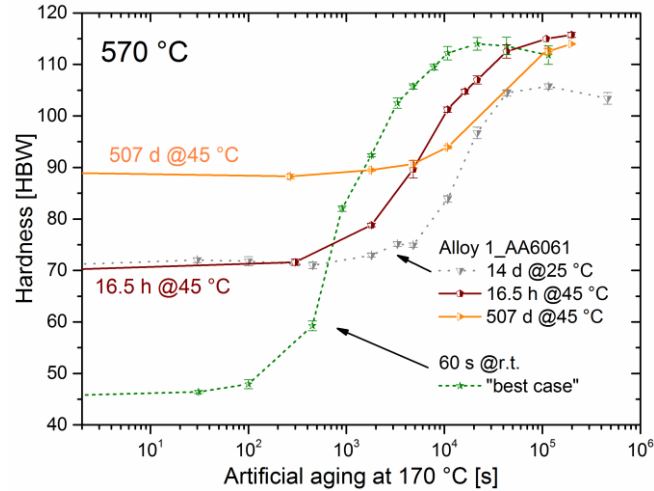
Fig. 11. Artificial aging (a.a.) of the "Sn-free" alloy 1 at 170 °C after natural aging for 16.5 h and 507 days at 45 °C compared to the "best case" of direct aging (60 s at r.t.) and a.a. after 14 days at 25 °C.

4. Discussion

Compared to the "Sn-free" alloy 1, the Sn- and Sn+In-added alloys 2 and 3 show a higher final hardness in stage II, a sharper stage II-III transition (Figs. 7-8), a tendency towards higher activation energies of clustering Q, and a higher temperature dependency in stage II (Fig. 9). DSC analysis shows that Sn reduces the cluster heat flow and shifts the cluster peaks and the β´´ peak to higher temperatures (Fig. 11a). Prolonged n.a. at 45 °C of alloy 1 in stage IV retards a.a. kinetics compared to direct a.a. and produces a β´´ double peak in DSC, but yields comparable peak hardness (Fig. 11). In contrast, a.a. after 14 days at 25 °C reduces the peak hardness. These results are interpreted based on the concise literature review in section 1.

The higher final hardness in stage II for trace element added alloys is explained as follows. If one assumes that quenched-in dissolved Sn and In atoms permanently bind most quenched-in excess structural vacancies, but like Cu take no part in the early clustering process due to repulsive interaction energies with Si [38], it seems reasonable that with fewer remaining (free) vacancies fewer Si-vacancy complexes in stage I are formed at low rates. At the transition to stage II fewer vacancies can detach to transport further atoms to the emerging vacancy-free clusters or to form new clusters. The result is a lower cluster density z, and thus the system strives for a larger average cluster radius r due to the inverse $z(r)$ relationship. This explains the (compared to the "Sn-free" alloy 1) higher final hardness in stage II and also the sharper transition to the "slow reaction" in stage III due to a possible higher vacancy $E_{b,cluster}$ of larger clusters [49] (Figs. 7 and 8). The reduction of the total DSC heat flow of clusters C1 (and C2) by Sn addition (Fig. 10a) also indicates a lower cluster number density formed during linear

heating, as also interpreted for Cu addition [8,29]. The further observed shift of clusters C1 and C2 and the β´´ peak, which with Sn becomes larger and broader, to higher temperatures (Fig. 10a) accords with the retardation of n.a. kinetics (compare Fig. 1) and a.a. kinetics at low a.a. temperatures [13].

While the concentration of quenched-in excess vacancies available for Si clustering in the "Sn-free" alloy 1 stays constant at each n.a. temperature, the higher temperature dependency of the Sn- or Sn+In-added alloys (Fig. 9) may result from the Arrhenius-like temperature dependency of solute-vacancy trapping by Sn or In [12,17], i.e. the trapping efficiency decreases with rising n.a. temperature. More untrapped vacancies may promote faster n.a. kinetics and cause the larger acceleration factors between 25 °C and 45 °C of stage I-II transition times and higher retardation factors between 5 °C and 25 °C (Table 3). Associated with the Sn and In E_b values, the thermally activated release of vacancies from Sn- or In-vacancy pairs is thus suggested as making an additional contribution to the effective activation energy Q of cluster C1 in stage II. This explains the tendency towards higher stage I-II transition Q values in Fig. 9a. Interestingly, the present results suggest that the n.a. stability of the alloy presented in ref. [17] increases from ~180-220 days at 25 °C to ~7 years at 5 °C.

Faster a.a. kinetics is observed in Fig. 11 for the "Sn-free" alloy 1 after n.a. for 16.5 h at 45 °C than after 14 days at 25 °C, although the alloys start early in stage IV with similar n.a. hardness (marked in Fig. 8a). For a.a. after n.a. at 45 °C this indicates the presence of a more beneficial n.a. microstructure than after n.a. at 25 °C, i.e. at 45 °C there exists a lower number density z of clusters with, on average, a larger radius r, as schematically shown in Fig. 4a. With a lower cluster density the dissolution of fewer unstable clusters during a.a. ends earlier, such that solutes are available earlier for re-precipitation and hardening. This assumption is supported by a smaller endothermic cluster dissolution trace and earlier β´´ peak temperature for 16.5 h n.a. at 45 °C in Fig. 10b compared to a DSC measurement after 14 days at 25 °C [58]. With a lower cluster density fewer n.a. clusters also exist for preferential growth to coarse, less hardenable β´´ needles. A higher ratio and larger number density of fine re-precipitated β´´ needles due to the fast cluster dissolution may thus generate the high a.a. strength, comparable to direct a.a. after 60 s at r.t.

With increasing n.a. time in stage IV the average cluster radius r is supposed to increase while the density $z(r)$ decreases, which causes the significant hardening in stage IV in Figs. 7 and 8. The retardation of the a.a. kinetics of the "Sn-free" alloy 1 after 507 days compared to after 16.5 h at 45 °C in Fig. 11 can thus be explained by the β´´ double peak in Fig. 10b for ~500 days of n.a. at 45 °C. This is also seen for the Sn-added alloy 2. The β´´ double peak phenomenon is known from literature [59] for a Si-rich alloy which has been strained by 5% after 1 week n.a. before the DSC measurement. There the first peak is attributed to coarse β´´

needles that evolve fast from n.a. clusters due to enhanced atomic transport along dislocations, and the second peak to fine β′′ needles that form retarded from newly available solutes after the dissolution of less stable clusters [59]. These explanations for a β′′ double peak are comparable to the negative effect of Mg/Si ≈ 1 and Mg-rich alloys where after n.a. until stage IV a coarsening of the a.a. microstructure follows (Fig. 5 and 6) [7,36]. Hence, the first β′′ peak after long-term n.a. at 45 °C (Fig. 10b) may result from the slow preferential growth of a few large Mg-rich n.a. clusters at possibly preferred sites such as dislocations [60]. Due to the high Mg/Si ratio of the alloy of ~2.3 (Table 2), larger clusters after prolonged n.a. need prolonged times to adopt a chemistry close to a Mg/Si ratio of ideally ~1 ($Mg_2Si_2Al_7$ [24]) up to perhaps ~1.5 according to the compositional variation of short-elongated precipitates [6,60]. This also accords with the highest Mg,Si co-cluster formation rates for DSC cluster C2 in Mg/Si ≈ 1-1.5 alloys [9]. Hence, Si addition is necessary for a structural and dynamic compositional change to β′′ with $(Al+Mg)_5Si_6$ [24,55] or a chemically lesser ordered Mg-rich variant [60,61], possibly provided by pipe diffusion along dislocations [60]. The second β′′ peak after ~500 days of n.a. at 45 °C may result from a retarded vacancy release for re-precipitation [19] due to slower dissolution of larger unstable Mg-rich n.a. clusters than after n.a. for 16.5 h, as perceived by the broader and deep cluster dissolution trace in Fig. 10b.

With regard to the negative effect, it may be concluded that prolonged n.a. in stage IV increasingly retards a.a. kinetics due to slower cluster dissolution kinetics and slower preferential growth of β′′ needles. The reachable strength, however, strongly depends on the ratio and size of less hardenable, coarse, preferentially grown β′′ needles and the increasing amount of fine re-precipitated β′′ needles. This agrees with TEM analysis in literature, which shows a fine uniform a.a. microstructure with high precipitate number density for direct a.a. [52,60], a coarse microstructure with low density at the beginning of stage IV [52,60], and, after prolonged storage at r.t. (Fig. 6), an intermediate density of both fine precipitates and smaller coarse β′′ needles [52].

8.5 Conclusions

Based on the literature review of natural aging (n.a.) in Al–Mg–Si alloys, n.a.'s effect on artificial aging (a.a.) and a refined picture of the underlying mechanisms, we interpret our results for alloys with and without trace element additions as follows.

- The trapping of quenched-in excess vacancies by Sn and/or In decreases the cluster number density while increasing the cluster size, which explains the more pronounced n.a. hardness increase in stage II and the low DSC heat flow of clusters.

- Sn or Sn+In addition increases the effective activation energy Q for early stage cluster formation, which is explained by an additional contribution of a thermally activated vacancy release from Sn- and In-vacancy pairs.

- N.a. hardness mainly depends on the cluster size, and to a lower degree the cluster number density.

- Prolonged n.a. lasting from weeks to years increasingly retards a.a. kinetics due to increasingly slower cluster dissolution kinetics and slower preferential growth of β´´ needles. The reachable strength, however, strongly depends on the ratio and size of less hardenable, coarse, preferentially grown β´´ needles and the increasing amount of fine re-precipitated β´´ needles.

Acknowledgements

References

[1] Banhart J, Chang C, Liang Z, Wanderka N, Lay M, Hill A. Advanced Engineering Materials 2010;12:559–71.

[2] Banhart J, Lay M, Chang C, Hill A. Physical Review B 2011;83:14101.

[3] Liu M, Čížek J, Chang C, Banhart J. Acta Materialia 2015;91:355–64.

[4] Chang C, Banhart J. Metallurgical and Materials Transactions A: Physical Metallurgy and Materials Science 2011;42:1960–4.

[5] Zandbergen MW, Cerezo A, Smith G. Acta Materialia 2015;101:149–58.

[6] Zandbergen MW, Xu Q, Cerezo A, Smith G. Acta Materialia 2015;101:136–48.

[7] Kim J, Kobayashi E, Sato T. Materials Transactions 2015;56:1771–80.

[8] Liang Z, Chang C, Banhart J, Hirsch J. The effect of Cu and Cr on clustering and precipitation in Al–Mg–Si alloys., in: ICAA13: 13th International Conference on Aluminum Alloys: John Wiley & Sons, Inc; 2012. p. 1125–1130.

[9] Kim S, Kim J, Tezuka H, Kobayashi E, Sato T. Materials Transactions 2013;54:297–303.

[10]   Wolverton C. Acta Materialia 2007;55:5867–72.

[11]   Hardy HK. Journal of the Institute of Metals 1950;78:169.

[12]   Pogatscher S, Antrekowitsch H, Werinos M, Moszner F, Gerstl S, Francis MF, Curtin WA et al. Physical Review Letters 2014;112:225701–5.

[13]   Werinos M, Antrekowitsch H, Kozeschnik E, Ebner T, Moszner F, Löffler JF, Uggowitzer PJ et al. Scripta Materialia 2016;112:148–51.

[14]   Werinos M, Antrekowitsch H, Fragner W, Ebner T, Uggowitzer PJ, Pogatscher S. Influence of Alloy Production History on Natural Aging of AA6061 Modified with Sn, in: GDMB (Ed.). Proceedings of European Metallurgical Conference (EMC) 2015. Clausthal-Zellerfeld: GDMB Verlag GmbH; 2015. p. 303–310.

[15]   Werinos M, Antrekowitsch H, Fragner W, Ebner T, Uggowitzer P, Pogatscher S. TMS Light Metals 2015:367–71.

[16]   Werinos M, Antrekowitsch H, Fragner W, Ebner T, Uggowitzer PJ, Pogatscher S. Influence of Sn-solubility on suppression of natural aging in an AA6061 aluminum alloy. Oral Presentation at Materials Science & Technology (MS&T) 2014. Pittsburgh, Pennsylvania, USA; 2014.

[17]   Werinos M, Antrekowitsch H, Ebner T, Prillhofer R, Curtin WA, Uggowitzer PJ, Pogatscher S. Design strategy for controlled natural aging in Al–Mg–Si alloys; submitted to Acta Materialia.

[18]   Werinos M, Antrekowitsch H, Fragner W, Ebner T, Uggowitzer PJ, Pogatscher S. Materials Science and Technology Conference and Exhibition 2014, MS and T 2014 2014;2:1283–9.

[19]   Pogatscher S, Antrekowitsch H, Leitner H, Ebner T, Uggowitzer P. Acta Materialia 2011;59:3352–63.

[20]   Strobel K, Lay M, Easton MA, Sweet L, Zhu S, Parson NC, Hill AJ. Materials Characterization 2016;111:43–52.

[21]   Lay M, Zurob HS, Hutchinson CR, Bastow TJ, Hill AJ. Metallurgical and Materials Transactions A: Physical Metallurgy and Materials Science 2012;43:4507–13.

[22]   Torsaeter M, Hasting H, Lefebvre W, Marioara C, Walmsley J, Andersen S, Holmestad R. Journal of Applied Physics 2010;108:073527-1 - 073527-9.

[23]   Serizawa A, Hirosawa S, Sato T. Metallurgical and Materials Transactions A: Physical Metallurgy and Materials Science 2008;39:243–51.

[24]   Chen JH, Costan E, van Huis MA, Xu Q, Zandbergen HW. Science 2006;312:416–9.

[25]   Pogatscher S, Kozeschnik E, Antrekowitsch H, Werinos M, Gerstl S, Löffler JF, Uggowitzer PJ. Scripta Materialia 2014;89:53–6.

[26]   Mantina M, Wang Y, Chen L, Liu Z, Wolverton C. Acta Materialia 2009;57:4102–8.

[27] Simonovic D, Sluiter M. Physical Review B - Condensed Matter and Materials Physics 2009;79.

[28] Chang C, Liang Z, Schmidt E, Banhart J. International Journal of Materials Research 2012;103:955–61.

[29] Liang Z. Clustering and Precipitation in Al-Mg-Si Alloys. PhD thesis. Berlin; 2012.

[30] Liu M, Čížek J, Chang C, Banhart J. Materials Science Forum 2014;794-796:33–8.

[31] Fallah V, Langelier B, Ofori-Opoku N, Raeisinia B, Provatas N, Esmaeili S. Acta Materialia 2016;103:290–300.

[32] Liang Z, Chang C., Wanderka N., Banhart J., Hirsch J. The Effect of Fe, Mn and Trace Elements on Precipitation in Al-Mg-Si Alloy, in: Proceedings of the 12th International Conference on Aluminium Alloys. p. 492–497.

[33] Brenner, P., Kostron, H. Zeitschrift für Metallkunde 1939;4:89–97.

[34] Hirth SM, Marshall GJ, Court SA, Lloyd DJ. Materials Science and Engineering A 2001;319-321:452–6.

[35] Gupta A, Lloyd D, Court S. Materials Science and Engineering A 2001;316:11–7.

[36] Tao GH, Liu CH, Chen J, Lai YX, Ma PP, Liu LM. Materials Science and Engineering A 2015;642:241–8.

[37] Zurob H, Seyedrezai H. Scripta Materialia 2009;61:141–4.

[38] Hirosawa S, Nakamura F, Sato T. Materials Science Forum 2007;561-565:283–6.

[39] Fickett FR. Cryogenics 1971;11:349–67.

[40] Hatch J. Aluminum: Properties and Physical Metallurgy: A S M International; 1984.

[41] Weisz T, Warczok P, Ebner T, Falahati A, Kozeschnik E. Materials Science Forum 2015;828-829:468–73.

[42] Panseri C, Federighi T. Journal of the Institute of Metals 1966;94:99–105.

[43] Røyset J, Stene T, Saeter JA, Reiso O. Materials Science Forum 2006;519-521:239–44.

[44] Kovaćs I, Lendvai J, Nagy E. Acta Metallurgica 1972;20:975–83.

[45] Seyedrezai H, Grebennikov D, Mascher P, Zurob H. Materials Science and Engineering A 2009;525:186–91.

[46] Esmaeili S, Poole WJ, Lloyd DJ. Materials Science Forum 2000;331-337 II:995–1000.

[47] Panseri C, Gatto F, Federighi T. Acta Metallurgica 1958;6:198–204.

[48] Nishimura K, Matsuda K, Komaki R, Nunomra N, Wenner S, Holmestad R, Matsuzaki T et al. Archives of Metallurgy and Materials 2015;60:925–9.

[49] Federighi T, Thomas G. Philosophical Magazine 1962;7:127–31.

[50] Liu M. Clustering Kinetics in Al-Mg-Si Alloys Investigated by Positron Annihilation Techniques. PhD thesis. Berlin; 2014.

[51] Ried A, Schwellinger P, Bichsel H. Aluminium 1977;53:595–9.

[52] Martinsen FA, Ehlers F, Torsæter M, Holmestad R. Acta Materialia 2012;60:6091–101.

[53] Chang C, Wieler I, Wanderka N, Banhart J. Ultramicroscopy 2009;109:585–92.

[54] Pogatscher S, Antrekowitsch H, Ebner T, Uggowitzer P. TMS Light Metals 2012:415–20.

[55] Zandbergen H, Andersen S, Jansen J. Science 1997;277:1221–5.

[56] Bale C, Chartrand P, Degterov S, Eriksson G, Hack K, Ben Mahfoud R, Melançon J et al. Calphad: Computer Coupling of Phase Diagrams and Thermochemistry 2002;26:189–228.

[57] Bale C, Bélisle E, Chartrand P, Decterov S, Eriksson G, Hack K, Jung I et al. Calphad: Computer Coupling of Phase Diagrams and Thermochemistry 2009;33:295–311.

[58] Pogatscher S, Antrekowitsch H, Leitner H, Pöschmann D, Zhang Z, Uggowitzer P. Acta Materialia 2012;60:4496–505.

[59] Birol Y, Karlik M. Scripta Materialia 2006;55:625–8.

[60] Pogatscher S, Antrekowitsch H, Leitner H, Sologubenko A, Uggowitzer P. Scripta Materialia 2013;68:158–61.

[61] Marioara C.D., Andersen S.J., Zandbergen H.W., Holmestad R. Metallurgical and Materials Transactions A: Physical Metallurgy and Materials Science 2005;36:691–702.

9 SUMMARY & OUTLOOK

9.1　Summary

Today Al-Mg-Si alloys (6xxx series) in wrought, cast or extruded form represent the commercially most important group of age hardenable aluminum alloys. The wish to control natural aging kinetics and to find a solution to the negative effect of room temperature storage on artificial aging, discovered in 1939, is of major importance for the aluminum manufacturing industry. Based on preliminary results of a preceding study, the main objectives of this thesis were the minimization of natural aging and maximization of the artificial aging potential of Al-Mg-Si alloys with and without trace element additions to commercial Al-Mg-Si alloys.

To obtain a general understanding how trace Sn additions to the alloy AA6061 are able to suppress natural aging for > 2 weeks after quenching from 570 °C with simultaneous enhancement of artificial aging kinetics, a thermodynamic model and first-principles computations of Sn-vacancy binding were necessary. The real Sn solubility in fcc aluminum in the alloy AA6061 was determined by atom probe tomography (APT) measurements with ~100 at.ppm. With this knowledge the mechanism controlling aging could be explained: The strong Sn-vacancy binding energy results in trapping of most quenched-in excess structural vacancies in predominantly Sn-vacancy pairs. This generates a reduced number of quenched-in vacancies in the matrix which can control diffusional processes of other alloying atoms (Mg, Si or Cu) and thus significantly retards all clustering processes. While suppression of natural aging prevails, the release of vacancies from Sn-vacancy pairs significantly enhances artificial kinetics at 170 °C in trace Sn-added AA6061 compared to the naturally pre-aged commercial case. The buffering of vacancies by Sn thus retards natural aging hardening and allows diffusion on demand for the precipitation of the peak hardening phase β´´ during artificial aging.

The observation of a change from a negative to a positive influence of natural pre-aging on subsequent artificial aging in the alloy AA6061 at temperatures above 210 °C led to the formulation of the "vacancy prison mechanism" by Pogatscher et al. in 2011. To shed more light on the mechanisms controlling aging at such unconventionally high temperatures a comparative analysis of direct artificial aging kinetics and the naturally pre-aged case with and without trace Sn addition was performed. The effect of Sn could be shown to be phenomenological similar to the positive effect of natural pre-aging at high temperatures in the commercial alloy. Additionally trace Sn addition generates both ultrafast artificial aging kinetics and superior peak hardness. This could be explained by a detailed analysis of the contribution of quenched-in excess structural vacancies to the nucleation and growth of age-hardening precipitates with and without Sn addition. It is supposed that besides the release of trapped vacancies, during artificial aging Sn-vacancy pairs contribute to diffusion and/or Sn retards the annihilation of quenched-in vacancies.

The results reported before were investigated at the solution treatment temperature of 570 °C and Sn addition to an AA6061 alloy with a fixed Mg, Si and Cu content. Conventionally processing parameters and compositional limits of different Al-Mg-Si alloys and products vary and therefore the influence on natural aging kinetics with and without trace element addition varies. A decrease in the solution treatment temperature from 570 °C to 510 °C results in a decreasing delay of natural aging hardening. This could be explained with thermodynamic calculations for the Sn-added alloy AA6061 that disclosed a decrease in the maximum quenchable Sn amount below 570 °C. Such calculations were also able to explain the effect of a systematic variation of the Mg, Si and Cu content. An increase in the Si content significantly decreases the suppressive effect of Sn during natural aging while Mg shows a comparable, but lower effect due to a reduction of the quenchable Sn solubility. Cu addition on the other hand does not influence the Sn solubility, but by trend retards early stage kinetics.

For a transfer of the trace element effect to industrial scale production the knowledge if material gravity mould-cast and rolled in laboratory behaves comparably as industrially produced wrought sheets or plates is important. Thus the influence of the industrial production route of AA6061 was investigated with and without Sn addition for two different solution treatment temperatures and two different combinations of the Mg, Si and Cu content. It could be shown that the suppressive effect of Sn on natural aging kinetics of the alloy AA6061 is similar for industrially produced material and material produced in laboratory with comparable composition. Industrially produced material only shows a higher as-quenched hardness than laboratory sheets. This initial hardness increase is suggested to result from higher degrees of deformation during industrial rolling that can cause smaller fragmented intermetallic phases and/or from the different texture of grains.

Through the investigation of the influence of the solution treatment temperature, the production history, the variation of the Mg, Si and Cu content and theoretical considerations, a design strategy for a maximum suppression of natural aging in Al-Mg-Si alloys was developed. The significant effect of Si addition on the suppressive effect of Sn can be interpreted when Si-related clustering is assumed to control the beginning of natural aging and its kinetics, while Si additionally lowers the quenchable Sn solubility. Therefore it has been proposed that the reduction of the free excess vacancy concentration by Sn is most important for early Si clustering. Cu does not influence the Sn solubility and is therefore believed to show a similar, but weaker effect as Sn, whereas Mg lowers the quenchable Sn solubility only. Exploration of combined trace element addition of Sn and In showed comparable natural aging kinetics after quenching from 530 °C and 570 °C which is explained by an increasing In solubility at low temperatures. Application of the new design strategy led to the development of a new Sn-

added Al-Mg-Si alloy that shows natural aging stability of > 6 months for high solution treatment temperatures and a significant artificial aging potential.

A maybe more difficult to control parameter than the guidelines proposed within the design strategy for controlled natural aging, is the storage temperature of solution heat treated material before the final artificial aging step. The investigation of storage temperatures between 5 °C and 45 °C on various AA6061 alloys (see also the Appendix) with and without trace element addition of Sn and/or In showed a strong dependence of natural aging hardening kinetics on temperature. Sn- and Sn+In-added alloys showed by trend higher activation energies for early stage clustering, which is explained by an additional contribution of a thermally activated vacancy release from Sn- and In-vacancy pairs. Applying this knowledge also the developed alloy should show up to one month of stability for natural aging at 45 °C and up to ~7 years of stability at 5 °C.

Based on a concise literature review with an in-depth analysis of recent literature and therefrom-generated new cross-links on natural aging in Al-Mg-Si alloys and its effect on artificial aging, suggestions of mechanisms underlying natural aging could be refined. Some parts of the review have been included in the introduction of this thesis. The derived overall mechanistic picture of natural aging enabled us to understand our results about the effect of natural aging temperature and prolonged storage (up to years) in Al-Mg-Si alloys with and without trace element additions. The trapping of quenched-in excess vacancies by Sn and/or In decreases the cluster number density during natural aging while increasing the cluster size, which explains the pronounced natural aging hardness increase in stage II and the low DSC heat flow of clusters compared to a commercial alloy. It could be interpreted from DSC measurements and artificial aging curves obtained after prolonged natural aging at 25 °C and 45 °C that prolonged natural aging between weeks and up to years increasingly retards artificial aging kinetics due to slower cluster dissolution kinetics and slower preferential growth of β´´ needles. The reachable strength though strongly depends on the ratio and size of less hardenable coarse preferentially grown β´´ needles and increasing amount of fine re-precipitated β´´ needles.

In this view, the project succeeded in a sustainable alloy development for industrial application with the simultaneous aim to significantly improve the current understanding of underlying mechanisms. The developed alloy shows maximum suppression of natural aging and simultaneous high artificial aging potential and may pave the way for a new class of Al-Mg-Si alloys with their own property profile. To capitalize on these great advantages, AMAG rolling has already filed patents which apply the above-described principles (*Age-hardenable aluminum alloy and method for improving the ability of a semi-finished or finished product to age artificially.*

WO2013124472A1. Annealable aluminium alloy and method for improving artificial ageing ability. EP2631317A1.).

9.2 Outlook

The following sections discuss additional preliminary results for the commercial alloys AA6061 and AA6016 with and without trace Sn addition and suggest further research topics.

9.2.1 Influence of stretching

Usually industrial plates are stretched several hours after an industrial solution heat treatment to reduce quenched-in internal stresses. Figure 9.1 shows the negligible influence of a stretching procedure performed in laboratory 2 h after the solution heat treatment on natural aging kinetics with and without Sn addition. This effect though depends on the alloy investigated, the heat treatment history and also on the natural aging clustering stage in which the plastic deformation is performed. Thus there exists a significant potential for further investigations in this field.
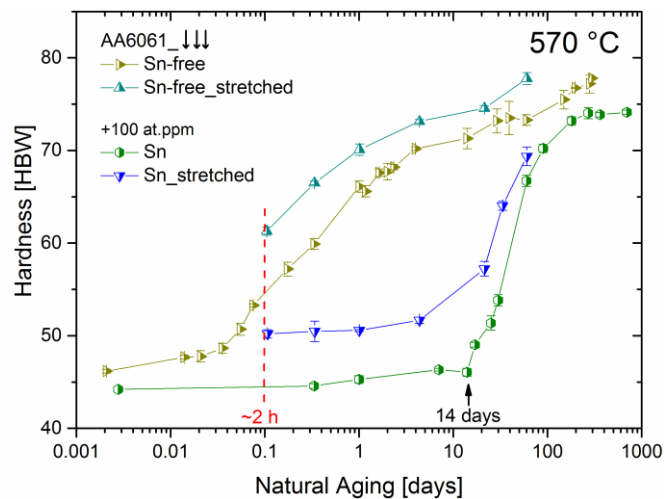

Figure 9.1. Influence of plastic deformation 2 h after quenching from 570 °C on natural aging kinetics with and without 100 at.ppm Sn addition to the alloy AA6061

9.2.2 Influence of quenching rate

In contrast to the trace Sn-added AA6061 alloys mostly investigated in this thesis, which show a significant dependence on the quenching rate, the trace Sn-added sheet alloy AA6016 showed no or negligible dependence on the solution treatment temperature or the quenching rate. As shown in Figure 9.2a, Sn additions of 100 at.ppm achieve to suppress natural aging for up to

8 h followed by comparable kinetics after a water-quench from both solution treatment temperatures for AA6016. Free cooling in air on an aluminum surface shows a similar retardation of hardening followed by slightly faster kinetics. Independently of the quenching rate trace Sn additions of 20 at.ppm similarly retard natural aging by ~8 h (Figure 9.2b).
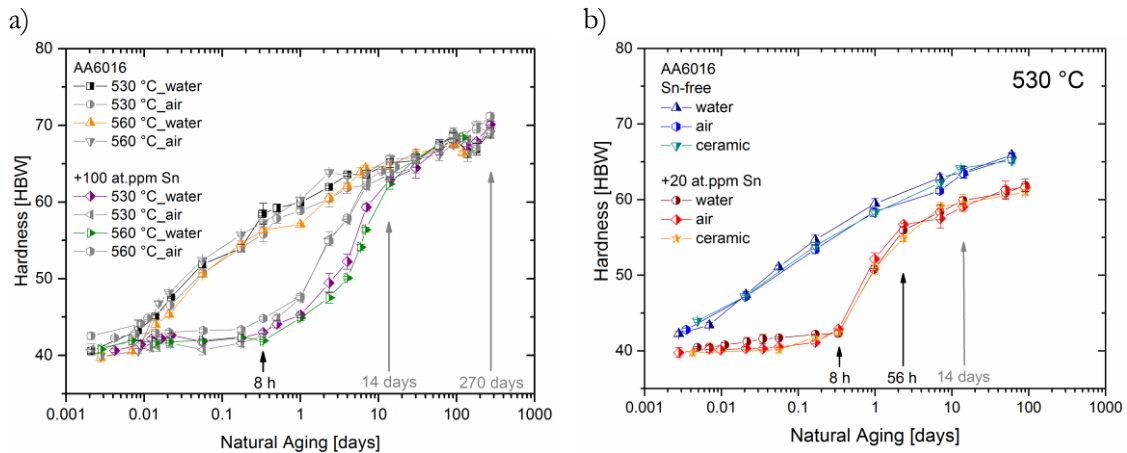

Figure 9.2. Natural aging kinetics for different quenching rates for the sheet alloy AA6016 with a) 100 at.ppm Sn addition and two solution treatment temperatures and b) with 20 at.ppm Sn addition

Based on thermodynamic calculations, a Sn solubility of > 100 at.ppm in the alloy AA6016 at both solution treatment temperatures is supposed to result in comparable natural aging kinetics after quenching from different temperatures. Compared to AA6061 alloys with and without Sn addition, the high Si-content of ~1 wt.% results in fast kinetics as Mg does not take part in early stage clustering.

The reason why 20 and 100 at.ppm Sn additions to the alloy AA6016 result in similar natural aging kinetics still has to be clarified, because of which there exists a significant potential for further investigations in this field.

In contrast to the alloy AA6016, the developed alloy and other AA6061 alloys investigated in this thesis show a significant influence of the quenching rate on natural aging kinetics (see Figures 9.3a and 9.3b). Scanning transmission electron microscopy (STEM) measurements in Figure 9.3c indicate that this results from the high content of dispersoid forming elements such as Fe, Cr and Mn in AA6061: With decreasing quenching rate an increasing amount of Sn-containing precipitates form on dispersoids. This reduces the quenchable, dissolved Sn concentration during natural aging and thus the maximum achievable suppression of natural aging.
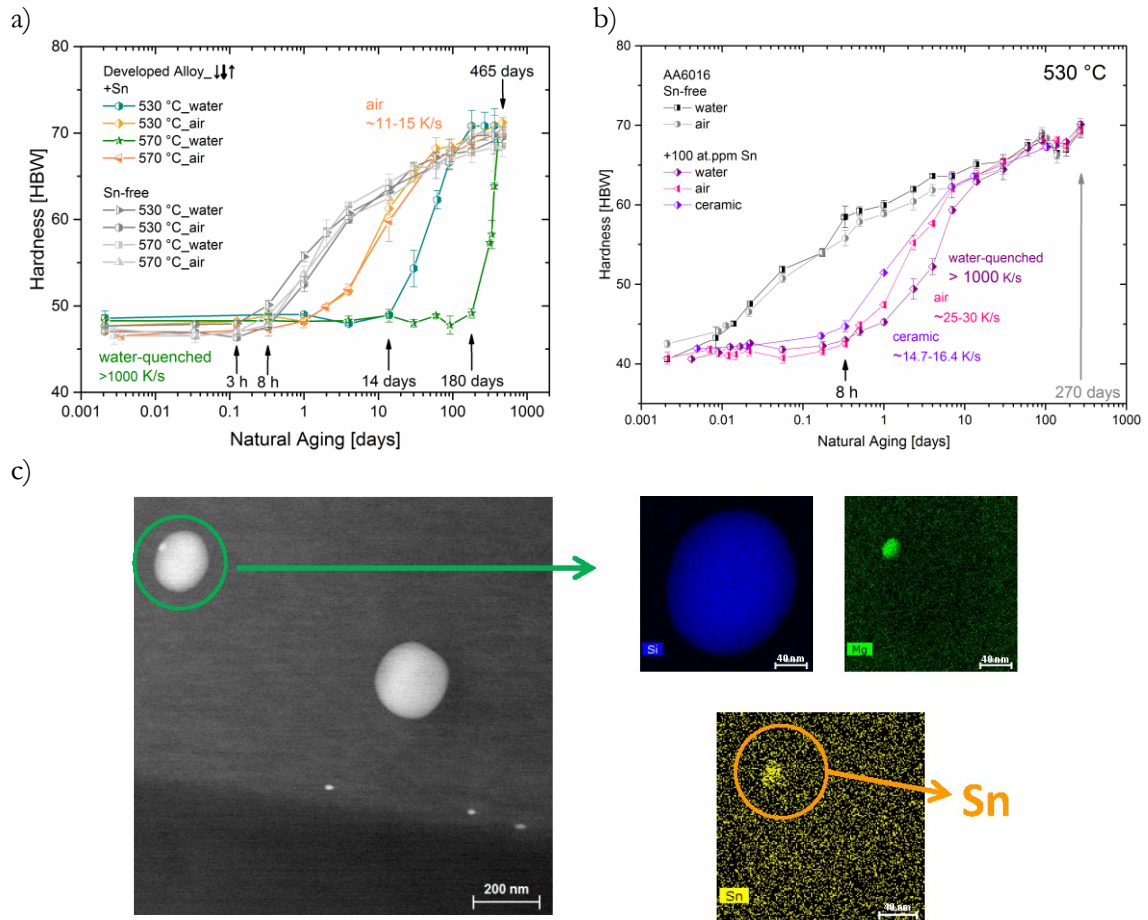
Figure 9.3. Influence of quenching rate on natural aging kinetics for the a) developed alloy and b) sheet alloy AA6016. c) Scanning transmission electron microscopy (STEM) measurements of Sn-containing precipitates on dispersoids formed at low quenching rates

Additionally, an air quench of the developed AA6061 alloy with and without Sn addition results in same natural aging kinetics for different solution treatment temperatures (Figure 9.3a). Due to the sharply decreasing Sn solubility at temperatures < 570 °C, during a slow air quench from 570 °C or 530 °C a much lower maximum Sn solubility present at a temperature << 530 °C will be quenched in for both temperatures. Also the maximum amount of Sn will precipitate on dispersoids in the time available.

Preliminary STEM measurements for the alloy AA6016 confirmed that the low concentration of Fe, Cr and Mn in the alloy results in the formation of few dispersoids and thus in a low quench sensitivity.

To avoid the negative influence of the quenching rate in industrial production, it has been recommended to produce the developed alloy with a reduced Fe, Cr and Mn content. As Fe, Ti etc. bind Si atoms, the Si content of the alloy has to be reduced to obtain the same quenchable, dissolved Si concentration.

Summing up, the gained knowledge is believed to facilitate the industrial implementation, i.e. to not only trigger the internal product development at AMAG rolling but for Al-Mg-Si alloys in general.

APPENDIX

CURRICULUM VITAE

Marion Werinos

Eschenweg 7, 8230 Hartberg, Austria

Telephone: 0043 664 5591918 / E-mail: marion.werinos@gmx.at

Professional Career

Since 2012   Research assistant at the Chair of Nonferrous Metallurgy, Montanuniversitaet Leoben, Austria

Education

Since 2012   PhD student at the Chair of Nonferrous Metallurgy, Montanuniversitaet Leoben; Several research stays at the Laboratory of Metal Physics and Technology, ETH Zurich, Switzerland

2006 – 2012   Diploma program in Materials Science, Montanuniversitaet Leoben, Austria (MSc)

Awards and Honors

2014   Graduate Excellence in Materials Science Sapphire Award, The Basic Science Division of the American Ceramic Society, US

2012   Rektor-Platzer-Ring, Montanuniversitaet Leoben, Austria

Publication List

Peer Reviewed Papers

Werinos M, Antrekowitsch H, Ebner T, Prillhofer R, Uggowitzer PJ, Pogatscher S. Hardening of Al-Mg-Si alloys: Effect of trace elements and prolonged natural aging. Submitted to Current Opinion in Solid State & Materials Science (2016)

Werinos M, Antrekowitsch H, Ebner T, Prillhofer R, Curtin WA, Uggowitzer PJ, Pogatscher S. Design strategy for controlled natural aging in Al-Mg-Si alloys. Submitted to Acta Materialia (2016)

Werinos M, Antrekowitsch H, Kozeschnik E, Ebner T, Moszner F, Löffler JF, Uggowitzer PJ, Pogatscher S. Ultrafast artificial aging of Al-Mg-Si alloys. Scripta Materialia 2016; 112:148–51.

Pogatscher S, Kozeschnik E, Antrekowitsch H, Werinos M, Gerstl S, Löffler JF, Uggowitzer PJ. Process-controlled suppression of natural aging in an Al-Mg-Si alloy. Scripta Materialia 2014; 89:53–6.

Pogatscher S, Werinos M, Antrekowitsch H, Uggowitzer PJ. The role of vacancies in the aging of Al-Mg-Si alloys. Materials Science Forum 2014; 794-796:1008–13.

Pogatscher S, Antrekowitsch H, Werinos M, Moszner F, Gerstl S, Francis MF, Curtin WA, Löffler JF, Uggowitzer PJ. Diffusion on Demand to Control Precipitation Aging: Application to Al-Mg-Si Alloys. Physical Review Letters 2014; 112:225701–5.

Proceedings

Werinos M, Antrekowitsch H, Fragner W, Ebner T, Uggowitzer PJ, Pogatscher S. Influence of Alloy Production History on Natural Aging of AA6061 Modified with Sn, in: GDMB (Ed.). Proceedings of European Metallurgical Conference (EMC) 2015. Clausthal-Zellerfeld: GDMB Verlag GmbH; 2015. p. 303–310.

Werinos M, Antrekowitsch H, Fragner W, Ebner T, Uggowitzer PJ, Pogatscher S. Influence of temperature on natural aging kinetics of AA6061 modified with Sn. TMS Light Metals 2015:367–71.

Pogatscher S, Antrekowitsch H, Werinos M, Rank G, Kaiß A, Prillhofer R, Löffler JF, Uggowitzer PJ. Statistical and Thermodynamic Optimization of Trace-Element Modified Al-Mg-Si-Cu Alloys. TMS Light Metals 2015:263–70.

Pogatscher S, Antrekowitsch H, Werinos M, Prillhofer R, Uggowitzer PJ. Optimierung der Wärmebehandlung von Aluminiumwerkstoffen der 6xxx-Familie, in: Chimani CM, Kraly A, Uggowitzer PJ (Eds.). 8. Ranshofener Leichtmetalltage 2014: Leichtmetalle - Prozesse - Anwendungen: Zukunftstechnologien als Basis für neue Mobilitätskonzepte; 2014. p. 136–142.

Werinos M, Antrekowitsch H, Fragner W, Ebner T, Uggowitzer PJ, Pogatscher S. Influence of Sn-solubility on suppression of natural aging in an AA6061 aluminum alloy. Materials Science and Technology Conference and Exhibition 2014, MS and T 2014 2014; 2:1283–9.

Talks

Werinos M, Antrekowitsch H, Fragner W, Ebner T, Uggowitzer PJ, Pogatscher S. Influence of Alloy Production History on Natural Aging of AA6061 Modified with Sn. Oral Presentation at EMC 2015. Düsseldorf, Germany; 2015.

Werinos M, Antrekowitsch H, Fragner W, Ebner T, Uggowitzer P, Pogatscher S. Influence of temperature on natural aging kinetics of AA6061 modified with Sn. Oral Presentation at TMS 2015. Orlando, USA; 2015.

Werinos M, Antrekowitsch H, Fragner W, Ebner T, Uggowitzer PJ, Pogatscher S. Influence of Sn-solubility on suppression of natural aging in an AA6061 aluminum alloy. Oral Presentation at Materials Science & Technology (MS&T) 2014. Pittsburgh, Pennsylvania, USA; 2014.

Werinos M, Pogatscher S, Antrekowitsch H, Ebner T, Moszner F, Uggowitzer PJ. Influence of Microalloying Elements on the Negative Effect of Natural Pre-Aging on Artificial Aging in Al-Mg-Si Alloys. Oral Presentation at LightMat 2013. Bremen; 2013.

Posters

Werinos M. Rapid artificial aging of Al-Mg-Si alloys. Poster at EMC 2015. Düsseldorf; 2015.

Werinos M. Rasche Warmauslagerung von Al-Mg-Si Legierungen. Poster at ASMET Forum 2015. Leoben, Österreich; 2015.

Kolb G, Kremmer T, Werinos M. Legierungsdesign von Aluminium-Knetlegierungen. Poster, in: Dipl.-Ing. Stephan Schuschnigg (Ed.). WerWasWo.Forschung@MUL, 2nd ed. Leoben, Österreich; 2014. p. 134.

Werinos M. Mikrolegierungselemente in 6xxx-Legierungen. Poster, in: Dipl.-Ing. Stephan Schuschnigg (Ed.). WerWasWo.Forschung@MUL, 2nd ed. Leoben; 2014. p. 242.

Werinos M. Einfluss von Mikrolegierungselementen auf das Ausscheidungsverhalten von Aluminiumlegierungen. Poster at ASMET Forum 2013; 2013.

Werinos M. Influence of Microalloying Elements on the Precipitation Behaviour of Aluminium Alloys. Poster and Poster Presentation at EMC 2013. Weimar; 2013.

Patents

Uggowitzer, P. J., S. Pogatscher, H. Antrekowitsch, M. Werinos, T. Ebner and C. Melzer: Age-hardenable aluminum alloy and method for improving the ability of a semi-finished or finished product to age artificially. WO2013124472A1.

Pogatscher S., M. Werinos, H. Antrekowitsch, P. J. Uggowitzer, T. Ebner und C. Melzer: Annealable aluminium alloy and method for improving artificial ageing ability. EP2631317A1.

UNPUBLISHED RESULTS

Figures 9.1-9.3 show unpublished results about the effect of natural aging temperature (5 °C, 25 °C and 45 °C) on hardening kinetics of various AA6061 alloys with (Fig. 9.2-9.3) and without (Fig. 9.1) Sn addition after annealing at 530 °C (Fig. 9.1-9.3a) or 570 °C (Fig. 9.1-9.3b). The data points assigned to clustering stages I, II and III are fitted with straight logarithmic lines. With decreasing natural aging temperature clustering stages are retarded and transition times delayed.
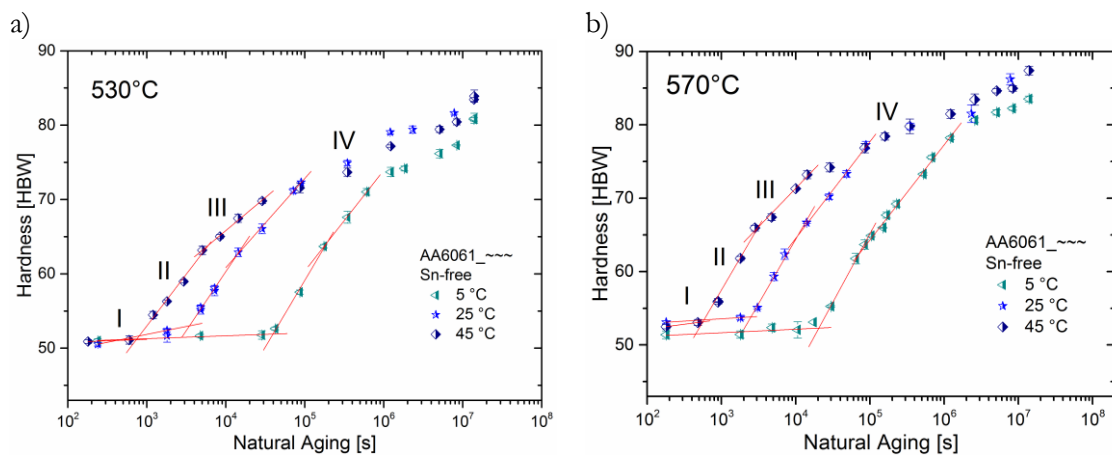

Figure 9.1. Effect of natural aging temperature (5 °C, 25 °C and 45 °C) on hardening kinetics in clustering stages I-IV of the commercial alloy AA6061 with 0.92 Mg, 0.70 Si and 0.26 Cu (in wt.%) after quenching from a) 530 °C and b) 570 °C
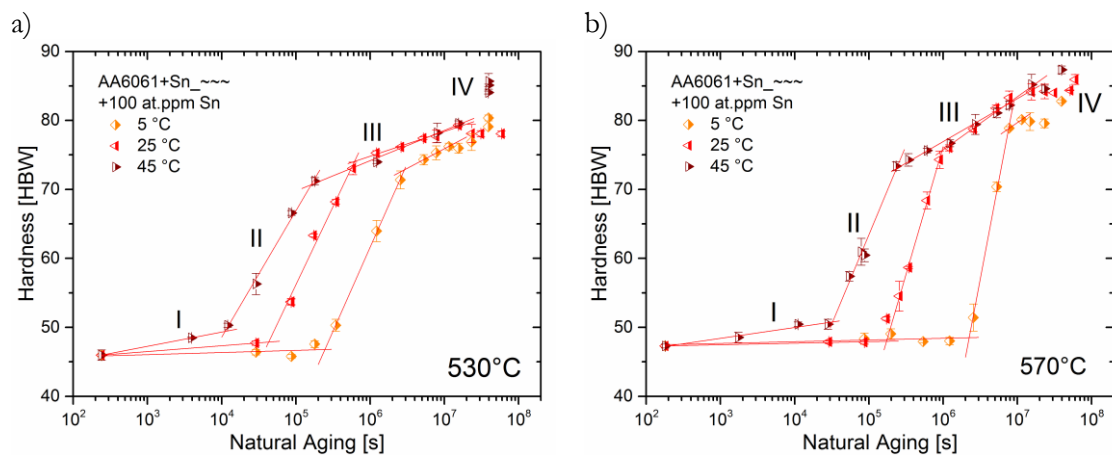

Figure 9.2. Effect of natural aging temperature (5 °C, 25 °C and 45 °C) on hardening kinetics in clustering stages I-IV of the commercial alloy AA6061 with 0.87 Mg, 0.72 Si and 0.30 Cu (in wt.%) after quenching from a) 530 °C and b) 570 °C
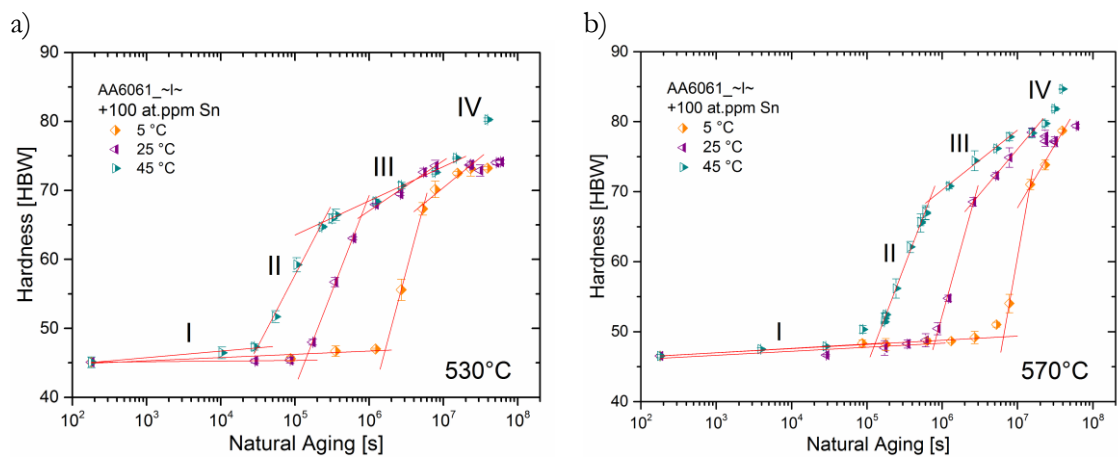
Figure 9.3. Effect of natural aging temperature (5 °C, 25 °C and 45 °C) on hardening kinetics in clustering stages I-IV of the commercial alloy AA6061 with 0.86 Mg, 0.61 Si and 0.245 Cu (in wt.%) after quenching from a) 530 °C and b) 570 °C